Clathrin Mediated Endocytosis in Alzheimer's Disease: Using Biomarkers to Uncover Disease Mechanism

By

Sierra Jaye Smith

A Dissertation

Presented to the Neuroscience Graduate Program at the Vollum Institute and the Oregon Health & Science University School of Medicine in partial fulfillment of the requirements for the Degree of Doctor of Philosophy

---

November 14, 2023

School of Medicine

Oregon Health & Science University

CERTIFICATE OF APPROVAL

This is to certify that the PhD dissertation of

Sierra J Smith

has been approved

Philip Copenhaver, Ph.D., *Committee Chair*

Julie Saugstad, Ph.D., *Advisor*

Kelly Monk, Ph.D.

Anusha Mishra, Ph.D.

Selva Baltan, Ph.D.

Joseph Quinn, M.D.

Table of Contents

List of Abbreviations

AD	Alzheimer's Disease
AMPAR	α-amino-3-hydroxy-5-methyl-4-isoxazolepropionic acid receptor
AP-2	Adaptor protein 2 complex
AP2A1	Adaptor protein 2 subunit A1
APOE e4	Apolipoprotein E4
APP	Amyloid precursor protein
APP_{SWE}	Amyloid precursor protein, Swedish mutation
Aβ	Amyloid beta
CLTA/B	Clathrin light chain A/B
CME	Clathrin mediated endocytosis
CNS	Central nervous system
CSF	Cerebrospinal fluid
CTL	Control
CTX	Cortex
DG	Dentate gyrus
DIV	Days *in vitro*
DNM2	Dynamin 2
DS	Down Syndrome
EPS15	Epidermal Growth Factor Receptor Pathway Substrate 15
FC	Frontal cortex
FCHO1,2	FCH and μ domain containing endocytic adaptor ½
FFPE	Formalin fixed paraffin embedded
GAK	G-associated kinase
HSC70	Heat shock protein 70

HP	Hippocampus
IHC	Immunohistochemistry
IPA	Ingenuity Pathway Analysis
iPSC	Induced pluripotent stem cell
ITSN1	Intersectin 1
LTD	Long-term depression
LTP	Long-term potentiation
MCI	Mild cognitive impairment
miRNA	microRNA
mRNA	Messenger RNA
PICALM	Phosphatidylinositol binding clathrin assembly protein
PSEN1	Presenilin 1
SEM	Standard error of the mean
UTR	Untranslated Region
WT	Wild type

List of Figures

List of Tables

Acknowledgements

I would first like to thank my advisor Dr. Julie Saugstad, for your guidance throughout the years and the freedom to make this project my own. I would also like to thank my lab members Dr. Ursula Sandau, Trevor McFarland, and Sarah Cate Baker, without whom the completion of this dissertation would not have been possible. It truly has been a team effort and all the hours we have spent together working through challenging problems, learning from one another, and laughing together will always mark a very special time in my journey.

Thank you to my committee members: Drs. Philip Copenhaver, Kelly Monk, Anusha Mishra and Selva Baltan. Your collective time and efforts have shaped how I ask and answer questions. I could always look forward to a lively discussion at each of our meetings, prompting me to think about my research in new and interesting ways. Your guidance allowed me to do good science and helped me to overcome many roadblocks when I didn't know what to do next.

I would also like to thank all of the other people that have provided help in my research and academic endeavors while here at OHSU: The Anesthesiology & Perioperative Medicine (APOM) Research group – for their support administratively and academically where someone was always willing to lend a hand. The OHSU Layton Aging & Alzheimer's Disease Research Center, and Dr. Randy Woltjer – for help in obtaining the human tissue used in my studies and providing expertise in interpreting the results. The OHSU Advanced Light Microscopy Core – for supporting my introduction into microscopy, which I have enjoyed thoroughly. The Copenhaver and Gray labs – who shared their reagents and expertise on growing primary hippocampal neurons. Dr. Joseph Quinn – for serving on my exam committee. And for their administrative and programmatic support – Jessica Parks, Dr. Kelly Monk and Dr. Kevin Wright.

Thank you to the Neuroscience Graduate Program and the Vollum institute for providing the opportunity to meet and enjoy the company of so many intelligent people who cultivate such a wonderful community. I have made so many amazing friends, who have supported me in more ways than I could ever have imagined. To my NGP cohort, thank you for always being friendly faces I knew I could count on. To Alex Houser, Mason Handford, Kate Bowie, Katy Lehman, Omar Koita, and many more, thank you for the many laughs and adventures. I wouldn't want to endure rainy camping trips, long hikes, or late nights with anyone else.

I am especially grateful for lifelong friends who have cheered me on from near and far away. Nai'a Turner, you are forever my sister and I am inspired by your perseverance and never-ending optimism. Thank you for giving me space to be myself. Belén Martinez Caro-Aguado, I have no words for what your support has meant to me. No matter what you had going on, you always gave me your unconditional friendship and believed in me when I was struggling, thank you.

To my family, thank you for your unconditional love. To my brothers Dylan and Wyatt Smith, you are my constants, I love you. To my father, Jay Smith, thank you for being a soft place to land when I need rest. Home will always be home because you are there.

Finally, to my mother, Carolyn Smith, I am who I am because of your unwavering love. Thank you for teaching me how to be a good human, how to trust and believe in myself, that I can do anything, and that wherever I am, you will be too. I love you all the time no matter what.

In loving memory of Carolyn Smith

Chapter 1. Introduction

1.1 Clathrin mediated endocytosis

Endocytosis is a ubiquitous and essential function of mammalian cells, it mediates many downstream pathways through internalization of material from the cell surface. Many types of endocytosis have been described, including clathrin-mediated endocytosis (CME), dynamin-dependent endocytosis, caveolin dependent endocytosis, micropinocytosis, and phagocytosis (*1*). Of these, CME is one of the most well characterized and mechanistically understood. Processes that rely on CME include uptake of intracellular signals, transmembrane receptor recycling, regulation of membrane composition, synaptic vesicle recycling, and initiation/regulation of many downstream intercellular signaling cascades such as the endo-lysosomal system. There are several distinct phases of CME: nucleation, cargo selection, coat assembly, scission and uncoating. Each phase is mediated by a host of proteins that have been described in detail through decades of studies (*1, 2*).

Briefly, as shown in **Figure 1**, CME is initiated by proteins involved in nucleation (**Figure 1, Step 1**), including FCH and μ domain containing endocytic adaptor 1/2 (FCHO1,2), Intersectin1 (ITSN1), and Epidermal growth factor receptor substrate 15 (EPS15). These cluster and bind to the plasma membrane to initiate membrane curvature and recruit other proteins, such as the Adaptor protein 2 complex (AP-2), for cargo selection (**Figure 1, Step 2**). Clathrin is also recruited by AP-2, which then begins the clathrin coat assembly (**Figure 1, Step 3**) of the endosome and curves the membrane further, forming the vesicle around the clustered cargo. The vesicle then undergoes scission from the membrane (**Figure 1, Step 4**) by BAR-domain containing proteins recruitment of Dynamin. Uncoating of clathrin (**Figure 1, Step 5**) is subsequently initiated by Auxilin of G-associated kinase (GAK), which recruits ATPase HSC70 to disassemble the clathrin coat allowing the machinery to be available for the next endocytosis

event. Cargo internalized through CME is typically sorted through the endolysosomal pathway for delivery to the appropriate cellular compartment (*3-5*).

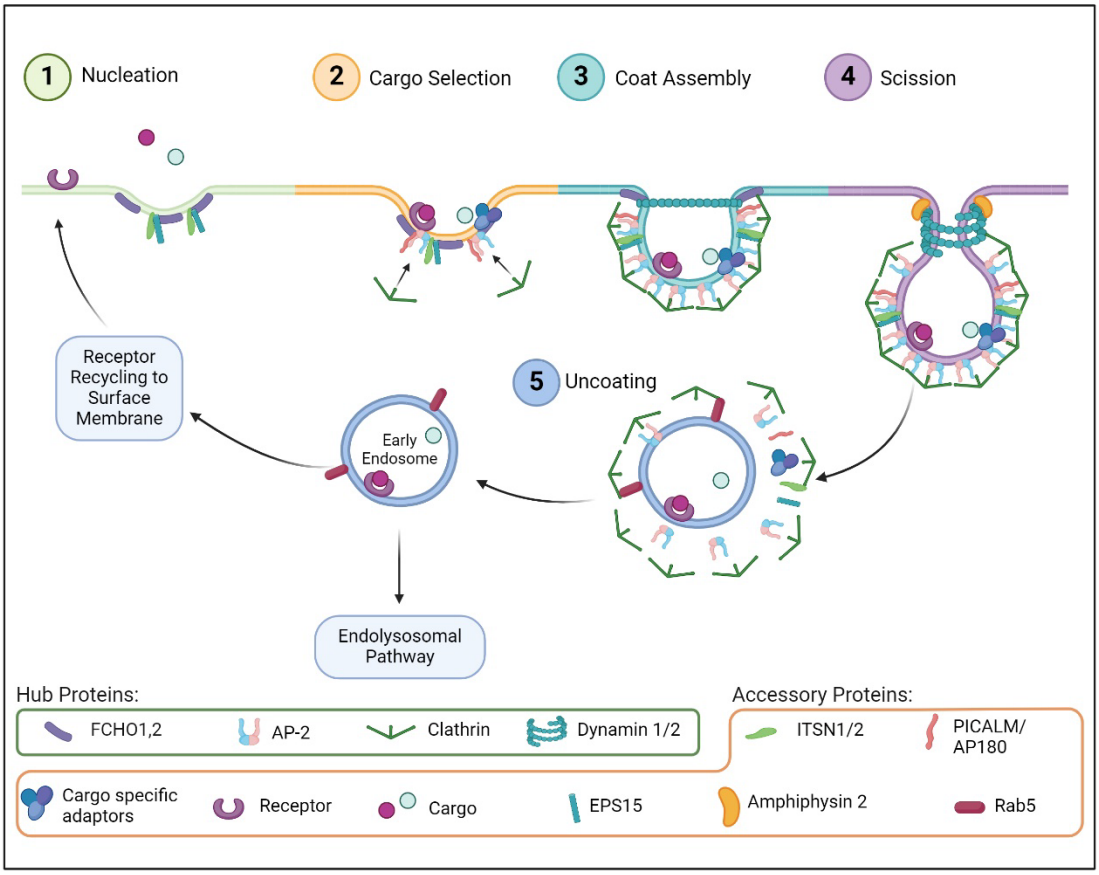

Figure 1.1 CME Step-by-step. *1) Nucleation:* Initial invagination of the membrane surface and recruits further proteins to the pit. *2) Cargo selection:* Couples with the intended cargo via receptors and adaptor proteins, which concurrently begin recruiting clathrin. *3) Coat assembly:* Clathrin begins forming a lattice around the budding vesicle. *4) Scission:* Dynamin assembles around the vesicle neck and with support from accessory proteins, the vesicle is removed from the extracellular membrane. *5) Uncoating:* The clathrin lattice disassembles and the early endosome can be trafficked through several pathways including back to the cell surface or through the endo-lysosomal pathway.

Given the fundamental need for cells to utilize this process, there are many diseases associated with disruption of CME. However, dysfunction is more common in accessory proteins, as genetic mutations of essential hub proteins, like those that make up the AP-2 complex, are typically embryonic lethal (*6, 7*). These changes can still have profound effects on CME function and are associated with cancer, psychiatric diseases, and various neurodegenerative diseases (*4*). For example, in Parkinson's disease, mutations in synaptojanin and auxilin have been shown to be causative for early onset Parkinson's (*8*). In Alzheimer's disease (AD), genetic links have been made to *AP-2* and importantly to the Phosphatidylinositol Binding Clathrin Assembly Protein gene (*PICALM),* one of the highest genetic risk factors in AD (*7, 9*).

AD is the most common form of dementia (*10*) and is characterized by the progressive development of amyloid beta (Aβ) plaques and neurofibrillary tau protein tangles in the brain (*11, 12*). AD is often diagnosed 15-20 years after pathology begins to develop, and there are no reliable tools to detect early brain changes that lead to it (*13*). As such, the effort to identify early cellular changes before onset of symptoms is of great importance. As AD progression is a highly complex process, many mechanisms have been associated with disease progression, such as neuroinflammation, impaired autophagy, oxidative stress, vascular dysfunction and endolysosomal dysfunction (*14, 15*). Perhaps one of the most widely referenced mechanisms is the Aβ cascade hypothesis, a well-established model of disease progression, in which intercellular Aβ accumulates as plaques in the brain, induces tau pathology, and ultimately neuronal death (*16, 17*). Others have since suggested that the imbalance of extracellular Aβ clearance and intracellular accumulation of Aβ initiates neuronal dysfunction rather than only accumulation of extracellular plaques (*12, 18, 19*). As such, the processes of Aβ production and clearance have been of particular interest in the field.

Amyloid precursor protein (APP) is endocytosed and processed in the endolysosomal pathway of neurons via a proteolytic cleavage which preferentially produces more pathogenic Aβ ($A\beta_{1-42}$) than non-pathogenic Aβ ($A\beta_{1-40}$) (*12, 20*). Although the endolysosomal pathway in AD has been extensively studied downstream of $A\beta_{1-42}$ production, few investigators have evaluated the upstream contribution of endocytosis, specifically CME. As the primary process that feeds into the endolysosome, disruption of CME has the potential to affect this and many other downstream cellular pathways implicated with AD. Yet how CME may change in the context of AD has not been evaluated carefully. Additionally, in other brain cell types like microglia and astrocytes, CME is implicated in extracellular debris uptake and could be important to $A\beta_{1-42}$ clearance, illustrating the potential for CME to affect the balance of both intra- and extra-cellular $A\beta_{1-42}$ accumulation in multiple ways via multiple cell types. Here, we will discuss how CME in different brain cell types has thus far been implicated in AD risk and progression, and illustrate the importance of examining CME further as a potential early disease modifier.

1.2 AD and Endolysosomal Function

The endolysosomal pathway systematically internalizes and sorts extracellular molecules that can be used in the cell, recycled back to the cell membrane, or degraded internally through lysosomes and autophagosomes. Classically, molecular cargo is internalized through CME or other endocytic pathways and trafficked to early endosomes, then late endosomes, recycled to the surface membrane, or sent to the lysosome for degradation (*21*). In AD, defects in this pathway cause cellular stress in multiple ways, including decreased endosomal transport, altered endosome signaling, reduction in vesicle recycling, decreased lysosomal acidification, and oxidative stress. These defects result in various neuropathological

outcomes such as $A\beta_{1-42}$ over production and clearance deficits, as well as dystrophic neurites (*22-24*).

Interestingly, the earliest presenting cytopathology in AD, even before accumulation of Aβ is observed, is enlargement of early endosomes containing accumulated APP in pyramidal neurons in the frontal cortex (*25*). This phenotype is specific to sporadic AD and has not been observed in familial AD or other neurodegenerative diseases like Parkinson's and Huntington's disease (*26*). Enlarged early endosomes are also observed in induced pluripotent stem cell (iPSC) derived neurons from sporadic AD patients (*27*) and iPSC lines with *APP* and presenilin 1 (*PSEN1*) mutations, both genetic risk factors for sporadic AD (*28*). Interestingly, endolysosomal dysregulation and enlarged early endosomes are also seen in Down syndrome (DS), a genetic disorder caused by a triplication of chromosome HSA21(*26*). People with DS have a significantly higher risk of developing AD, with nearly all patients developing neuropathology and symptoms by age 65 (*29, 30*). This phenomenon is thought to be due to several AD related genes encoded on HSA21, such as *APP* and *PSEN1* (*23, 31-33*). This connection between DS and AD could point towards endocytic processes as a potential driver of early endolysosomal dysfunction in AD.

Increased size and/or number of early endosomes is thought to correlate with an increase in general endocytosis, which results in the enlarged endosomal phenotype (*34*). This effect could indicate that changes in upstream endocytosis are important factors in downstream endolysosomal dysfunction in AD. The impact of cargo processed into this pathway has also been shown to alter endosomal function. For instance, in primary cortical rat neurons, internalization of $A\beta_{1-42}$ resulted in increased levels and altered distribution of endosomal-lysosomal markers, as well as triggered neuronal degeneration. Inhibiting general endocytosis, and CME specifically, attenuated this effect and returned endo-lysosomal markers to normal, suggesting that endocytosis of pathogenic $A\beta_{1-42}$ contributes to downstream endosomal

dysfunction (*35*). Therefore, changes in CME may contribute to AD endolysosomal dysregulation in multiple ways.

Kimura & Yanagiwasa summarized many of these endolysosomal disruptions into the "traffic jam" hypothesis (*36*). This hypothesis posits how disruptions in endocytosis and downstream endosome trafficking could be involved in altering the metabolism of AD related proteins and thus contributes to AD pathogenesis. Similarly, Limone et al., proposed using the related genetic changes in endolysosomal trafficking as a "genetic hub" of AD which could contribute to many pathological events and illuminate potential drug targets (*37*). However, as these hypotheses focus primarily on trafficking of endosomes after endocytosis, how endocytosis itself may be altered and affect cellular phenotypes needs to be considered.

1.3 Clathrin Mediated Endocytosis in AD

CME has been well studied under normal physiological conditions, but little is known about how it may be changed during AD progression. In addition to its downstream connection with the endolysosomal pathway, several studies have indirectly implicated CME in AD in humans and animal models through genomics, transcriptomics, and proteomics of CME-related genes and proteins. See **Table 1** for a summary of CME proteins associated with AD, their function in CME, and the AD brain regions where they are changed.

Table 1.1 CME Proteins in AD.

Gene	Protein Name	Role in CME	Changed in AD?	Method	Brain Region	References
			decreased	IHC	layer II superior frontal gyrus	Yao, 2000 PMID: 11124443
			no change	WB	total superior frontal gyrus, total hippocampus	
AP2A1	AP-2 complex subunit alpha-1	Nucleation	localized to NFTs	IHC	temporal neocortex	Srinivasan, 2021 PMID: 34820873
FCHO1	FCH and mu domain containing endocytic adaptor 1	Nucleation	unknown	-	-	
			decreased	IHC	all layers superior frontal gyrus, hippocampus CA3/hilus	Yao, 1999 PMID: 10579202
SNAP91	Clathrin coat assembly protein AP180	paralog of CALM, Cargo Selection	decreased	IHC, WB	Dentat Gyrus, CA3, Entorhinal cortex, temporal cortex	Cao, 2010 PMID: 20847448
			increased	RT-PCR	frontal cortex	Wilmot, 2008 PMID: 17174450
ITSN1	Intersectin 1	Nucleation, Cargo Selection	no change	WB	frontal cortex, temporal cortex	Malakooti, 2019 PMID: 31263630
			increased	RT-PCR	frontal cortex	Baig, 2010 PMID: 20838239
	Phosphatidylinositol-binding clathrin		localzed with NFTs	IHC	Hippocampus CA4	Ando, 2013 PMID: 23589030
PICALM	assembly protein	Cargo Selection	decreased	WB	neocortex	
CLTA	Clathrin, light chain	Coat Assembly,	localized to some NFTs	IHC	Hippocampus	Nakamura, 1994 PMID: 814089
CLTC	Clathrin, heavy chain	Scission, Uncoating	increased	IHC	frontal cortex	Alsquati, 2023 PMID: 37449017
DNM1	Dynamin 1	Scission	decreased	IHC	Hippocampus, entorhinal cortex	Cao, 2010 PMID: 20847448
			decreased	qRT-PCR	Hippocampus	Aidaraleiva, 2008 PMID: 18236001
DMN2	Dynamin 2	Scission	decreased	RT-PCR	temporal cortex	Kamagata, 2009 PMID: 19126407
			increased	PCR	frontal cortex	Chapuis, 2013 PMID: 23399914
BIN1	Amphiphysin 2	Scission	decreased	WB	frontal cortez	De Rossi, 2016 PMID: 27488240
AMPH	Amphyphysin 1	paralog of BIN1, Scission	decreaed	WB	frontal cortex	De Jesús-Cortés, PMID: 22975846
		Uncoating, early	increased	WB	frontal cortex	Alsquati, 2023 PMID: 37449017
RAB5A	Ras-related protein Rab-5A	endosome fusion	increased	WB	hippocampus, frontal cortex	Ginsberg, 2010 PMID: 20847427

In 2018, Ahmad et al., calculated weighted genetic risk scores by combining data from the longitudinal AD Rotterdam Study (*38*) and 20 AD genetic risk variants. These risk scores were then clustered within cellular pathways and associated with AD, mild cognitive impairment (MCI), and brain MRI phenotypes. The risk score of endocytic pathways was significantly associated with MCI, and interestingly, the clathrin/AP-2 adaptor complex pathway was modestly associated with white matter lesions (*39*). These associations suggest an early involvement of endocytosis, specifically CME, in AD risk/etiology. Indeed, proteins involved in CME such as AP180 (cargo selection), AP-2 (cargo selection/clathrin recruitment), and Dynamin I (scission) are shown to be decreased in AD in various regions of human post-mortem brains at the RNA and protein level (*40-44*). Together, the changes of CME protein levels point towards involvement of the pathway in AD, but each protein must be evaluated individually to understand how its changes may affect or contribute to potential CME dysfunction in AD.

Several of these protein changes also translate to a transgenic mouse model of AD with a mutation in humanized *APP* (APP_{SWE}) (*45*). Dynamin I and AP180 were decreased in APP_{SWE} brains versus control, with varying degrees of specificity in subregions of the hippocampus, entorhinal cortex, and temporal cortex, similar to their changes in human AD brains (*44*). Interestingly, a separate study of the cortex in APP_{SWE} mice, showed several CME proteins (APP, clathrin, Dynamin II, and PICALM) were upregulated, not downregulated as was observed in other brain areas. Importantly, proteins related to clathrin-independent endocytosis such as flotillin-1, and caveolin-1 and -3 were not changed (*46*). These observations demonstrate that proteins specific to CME, and not to other common endocytic pathways, are changed and could point towards CME being specifically responsible for downstream endocytic abnormalities in APP_{SWE} mice. However, it is unknown whether more recently studied AD models with multiple transgenes, such as the 3xTg (*47*) or 5xFAD lines (*48*), recapitulate these changes or have CME disruptions.

Another consideration is whether normal aging affects levels of CME proteins and CME function. It is well known that the biggest risk factor of developing AD is aging, and a change in CME proteins over time could suggest a possible connection between this risk and early cellular phenotypes. To date, only one study has attempted to address this possible connection. In 2018, Alsquati et al., examined how endocytosis-related proteins change in the frontal cortex of neurologically normal males from different age groups; 20-30 (young), 45-55 (middle aged), and 70-90 (old) (*49*). Interestingly, both CME and clathrin-independent proteins were changed in an age-dependent manner. Four CME proteins, dynamin I, isoform 4 of PICALM, AP180, and Rab5, were all significantly increased from young to old age groups. Clathrin-independent proteins such as caveolin-2 and flotillin-2, increased with age, while caveolin-3 was decreased.

Of note, some of these protein changes contrast with those seen in AD brains in studies described above and may be related to general endocytosis changes, rather than specifically to

CME. It is unclear whether this effect may be due to evaluation of different brain regions or exclusion of females from the aging study. Prior studies examining CME proteins in AD included both females and males in their cohorts, which is important, as females have a much higher incidence of AD (*50, 51*). Examining protein levels in males only does not explore a potential sex difference in endocytosis during aging, which could be a factor in why there is a difference in the direction of expression change between the aging study and others mentioned above. Additionally, the 15-year gap between each age group in these data should be considered. While the average age of AD diagnosis is about 75 years of age (*52*), brain changes can occur for many years beforehand; thus, the 15 year difference between the middle aged and old aged groups could be an illuminating time point to evaluate. While a very promising initial study, more research is needed to elucidate the potential role of CME in early AD and if, or how, aging may be involved.

When thinking about how these observed differences in AD CME proteins may affect function, we must also consider the potential for specific CME functions in different brain regions. As illustrated above, CME proteins show different changes, depending on what brain region was analyzed. The effect on overall CME function could be different in each brain region, depending on how a specific protein, or set of proteins, is changed. An increase in one protein may reduce CME, while the same increase in a different protein could decrease CME in a different brain region. Additionally, many CME proteins are not only expressed in a single cell type. As AD has an observed effect on many brain cell types (e.g., neurons, astrocytes, and microglia), which have varying phenotypes throughout disease progression, CME proteins may not change in the same way in all cells. Thus, depending on the cell type, dysregulation of CME proteins and resulting downstream dysfunction may have distinct cellular outcomes. Studies using whole brain lysate are not able to distinguish protein expression in different cell types. Thus, studies focused on individual cell types are needed to establish whether CME is altered in

distinct ways. Although brain region-specific changes are more difficult to evaluate due to difficulty obtaining the appropriate samples, many studies have begun to tease apart the potential cell type differences of CME proteins in AD, and will be further described in the remainder of this review.

1.4 CME in Neurons

1.4.1 CME in Synaptic Dysfunction

As AD is characterized by increasing loss of neurons throughout disease, most studies to date have focused on how altered neuronal functions may affect disease progression. It is well established that synaptic dysfunction, loss, and subsequent neuronal degeneration contributes to the progressive nature of AD. Reduced synapse numbers are observed throughout disease progression and are strongly correlated with cognitive decline (*53*), but synapses start to show dysfunction even before measurable cellular degeneration. Normally functioning synapses rely on the quick release of pre-synaptic vesicles, which are rapidly recycled via CME to maintain the pool of vesicles available for transmission (*54*). Synaptic disruption in AD can be induced by both extracellular $A\beta_{1\text{-}42}$ oligomers and intracellular hyperphosphorylated tau, and as such, may be connected to other aspects of AD neuropathology, such as altered APP processing, abnormal phosphorylation, and calcium imbalance (*55-57*). Of note, synaptic vesicle recycling is reduced in AD, and multiple CME proteins that are involved in maintenance of synaptic vesicle size, uniformity, and turnover, are clustered at pre-synaptic sites (*58, 59*). While several other mechanisms work in parallel to CME to maintain the synaptic vesicle pool, studies have shown that blocking CME significantly reduces synaptic vesicle recycling (*54*), indicating that CME is a major recycling mechanism, and that disruption of this machinery could contribute to AD synapse dysfunction.

Another source of synaptic dysfunction in AD results from disrupted regulation of AMPA receptors (AMPARs) in the post-synaptic cleft. Regulation of AMPARs at the membrane is involved in learning and memory, with receptor presentation leading to long-term potentiation (LTP) and internalization leading to long-term depression (LTD) (*60*). In AD, AMPAR trafficking is changed such that LTP is impaired and LTD is enhanced, which contributes to cognitive deficits (*56, 61, 62*). In LTD, AMPARs are internalized via CME, and internalization can be induced by interaction with $A\beta_{1\text{-}42}$ (*63-66*), suggesting that CME could be involved in the LTP/LTD changes in AD. Additionally, the AD risk factor and CME protein PICALM is involved in surface regulation of AMPARs. Loss of PICALM in mice initiates LTP and reduces LTD which improves learning (*67*). This directly implicates CME to AMPAR trafficking alterations and potential effects on learning and memory in AD. If CME dysfunction is an initial contributor to this early synaptic dysfunction in multiple contexts, it could very well be an upstream driver in disruption of many neuronal functions.

1.4.2 CME in Aβ Processing and Uptake

As briefly mentioned above, APP processing shifts towards producing more the amyloidogenic $A\beta_{1\text{-}42}$ in the endo-lysosomal pathway of neurons after internalization via CME (*20, 68*). This processing occurs in the early endosome, where the enzyme BACE1 and APP are individually delivered, and APP is cleaved by BACE1 and α-secretase into the pathogenic $A\beta_{1\text{-}42}$. Regulators of endosomal trafficking, which normally prevent BACE1 and APP from being delivered to the same compartment, have been identified as genetic risk factors for AD (*APOE4, PICALM, BIN1*). Disrupted expression of these regulators could contribute to the increased production of $A\beta_{1\text{-}42}$ in the endosome (*69, 70*). After amyloidogenic cleavage of APP, $A\beta_{1\text{-}42}$ peptides are secreted from the cell and aggregate to form toxic fibrils and plaques (*71*). In aged mouse hippocampal neurons, APP endocytosis is reduced with CME inhibition, but it is unclear

if this directly results in less $A\beta_{1-42}$ production (*72*). How CME alterations directly affect APP internalization and $A\beta_{1-42}$ production in an AD model has not yet been closely studied, but it is plausible that increased CME could cause a subsequent increase in APP internalization and processing, and conversely, that decreased CME may therefore decrease $A\beta_{1-42}$ production.

The production of $A\beta_{1-42}$ has also been connected to synaptic activity, which can stimulate CME and increase the internalization of APP. In fact, electrical stimulation in the hippocampus of the APP_{swe} mouse model increased $A\beta_{1-42}$ in brain interstitial fluid but was prevented up to 70% by CME inhibition (*73, 74*). This result suggests that endocytosis, both synaptic activity-mediated and clathrin-mediated, affects the levels of $A\beta_{1-42}$ produced and released from neurons, which could contribute to the development of extracellular $A\beta_{1-42}$ aggregation and spreading.

In addition to APP being endocytosed through CME, different forms of processed Aβ have also been shown to be internalized into neurons and accumulate in insoluble aggregates within endolysosomal compartments in AD brains (*75*). This accumulation of $A\beta_{1-42}$ in late endosomes and lysosomes could contribute to endo-lysosomal dysfunction and associated cellular disruptions(*23, 76*). Furthermore, endocytosed $A\beta_{1-42}$ can also cause intraneuronal dysfunction outside of lysosomal accumulation; for example, cultured rat hippocampal neurons treated with $A\beta_{1-42}$ showed decreased synaptic vesicle endocytosis and Dynamin1 expression after stimulation, indicating that the replenishing of vesicles to the readily available pool is impaired by $A\beta_{1-42}$ (*44*). Another of many observed intercellular effects of $A\beta_{1-42}$ fibrils is the induction of neuritic defects and growth cone collapse. In cultured cortical neurons, $A\beta_{1-42}$ internalization can result in failure of axonal repair and contribute to axonal degeneration (*77, 78*). It has since been shown that endocytosis in growth cones is increased after $A\beta_{1-42}$, and that inhibition of CME prevents the cone collapse (*79*) suggesting that CME is a primary mechanism driving downstream effects of $A\beta_{1-42}$.

However, there are conflicting reports as to which endocytic mechanism is responsible for taking up each form of processed Aβ (e.g. monomeric, oligomeric, or fibrillar $Aβ_{1-42}$). One study that evaluated the uptake of monomeric non-pathogenic $Aβ_{1-40}$ and pathogenic $Aβ_{1-42}$ in SH-Sy5Y neuroblastoma cells found that uptake of $Aβ_{1-42}$ is twice as efficient as that of $Aβ_{1-40}$ and is primarily independent of CME (*80*). A subsequent study from the same group found that while the mechanism of Aβ uptake observed was similar to some established endocytic pathways, there are likely more undiscovered molecular components regulating $Aβ_{1-42}$ uptake (*81*). Yet other groups report several forms of Aβ being internalized through CME in different cell types. For example, in rat primary hippocampal neurons, prefibrillar oligomeric forms of $Aβ_{1-42}$ were rapidly taken into cells in a dynamin-dependent manner, accumulated in lysosomes, and caused disruption to endo-lysosomal function. Importantly, a non-misfolded variant of $Aβ_{1-42}$ was not internalized and did not show any effects on endo-lysosomal function (*82*). In addition, in mouse neuro-2a cells, both $Aβ_{1-42}$ monomers and oligomers showed minimal capacity for binding with the membrane itself but were not able to enter cells under CME inhibition (*83*), meaning that toxicity of $Aβ_{1-42}$ fragments could be due to their internalization through receptors.

These observed differences in uptake methods for each $Aβ_{1-42}$ form could be due to the use of multiple experimental models or structural changes in receptor binding to initiate endocytosis. They point to aggregation state of $Aβ_{1-42}$ as an important factor to consider when evaluating the mechanisms and further effects of $Aβ_{1-42}$ internalization. Indeed, several studies have shown that oligomeric and aggregated $Aβ_{1-42}$ are internalized more and are more toxic to neurons than fibrillar or monomeric $Aβ_{1-42}$ (*84, 85*). However, these studies do not clarify which mechanism of endocytosis is involved, clathrin mediated or otherwise. Additionally, when comparing uptake of pathogenic $Aβ_{1-42}$ vs. non-pathogenic $Aβ_{1-40}$, $Aβ_{1-42}$ and not $Aβ_{1-40}$ is internalized by Dynamin dependent endocytosis (*86*). Taken together, it is still unclear how each different form of Aβ fragment is internalized into neurons and what downstream effects they may

have inside the cell. Nevertheless, there are many indications that CME is clearly an important player in neuronal AD mechanisms and should be studied further to tease the emerging nuances apart.

1.4.3 CME Involvement in Tau Dysfunction

While we have thus far focused on how CME disruptions may relate to Aβ pathology, it may also play a role in tau dysfunction. During its propagation, pathological tau is excreted and then internalized by neighboring cells (*87*). Internalization of extracellular tau aggregates, as opposed to monomers, has recently been suggested to initiate tau propagation in recipient cells (*88, 89*). Internalization of tau has been observed to occur through several types of endocytosis, including phagocytosis, bulk endocytosis, and CME (*90, 91*). However, as with CME effects on Aβ there are few direct experiments that examine how CME disruption may affect Tau propagation and resulting neuronal dysfunction. Additionally, it may be difficult to distinguish AD-specific changes from changes in other tauopathies. Thus, although the potential cellular effects of tau internalization by CME are substantial, there is less evidence that CME is as prominent mechanism of tau endocytosis as it is for Aβ.

1.5 CME in Non-Neuronal Cell Types

As CME is a ubiquitous process, how it is changed in non-neuronal cell types during AD must be considered. Here, we will focus on astrocytes and microglia, which have myriad functions essential for maintaining a healthy nervous system and respond quickly to changes in environment (*92*). Both have been implicated in reactivity to and protection from AD pathology, often in synchrony (*93*).

1.5.1 CME in Astrocytes

Astrocytes perform many essential functions in a healthy central nervous system (CNS), including regulating synapse activity, interactions with blood vessels and endothelial cells to facilitate the blood brain barrier, neurogenesis, and maintenance of neuronal homeostasis. Astrocytes have diverse morphology and mechanisms of action for these functions (*94-97*). In AD, many astrocytes become reactive, localize around $A\beta_{1-42}$ plaques, and excrete inflammatory cytokines that contribute to widespread neuroinflammation and subsequent neuronal dysfunction (*93*). It has also been shown that astrocytes can be induced to lose the ability to support neurons by activated microglia, and these neurotoxic astrocytes are abundant in AD and other neurodegenerative diseases (*98*).

Astrocytes are closely tied to the clearance of dying neurons and take up large amounts of neuronal $A\beta_{1-42}$ and debris (*99*). However, astrocytes can become overburdened with Aβ, resulting in impaired phagocytosis of diseased synapses and potentially contributing to the increased amount of dystrophic neurites seen in early stages of AD (*100*). Additionally, internalization of Aβ protofibrils engulfed by mouse primary astrocytes are not degraded in the cell and induce lysosomal dysfunction within them (*101*). Astrocytes of aged primate brains show enlarged early endosomes filled with Aβ, suggesting that aging may also play a role in astrocytic dysfunction (*102*). And while it is largely thought that astrocytes internalize Aβ through phagocytosis, it has recently been shown that multiple forms of Aβ (1-40 and1-42) are internalized via clathrin-coated vesicles in rat primary astrocytes, where they induce increased reactive oxygen species production and decreased cell viability. When treated with pharmacological inhibitors of CME, astrocytes exhibit significantly decreased uptake of $A\beta_{1-42}$ and a partial rescue of $A\beta_{1-42}$ induced cell death (*103*).

Another consideration of astrocytic involvement in AD is their connection to the genetic risk factor of apolipoprotein E4 (*APOE4*). *APOE* is mainly expressed in astrocytes as their primary cholesterol carrier, and expressing the *APOE4* allele is one of the biggest risk factors for developing AD (*104*). Many AD phenotypes are affected by *APOE* status, including Aβ clearance and lipid metabolism (*105-107*). Human iPSC-derived astrocytes expressing *APOE4* exhibit both decreased CME and early endosomal markers, suggesting that *APOE4* disrupts CME. Interestingly, increased expression of *PICALM* rescues endocytic defects in the APOE4 astrocytes (*108*). The connection of these two major genetic risk factors of AD through CME suggests that CME is instrumental in disease development. It is also possible that the changes in CME protein levels observed in AD post-mortem brains contribute to the dysfunction of astrocytes and their role in driving subsequent AD pathology. Moreover, the involvement of CME in astrocytic responses to $A\beta_{1-42}$ illustrates the importance of evaluating CME in cell types other than neurons. It also opens up questions regarding how aberrant CME early in AD contributes to non-neuronal disease phenotypes.

1.5.2 CME in Microglia

Microglia, CNS-resident phagocytes, are well recognized to have a dual role in AD, as reviewed recently (*93, 109-111*). Briefly, microglia can act in both a neurotoxic and neuroprotective role in AD, and which role they perform depends on many factors. Microglia activated from their resting state into neurotoxic phenotypes promote neuroinflammation through release of neurotoxic cytokines and other inflammatory factors. Contrasting this response, activated microglia in their neuroprotective phenotype can limit plaque formation by clearing extracellular $A\beta_{1-42}$. Paradoxically, both phenotypes can be initiated by $A\beta_{1-42}$. One prominent hypothesis in AD pathogenesis is that an initial problem that arises in disease progression is the loss of neuroprotective microglial function due to age-associated microglial

senescence, which in turn leads to loss of $A\beta_{1-42}$ clearance and accumulation of $A\beta_{1-42}$. This accumulation of $A\beta_{1-42}$ then activates microglial neurotoxic states, which increase neuroinflammation and eventually leads to dementia (*112*). This idea implicates microglia, and specifically a disruption in $A\beta_{1-42}$ clearance, in early stages of AD.

Endocytic clearance of $A\beta_{1-42}$ by microglia can occur through several mechanisms, the most commonly studied being micropinocytosis and phagocytosis. However, recent studies have begun to implicate CME in this process. In HMO6 cells, a human microglial cell line, treated with an amyloid-degrading enzyme activator, $A\beta_{1-42}$ uptake was significantly increased, and both clathrin and caveolin expression were upregulated (*113*). However, no studies were done to examine the effect of inhibiting clathrin- or caveolae-dependent endocytosis independently, so it is unclear whether one process is more prominent that the other. Nevertheless, these findings suggest an involvement of CME in microglial $A\beta_{1-42}$ clearance, although it may not be the only mechanism at play.

More recently, a study using a mouse microglial cell line treated with fibrillar $A\beta_{1-42}$ found that clathrin colocalized with internalized $A\beta_{42}$ and that inhibition of CME resulted in 80% reduction of $A\beta_{1-42}$ uptake (*114*), further supporting the hypothesis that CME is involved in microglial Aβ uptake. Additionally, in another mouse microglia cell line, a novel form of endocytosis has been described, LC3-associated endocytosis (LANDO) (*115*). LANDO supports the clearance of Aβ and prevents activation of inflammatory microglia, yet inhibition of actin polymerization and phagocytosis had no effect on internalization of Aβ. This finding suggests that LANDO occurs though CME, as LC3 is colocalized with clathrin and Rab5 early endosomes (*115*).

Also, it is important to note that these studies have not yet been replicated *in vivo* and should be validated further, as microglia function is strongly influenced by the surrounding environment. Hower, the recent evidence of CME in microglial clearance of $A\beta_{1-42}$ does point

towards another potential effect of CME disruption in AD. CME in microglia needs to be further investigated to clarify what degree it and other endocytic mechanisms are disrupted in AD. Reduction in CME could contribute to neurotoxic microglial function through reduction of $A\beta_{1-42}$ clearance. Alternatively, if CME is not changed or is increased in AD microglia, it could be driving neuroprotection of microglia, whereby $A\beta_{1-42}$ clearance is actually contributing to a slowing of disease progression.

1.6 Conclusion

In conclusion, CME is emerging as a critical player in the development and progression of AD in multiple brain cell types. CME is an important intersection between early neuronal dysfunction via $A\beta_{1-42}$ accumulation and downstream effects that contribute to neuronal viability, such as synaptic vesicle recycling deficits and disruption of AMPAR regulation. Not only is $A\beta_{1-42}$ produced following CME of APP, but internalization of multiple forms of extracellular $A\beta_{1-42}$ contribute to downstream neuronal pathology. In astrocytes and microglia, which are heavily involved in clearance of extracellular $A\beta_{1-42}$ in the brain, CME disruptions reduce internalization of $A\beta_{1-42}$. Importantly, other brain cell types, including endothelial cells, oligodendrocytes, and ependymal cells that are not reviewed herein, should also be considered in the context of CME and AD, as they could also be affected by changes in CME. Ultimately, CME appears to be involved in dysfunction in multiple cell types across early and late stages of AD. Thus, elucidating the mechanisms of CME and how their disruption is related to AD pathogenesis or neuroprotection in each brain cell type would both lead to a better understanding of AD mechanisms and potentially point to novel targets for the treatment or prevention of AD. In this dissertation work, I have begun to assess CME in the context of AD, using human post-mortem samples and the 5xFAD AD mouse model.

Chapter 2. Intersectin 1 is Changed in an Isoform and Brain Region Specific Manner in Alzheimer's Disease Brains

Data shown in Figure 2.1 of this chapter is published in Sandau et al, 2020 (*116*). Therein, I developed the target prediction pipeline and performed the subsequent target prediction analysis.

2.1 Abstract

Alzheimer's disease (AD) is the most common form of dementia and is characterized by the accumulation of amyloid-beta (Aβ) plaques and neurofibrillary Tau tangles in the brain. We previously identified a set of candidate AD microRNAs (miRNAs) in human cerebrospinal fluid (CSF) and used a target prediction pipeline to identify mRNAs and pathways that could be regulated by the miRNAs. Of these pathways, clathrin mediated endocytosis (CME) was selected for further investigation. CME is altered in multiple brain cell types in AD and is implicated in early cellular phenotypes such as enlarged early endosomes and pathogenic processing of Aβ. However, a comprehensive evaluation of major CME hub proteins in AD across multiple brain regions is lacking. Thus, we used immunoblot analysis to evaluate human post-mortem AD and control (CTL) frontal cortex (FC; AD n=22, CTL n=23) and hippocampus (HP; AD n=34, CTL n=22) for changes in Intersectin 1 (ITSN1), Phosphatidylinositol Binding Clathrin Assembly Protein gene (PICALM), Clathrin Light Chain (CLT), FCH and mu domain containing endocytic adaptor 1 (FCHO1), AP2 subunit alpha 1 (AP2A1), and Dynamin 2 (DNM2). Of these, we found that in AD ITSN1-long was decreased in the FC of males and HP of females; while ITSN1-short was increased in the HP of both males and females. Further, by immunohistochemistry we showed a potential association of ITSN1 with Tau pathology in AD

brains. Here we illustrate the possibility of CME changes affecting AD and pose specific functional differences between the ITSN1 isoforms that are brain region dependent.

2.2 Introduction

Alzheimer's Disease (AD) is characterized by the accumulation of amyloid beta (Aβ) plaques and neurofibrillary Tau protein tangles as the disease progresses (*11, 12*). However, as there are no reliable tools to detect early brain changes, patients are often diagnosed 15-20 years after the onset of neuropathology (*13*). Many scientists and clinicians are now focused on the development of more sensitive, affordable, and less invasive diagnostic tools, as well as disease modifying treatments to halt disease progression. To that end, we previously discovered (*117*) and validated (*118*) a set of candidate microRNA (miRNA) biomarkers in human cerebrospinal fluid (CSF) that distinguish AD patients from neurologically normal controls (CTL). Five of the miRNAs (miRs-142-3p, 146a-5p, 146b-5p, 193a-5p, 365a-3p) showed a trend towards decreased median expression across ordered diagnoses from normal control to mild cognitive impairment (MCI) to AD (*119*), suggesting that these miRNAs track with disease progression.

MiRNAs regulate protein expression via complementary binding to targeted messenger RNA (mRNA) sequences. This leads to suppression or degradation of the targeted mRNA transcripts (*120-122*) and subsequently reduced translation of the corresponding protein. As miRNAs themselves are also highly regulated, factors that alter their expression can affect target mRNA protein translation (*122*). It is currently unknown how CSF miRNAs may reflect or affect brain changes in AD through protein regulation.

The purpose of the current study is to utilize these novel candidate miRNA biomarkers to uncover potential cellular pathways involved in AD and to examine how the expression of proteins in these pathways may be altered in human postmortem AD brains. Using our miRNA

target prediction pipeline, we found that a significant number of proteins involved in clathrin mediated endocytosis (CME) may be regulated by AD CSF miRNAs, including Intersectin 1 (ITSN1), Phosphatidylinositol Binding Clathrin Assembly Protein gene (PICALM), and Clathrin Light Chain A (CLTA). Many cellular processes rely on CME such as synaptic vesicle recycling, uptake of intracellular signals, and regulation of downstream cellular functions such as the endolysosomal system (*1, 2*). Additionally, changes in endocytosis is one of the earliest pathologies of AD (*123*) and CME has been directly implicated in Aβ processing in neurons (*72*) and Aβ clearance in astrocytes (*108*).

PICALM is one of the highest genetic risk factors in AD (*7, 9*) and has been shown to have isoform specific changes in ageing and in male AD brains (*49, 124*). Another study reported that in AD there is an increase of the CME proteins Clathrin Heavy Chain, Dynamin 1, and Adaptor Protein 2 (AP2) (*125*). However, prior studies were limited in that they evaluated few proteins involved in CME in a small number of only male brains (*49, 124, 125*). Here, we examined, in both males and females, levels of CME hub proteins that have been previously implicated in AD: ITSN1 (*126, 127*), and CLTA (*128*), PICALM (*7, 9*), FCH and mu domain containing endocytic adaptor 1 (FCHO1) (*129*), AP2 subunit alpha 1 (AP2A1) (*41, 130*), and Dynamin 2 (DNM2) (*131-133*). Furthermore, PICALM, ITSN1, and CLTA are predicted targets of candidate AD miRNAs. We found that only ITSN1, a scaffolding protein that interacts with all CME hub proteins(*4*), is altered in AD brains compared to age-matched CTLs in an isoform and brain region specific manner. Our data suggest that CME dysfunction in AD may not be caused by a change in most CME hub proteins, and may be a product of disrupted interactions between supporting proteins such as ITSN1.

2.3 Methods

Target Prediction

We used TargetScan 7.2(*134*) and miRDB (*135, 136*) to predict target mRNAs of the top five miRNAs that show a trend in decreased median expression in the ordered diagnosis of CTL, MCI, and AD (miRs-142-3p, 146a-5p, 146b5p, 365a-3p, 193a-5p) from our previous study (*116*). These algorithms use the miRNA sequence and properties of mRNA sequences to predict the likelihood of a miRNA binding to an mRNA (*137*). To limit number of genes input for later pathway analysis, predicted targets were excluded if they had a Cumulative Weighted Context Score above –0.3 in TargetScan or a target score of below 60 in miRDB. To increase sensitivity and potential for predicting novel targets, we used the union of targets predicted by both TargetScan and miRDB (*137, 138*). The sensitivity, specificity, and precision of this method were calculated using validated miRNA-target pairs from miRTarBase, a database of experimentally validated miRNA-target interactions (*139*). The resulting values ranged from 0-1 with high quality results performing closer to 1 (*137, 138*). The union of TargetScan and miRDB resulted in higher values of sensitivity (0.35), specificity (0.833), and precision (0.98) when compared with an intersection (only targets predicted by both algorithms). Pathway analysis of the union set of 1214 predicted targets with QIAGEN Ingenuity Pathway Analysis (IPA) revealed 214 pathways in which the targets are significantly overrepresented. For this analysis we excluded cancer cell lines and related tissues to avoid the knowledge bias towards cancer in the IPA database.

Human Brain Samples

This study consisted of post-mortem tissue of 121 donors from the Oregon Brain Bank. All patients were aged individuals from the community and had either no known neurological disease (CTL) or a clinical history of AD established as previously described (*140, 141*). After

consent was given from the next of kin, brain autopsy was performed on all participants in accordance with Oregon Health & Science University IRB guidelines. Tissue was either stored unfixed at -80ºC, or formalin fixed and paraffin embedded.

Immunoblots

Archived frozen brain tissue was thawed and while thawing white matter and leptomeninges were dissected away. 40-60 mg of post-mortem grey matter from AD and CTL frontal cortex (FC; AD n=22, CTL n=23) and hippocampus (HP; AD n=34, CTL n=22) was collected and total protein extracted by sonication for 25 seconds in lysis buffer (62.5 mM Tris pH 6.8, 2% SDS and 10% glycerol) followed by centrifugation at 14,000 x g for 10 minutes. The supernatant was aliquoted and stored at -80ºC until used for immunoblot analysis. Before use, protein lysates were analyzed for protein content using the Pierce BCA Protein Assay kit (ThermoFisher Scientific), loading buffer (50 mM DTT, 0.01% bromophenol blue) added, boiled and cooled before protein (50 µg: ITSN1, 40 µg: AP2A1, FCHO1, 20 µg: CLT, DNM2, PICALM) was loaded onto precast NuPAGE 3-8% Tris-Acetate gels (Invitrogen) and separated by electrophoresis. Protein was then transferred onto polyvinylidene difluoride (PVDF) membranes in transfer buffer containing 10% methanol for better transfer of high molecular weight proteins. Before primary antibody incubation, membranes were dried overnight at 4ºC then activated with methanol and stained with Revert 700 Total Protein Stain Kit Total protein stain (TPS, LI-COR Biosciences), imaged on the Odyssey CLx Imager (LI-COR Biosciences), then destained and blocked with Intercept (TBS) Blocking Buffer (LI-COR Biosciences). After blocking, membranes were incubated with the specified primary antibodies (**Table 2.1**) for two hours at room temperature in Intercept blocking buffer (LI-COR Biosciences) with 0.2% Tween-20. After washing (4 x 5 min, TBS-T, 0.2% Tween-20). Membranes were then incubated with the appropriate IRDye secondary antibodies (LI-COR, **Table 2.1**) in Intercept blocking buffer with 0.2% Tween-20 and

0.02% SDS for 1 hour at room temperature. Membranes were washed (4 x 5 min, TBS-T) and bands visualized on the Odyssey CLx Imager. For low abundance proteins with high signal to noise ratios, such as ITSN1, we used the automated iBind Flex Western System (Thermo Fisher), which has been shown to increase sensitivity (*142*). The intensity of each signal was determined with Empiria Studio software version 2.2 (LI-COR Biosciences) using the Quantitative western blot function that employs automatic lane detection and background subtraction to reduce variability of between gel analyses. Signals were first normalized within gels to TPS, and as multiple gels were needed to include all samples, bands were normalized to a repeated sample run on every gel to account for between gel variation.

Table 2.1. Antibodies Used in This Study. Primary and secondary antibodies used for immunoblots (IB) and IHC.

Antibody	Host Species	Dilution	Vendor, Product #
ITSN1	Rabbit	IB: 1:2500 IHC: 1:500	Novus Biologicals, NBP1-87806
CLTA	Rabbit	1:2500	Novus Biologicals, NBP2-38638
DNM2	Rabbit	1:1000	Novus Biologicals, NBP2-47477
PICALM	Rabbit	1:1000	Atlas Antibodies, HPA019053
FCHO1	Rabbit	1:200	Invitrogen, PA5-31603
AP2A1	Goat	1:16000	LSBio, LS-B9566
Aβ	Mouse	1:5000	BioLegend, 87001
Tau	Mouse	1:5000	Gift from Dr. Peter Davies (*143*)
IRDye 800CW Donkey anti-Rabbit	Donkey	1:20000	LI-COR Biosciences, 926-32213
IRDye 680RD Donkey anti-Mouse	Donkey	1:20000	LI-COR Biosciences, 926-68072
Horse Anti-Mouse IgG Antibody (H+L), Biotinylated	Horse	1:250	Vector Laboratories, BA-2000
Goat Anti-Mouse IgG Antibody (H+L), Biotinylated	Goat	1:250	Vector Laboratories, BA-1000

Peptide block for ITSN1 antibody specificity

Hippocampal AD and CTL protein lysate samples were prepared and immunoblot was performed as described above. Before applying primary antibody to the membrane, the ITSN1 antibody was incubated overnight with the peptide used to develop the antibody (Novus Biologicals, NBP1-87806PEP). ITSN1 peptide was applied in excess of the primary antibody at ratios of 5:1 and 10:1 peptide to antibody. Bands were assessed for presence or absence after the peptide block to determine specificity of the antibody.

Immunohistochemistry (IHC)

Archival formalin fixed paraffin embedded (FFPE) tissue was cut at 7 um and mounted on superfrost plus glass slides. Tissue was deparaffinaized and incubated in formic acid for 5 minutes then citrate buffer (0.2% citric acid in DI water) for 45 minutes in an 80º-85ºC water bath for antigen retrieval. After a 15-minute block with milk (3% in PBS), slides were incubated with primary antibodies for Tau, Aβ, and ITSN1 (**Table 2.1**) diluted in TBS-T with BSA overnight at 4ºC. After washing, biotinylated-secondary antibodies (**Table 2.1**) diluted in TBS-T with BSA were applied for 1 hour at room temperature. Sections were then washed for 10 minutes in methanol and treated with Avidin / Biotin Complex solution (Vectastain ABC Kit, Vector Labs) to reduce background staining before DAB (3,3′-Diaminobenzidine) was applied.

Image Acquisition

All images were taken in brightfield using a Zeiss Axioscan 7 Slidescanner and a Plan-Apochromat 10X/0.45 M27 objective. Tiles were stitched together and then images compressed using the Zeiss JpgXr compression method.

Statistical Analysis

For pathway analysis, IPA performs an overrepresentation analysis using Fishers Exact Test. For both the immunoblots and IHC, the experimenter was blinded to participant demographics until all data were collected. Immunoblot data were analyzed with GraphPad Prism software v10.1.0 (GraphPad Software, Inc., San Diego, CA). For immunoblots all hippocampal samples were run together and probed for antibody together, while all FC samples were grouped in the same way for each protein. Prior to running the immunoblot gels all protein lysates within each brain region were randomized for disease and sex. Immunoblot data are shown as mean protein levels ± the standard error of the mean (SEM) normalized to TPS versus experimental groups in both the FC and HP: CTL-male (FC n=12; HP n=11), AD-male (FC n=10; HP n=17), CTL-female (FC n=11; HP n=11), AD-female (FC n=12; HP n=17). Biological replicates are displayed as individual symbols on each graph. To assess differences between protein levels in AD and CTL groups while considering both males and females we used a two-way ANOVA (disease x sex) followed by a Šídák multiple comparisons post hoc test, when appropriate. A $p < 0.05$ was considered to be a significant difference between groups.

2.4 Results

AD CSF MiRNAs Predict Relevant Mechanistic Pathways

To discover potential pathways regulated by the candidate AD miRNA biomarkers, we queried TargetScan 7.2 and miRDB with our previously discovered 5 trending AD CSF miRNAs (miRs-142-3p, 146a-5p, 146b-5p, 193a-5p, 365a-3p) (*116, 118*) as shown in **Figure 2.1A**. This resulted in 367 predicted mRNA targets from TargetScan and 1096 predicted targets from miRDB. Of these, 249 targets were predicted by both TargetScan and miRDB. The combined 1214 unique predicted targets were input to IPA to discover which cellular pathways have a significant overrepresentation of predicted targets. 353 predicted targets were found to be overrepresented in 214 pathways. In the top 50 pathways, several were already known to be related to or altered in AD (**Figure 2.1B**). Notably, CME emerged as a pathway of interest that is predicted to be targeted by the AD CSF miRNAs. **Table 2.2** lists proteins involved in CME whose mRNA are predicted targets of AD CSF miRNAs. We chose several of these to evaluate for changes between male and female CTL and AD brain.

A

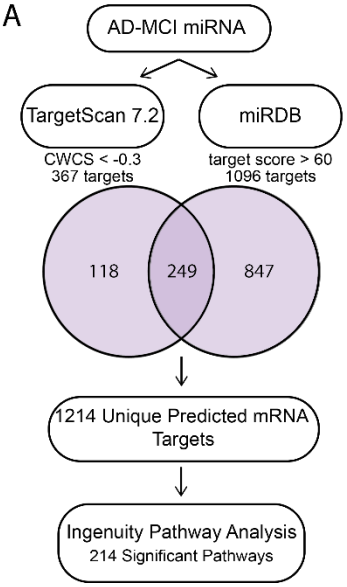

B

Ingenuity Canonical Pathways	-log(p-value)
Axonal Guidance Signaling	6.24
Synaptic Long-Term Potentiation	4.98
Synaptogenesis Signaling Pathway	4.82
Neuroinflammation Signaling Pathway	4.79
ERK/MAPK Signaling	4.19
Actin Cytoskeleton Signaling	3.38
Clathrin-mediated Endocytosis Signaling	2.97

Figure 2.1. Predicted mRNA Targets of AD MiRNAs are Represented in AD Related Pathways. (A) Target prediction pipeline in which five candidate AD miRNA biomarkers were analyzed for potential regulated mRNAs using TargetScan 7.2 and miRDB. There were 1214 predicted mRNAs with a CWCS < -0.3 or a target score > 60 in TargetScan and miRDB, respectively. mRNAs predicted by both algorithms are shown in the overlap of the Venn diagram. Ingenuity Pathway Analysis (IPA) was used to identify pathways with significant overrepresentation of these mRNA targets, which identified 214 significant pathways that included 353 mRNA targets. (B) Canonical pathways known to be related to AD that have significant overrepresentation of the predicted mRNA targets using a Fishers Exact test in IPA.

Table 2.2. Proteins Involved in CME are Targeted by One or More Candidate AD CSF MiRNA Biomarkers. The predicted mRNA targets of candidate AD miRNAs that are involved in clathrin mediated endocytosis (CME). Target mRNA symbol, miRNAs predicted to regulator the target, and target name are shown in alphabetical order. Targets we performed immunoblot on are indicated in bold.

mRNA Target Symbol	**MiRNA (hsa-miR)**	**mRNA Target Name**
CHP1	365a-3p	Calcineurin Like EF-Hand Protein 1
CLTA	142-3p	Clathrin Light Chain A
CTTN	142-3p	Cortactin
EPN1	142-3p	Epsin 1
FGF1	365a-3p	Fibroblast Growth Factor 1
FGF9	142-3p	Fibroblast Growth Factor 9
HGS	142-3p	Hepatocyte Growth Factor-Regulated Tyrosine Kinase Substrate
HSPA8	365a-3p	Heat Shock Protein Family A (Hsp70) Member 8
ITGB8	142-3p	Integrin Subunit Beta 8
ITSN1	193a-5p	Intersectin 1
NUMB	146a-5p 146b-5p	NUMB Endocytic Adaptor Protein
PICALM	142-3p	Phosphatidylinositol Binding Clathrin Assembly Protein
PIK3R3	365a-3p	Phosphoinositide-3-Kinase Regulatory Subunit 3
PIK3R6	142-3p	Phosphoinositide-3-Kinase Regulatory Subunit 6
PPP3R1	142-3p	Protein Phosphatase 3 Regulatory Subunit B, Alpha
RAC1	142-3p 146a-5p 146b-5p 365a-3p	Rac Family Small GTPase 1
STAM	142-3p	Signal Transducing Adaptor Molecule
SYNJ1	365a-3p	Synaptojanin 1
VEGFB	193a-5p	Vascular Endothelial Growth Factor B
WASL	142-3p	WASP Like Actin Nucleation Promoting Factor

Donor Demographics for Post-Mortem Brain Tissues

Both fresh frozen and FFPE postmortem brain samples from AD and CTL donors were obtained from the Oregon Health & Science University Layton Aging and Alzheimer's disease research center. Specific demographics can be found in **Tables 2.3 and 2.4**. The samples included 45 fresh frozen samples from the FC (23 CTL, 22 AD) and 56 samples from the hippocampus (22 CTL, 34 AD) for a total of 101 samples used for immunoblot in four groups (disease by sex) with $n \geq 10$. Disease state of all samples used were confirmed by post-mortem assessment with CTLs being Braak stage I/II and AD being Braak V/VI. There was no significant difference in the number of males to females and age at time of death between groups. All samples had PMI of less than 24 hours but given the constraints in availability of tissue there was a significant difference of PMI between male AD and CTL in both the FC ($p = 0.02$) and HP ($p = 0.005$). FFPE samples were used for IHC and included the FC and matching HP from 40 cases (20 CTL, 20AD) for a total of 80 samples. CTLs used for IHC were all Braak stage I/II and AD were all Braak stage VI. There was no significant difference in number of males to females, age at time of death, or PMI between groups.

Table 2.3. Participant Demographics for Immunoblots. Sex, mean age ± standard deviation (SD), and mean PMI ± SD of participant samples used for immunoblots. The sex, age, and PMI were matched across groups to the best of our ability in order to mitigate these factors as potential confounds.

	FC		HP	
	CTL	**AD**	**CTL**	**AD**
Sex				
Female	11	12	11	17
Male	12	10	11	17
Total	23	22	22	34
Age (Mean ± SD)				
Female	70 ± 10	76 ± 6	71 ± 11	74 ± 9
Male	68 ± 9	76 ± 5	70 ± 10	74 ± 8
Total	69 ± 9	76 ± 6	70 ± 10	74 ± 8
PMI (Mean ± SD)				
Female	11 ± 7	14 ± 7	13 ± 8	9 ± 7
Male	17 ± 6	10 ± 6	19 ± 3	11 ± 7
Total	14 ± 7	12 ± 7	16 ± 6	10 ± 7

Table 2.4. Participant Demographics for Immunohistochemistry. Demographics of the paired cases of postmortem FC and hippocampus used for immunohistochemistry. The sex, mean age ± standard deviation (SD), and PMI ± SD were matched across groups to the best of our ability in order to mitigate these factors as potential confounds.

	CTL	**AD**
Sex		
Female	10	8
Male	9	10
Total	19	18
Age (Mean ± SD)		
Female	67 ± 5	67 ± 6
Male	67 ± 5	66 ± 6
Total	67 ± 5	67 ± 6
PMI (Mean ± SD)		
Female	26 ± 6	23 ± 7
Male	28 ± 12	24 ± 14
Total	27 ± 9	24 ± 11

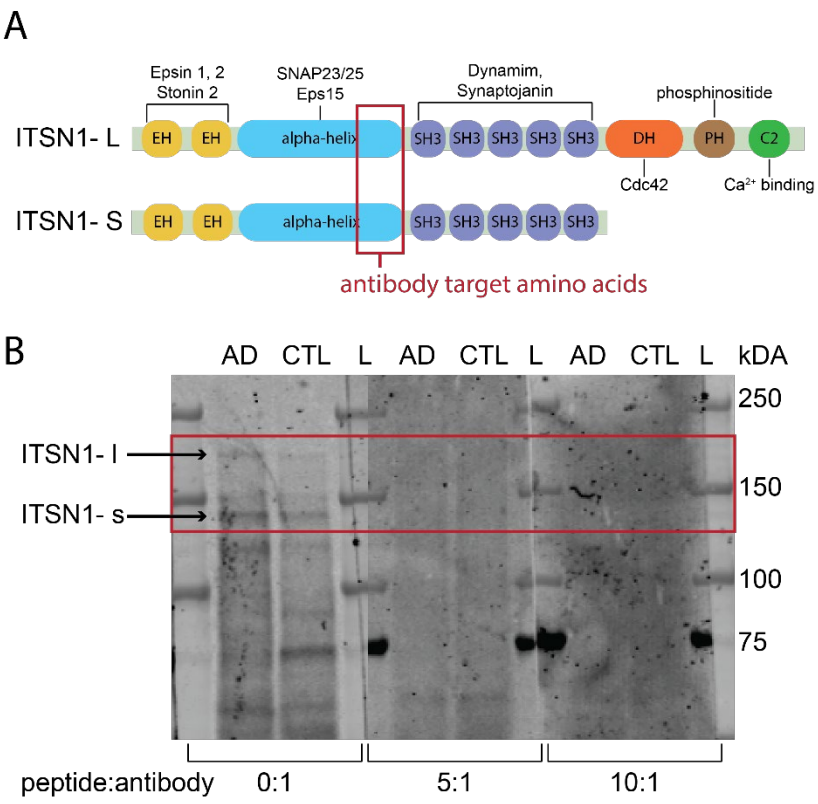

Figure 2.2. ITSN1 Antibody Binding is Confirmed by Peptide Block. (A) Schematic of functional domains in ITSN1-L and ITSN1-S indicate the location where other CME proteins interact with ITSN1. The red box indicates the region of ITSN1 used as the antigen for the ITSN1 antibody and the peptide used in blocking experiment. (B) AD and CTL HP samples were used for immunoblots with ITSN1 primary antibody without ITSN1 peptide (0:1) and ITSN1 primary antibody incubated ITSN1 peptide at 5:1 and 10:1 peptide:antibody ratios. Bands corresponding to ITSN1-L (190 kDa) and ITSN1-S (140 kDa) correspond to the expected molecular weights of the isoforms. Ladder (L).

ITSN1 is Decreased in AD FC and HP

We first investigated ITSN1, as it is the interactor of many hub proteins in CME (*144*).There are two isoforms resulting from alternative splicing (*145, 146*): a neuronal specific long form (ITSN1-L) and a ubiquitous short form (ITSN1-S) (**Figure 2.2A**). The ITSN1 antibody is expected to detect both ITSN1-L (190 kDa) and ITSN1-S (140 kDa) isoforms, which we observe in immunoblots using CTL and AD hippocampal protein lysates (peptide:antibody = 0:1, **Figure 2.2B**). We performed a peptide blocking test (**Figure 2.2B**) to confirm the antibody binds to the expected peptide. Before application to immunoblots the ITSN1 primary antibody was incubated with an excess of a peptide that corresponds to the amino acids/antigen used produce the antibody. In peptide:antibody ratios of 5:1 and 10:1, we do not observe the expected bands for ITSN1-L (190 kDa) and ITSN1-S (140 kDa) (**Figure 2.2B,** red box). This indicates that the antibody is indeed binding to the antigen for both ITSN1-L and ITSN1-S.

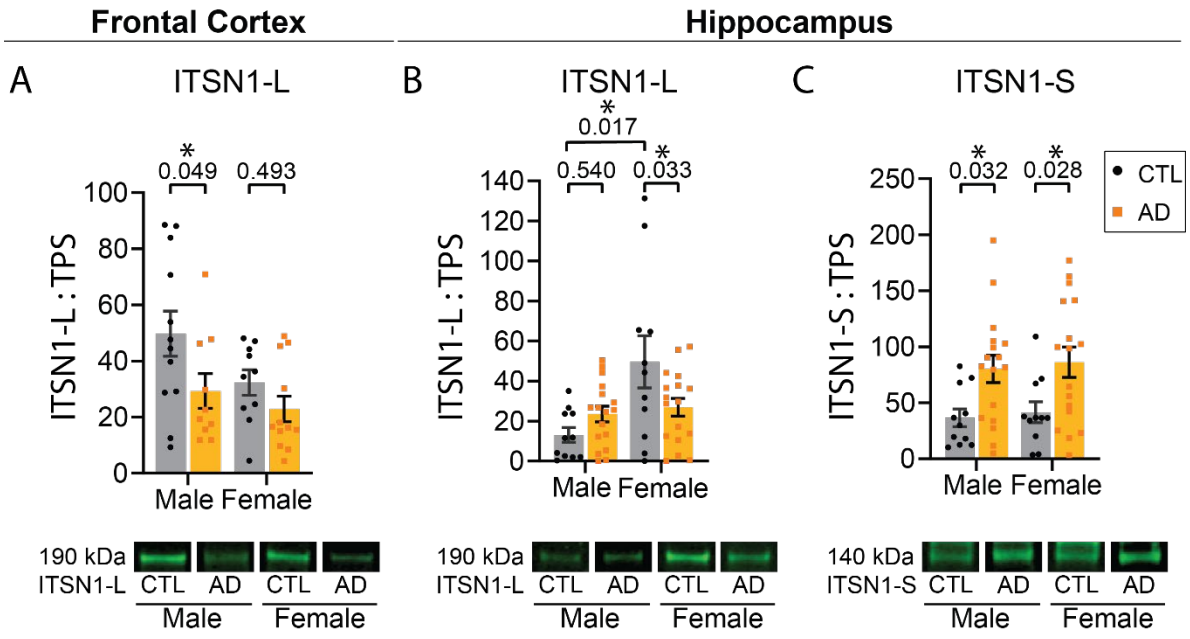

Figure 2.3. ITSN1-L and ITSN1-S are Altered in AD brain. (A) Comparison of ITSN1-L in the frontal cortex (FC) of male and female AD and CTL protein lysates. (B) Comparison of ITSN1-L and (C) ITSN1-S in the hippocampus of male and female AD and CTL protein lysates. For each analysis, all graphs (A, B, C) show protein intensity values normalized to total protein stain (TPS) with representative immunoblot bands underneath. Data are represented as mean ± SEM. Statistical significance was determined by two-way ANOVA, with post-hoc Šídák multiple comparisons tests for analyses with significant group effects. *P<0.05.

Next, to determine if there is an effect of disease on ITSN1 levels in AD and CTL FC and HP, we performed immunoblots with fresh frozen post mortem tissue and evaluated signal intensity normalized with TPS (**Figure 2.3A**). In the FC there was a significant effect of disease on ITSN1-L levels (p = 0.021) (**Figure 2.3A**). Post-hoc multiple comparisons tests showed a significant decrease of ITSN1-L in AD males as compared to CTL males (p = 0.049), but no difference between AD and CTL females (p = 0.493). FC ITSN1-S signal was very faint and quantification attempts resulted in high signal to noise ratios. Thus, ITSN1-S levels were not

evaluated in the FC. In the HP, there was a main effect of sex on ITSN1-L levels ($p = 0.004$) and a significant interaction between disease and sex ($p = 0.017$) (**Figure 2.3B**). Post-hoc tests demonstrated that in AD females there was a significant decrease in ITSN1-L, as compared to CTL females ($p = 0.033$), but no difference between CTL and AD males ($p = 0.540$). We also show that in CTL males ITSN1-L is decreased, as compared to CTL females ($p = 0.028$). Also in the HP, ITSN1-S levels also showed a significant main effect of disease ($p = 0008$), with significant increases in both male ($p=0.032$) and female ($p=0.028$) AD versus CTL (**Figure 2.3C)**. All statistics are shown for the FC in **Table 2.5** and HP in **Table 2.6**.

Table 2.5. Statistics for Frontal Cortex Immunoblot Results. This table shows the 2-way ANOVA results for frontal cortex (FC) immunoblots. Statistically significant results are in bold and trends are italicized.

	2-way ANOVA			Post-Hoc tests	
FC		F(DFn, DFd)	p-value	Šídák's multiple comparisons test	
ITSN1-L	Interaction	F (1, 40) = 0.792	P=0.379	Male CTL-AD	**P=0.049**
	Sex	F (1, 40) = 3.718	*P=0.061*		
	Diagnosis	F (1, 40) = 5.820	**P=0.021**	Female CTL-AD	P=0.493
CLTa	Interaction	F (1, 41) = 2.654	P=0.111	CTL Male-Female	**P=0.024**
	Sex	F (1, 41) = 4.201	**P=0.047**		
	Diagnosis	F (1, 41) = 1.684	P=0.202	AD Male-Female	P=0.947
CLTb	Interaction	F (1, 41) = 0.3835	P=0.539	CTL Male-Female	*P=0.066*
	Sex	F (1, 41) = 6.012	**P=0.019**		
	Diagnosis	F (1, 41) = 2.439	P=0.126	AD Male-Female	P=0.373
PICALM isoforms 1,2	Interaction	F (1, 41) = 0.829	P=0.368	_	_
	Sex	F (1, 41) = 1.185	P=0.283		
	Diagnosis	F (1, 41) = 0.372	P=0.545		
PICALM isoform 4	Interaction	F (1, 39) = 2.589	P=0.116	_	_
	Sex	F (1, 39) = 0.0002	P=0.989		
	Diagnosis	F (1, 39) = 2.232	P=0.143		
AP2A1	Interaction	F (1, 40) = 1.177	P=0.284	_	_
	Sex	F (1, 40) = 0.802	P=0.376		
	Diagnosis	F (1, 40) = 0.802	P=0.376		
FCHO1	Interaction	F (1, 50) = 0.085	P=0.772	_	_
	Sex	F (1, 50) = 0.022	P=0.883		
	Diagnosis	F (1, 50) = 1.487	P=0.229		
DNM2	Interaction	F (1, 52) = 0.08036	P=0.778	_	_
	Sex	F (1, 52) = 1.089	P=0.302		
	Diagnosis	F (1, 52) = 1.239	P=0.271		

Table 2.6. Statistics for Hippocampus Immunoblot Results. This table shows the 2-way ANOVA results for hippocampal immunoblots. Statistically significant results are in bold and trends are italicized.

		2-way ANOVA		Post-Hoc tests	
HP		F(DFn, DFd)	p-value	Šídák multiple comparisons test	
ITSN1-L	Interaction	F (1, 53) = 6.1	**P=0.017**	Male CTL-AD	P=0.540
	Sex	F (1, 53) = 9.0	**P=0.004**	Female CTL-AD	**P=0.033**
	Diagnosis	F (1, 53) = 1.2	P=0.287	CTL Male-Female	**P=0.002**
				AD Male-Female	P=0.897
ITSN1-S	Interaction	F (1, 52) = 0.002	P=0.966	Male CTL-AD	**P=0.020**
	Sex	F (1, 52) = 0.198	P=0.658		
	Diagnosis	F (1, 52) = 12.65	**P=0.0008**	Female CTL-AD	**P=0.028**
CLTa	Interaction	F (1, 52) = 1.826	P=0.183	_	_
	Sex	F (1, 52) = 2.352	P=0.131		
	Diagnosis	F (1, 52) = 0.01390	P=0.907		
CLTb	Interaction	F (1, 52) = 1.516	P=0.224	_	_
	Sex	F (1, 52) = 3.422	*P=0.070*		
	Diagnosis	F (1, 52) = 0.1746	P=0.678		
PICALM isoforms 1,2	Interaction	F (1, 52) = 1.825	P=0.183	_	_
	Sex	F (1, 52) = 1.517	P=0.224		
	Diagnosis	F (1, 52) = 0.1412	P=0.709		
PICALM isoform 4	Interaction	F (1, 52) = 3.981	*P=0.051*	_	_
	Sex	F (1, 52) = 1.496	P=0.227		
	Diagnosis	F (1, 52) = 0.5529	P=0.461		
AP2A1	Interaction	F (1, 51) = 0.6190	P=0.435	_	_
	Sex	F (1, 51) = 1.999	P=0.163		
	Diagnosis	F (1, 51) = 0.1116	P=0.740		
FCHO1	Interaction	F (1, 50) = 0.08526	P=0.772	_	_
	Sex	F (1, 50) = 0.02193	P=0.883		
	Diagnosis	F (1, 50) = 1.487	P=0.229		
DNM2	Interaction	F (1, 41) = 0.06373	P=0.802	_	_
	Sex	F (1, 41) = 0.08897	P=0.767		
	Diagnosis	F (1, 41) = 0.2218	P=0.640		

ITSN1 is Associated with Tau Pathology in Human AD Brain

To determine if ITSN1 is associated with AD pathology, we performed IHC on 20 AD and 20 CTL samples, including males and females, with matching FC and HP sections. There was no appreciable difference between male and female staining patterns so representative images are from male AD and CTL cases. AD cases showed expected Aβ plaques (**Figure 2.4A**) and Tau tangles (**Figure 2.4B**) which are not present in CTL brains (**Figure 2.4C, D**). There is ITSN1 staining that appears in AD cases, but not in CTL (**Figure 2.5**). The staining ranges from subtle cytoplasmic staining (**arrow heads, Figure 2.5A, B**) and tangle-like structures (**Figure 2.5C, D**) in both the HP and FC. In general, most neurons do not show ITSN1 staining in AD, and in all cases ITSN1 is less abundant than Tauopathy in adjacent sections (**Figure 2.4B, D)**.

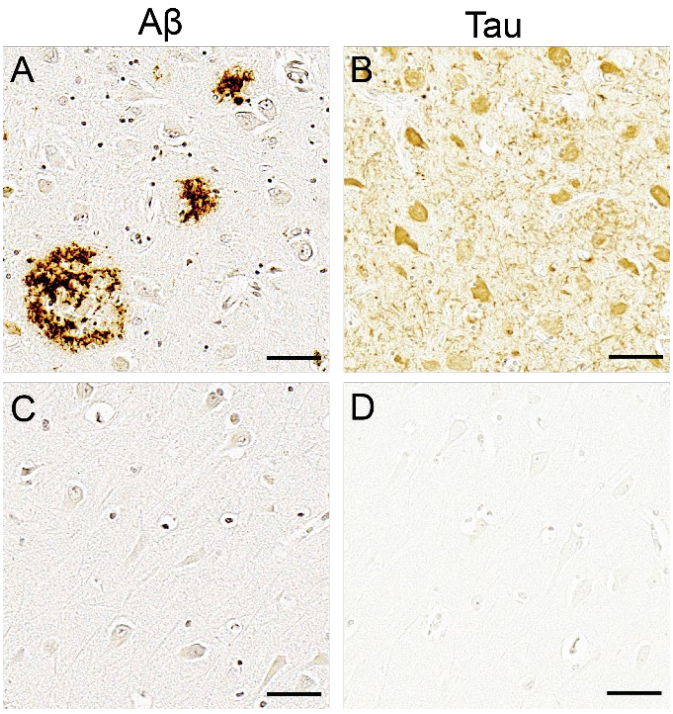

Figure 2.4. Aβ and Tau are Present in AD Hippocampus. Representative brightfield images of Aβ (A, C) and Tau (B, D) immunohistochemistry in the CA1 subregion of AD (A, B) and CTL (C, D) hippocampus. Scale bars = 50 μm.

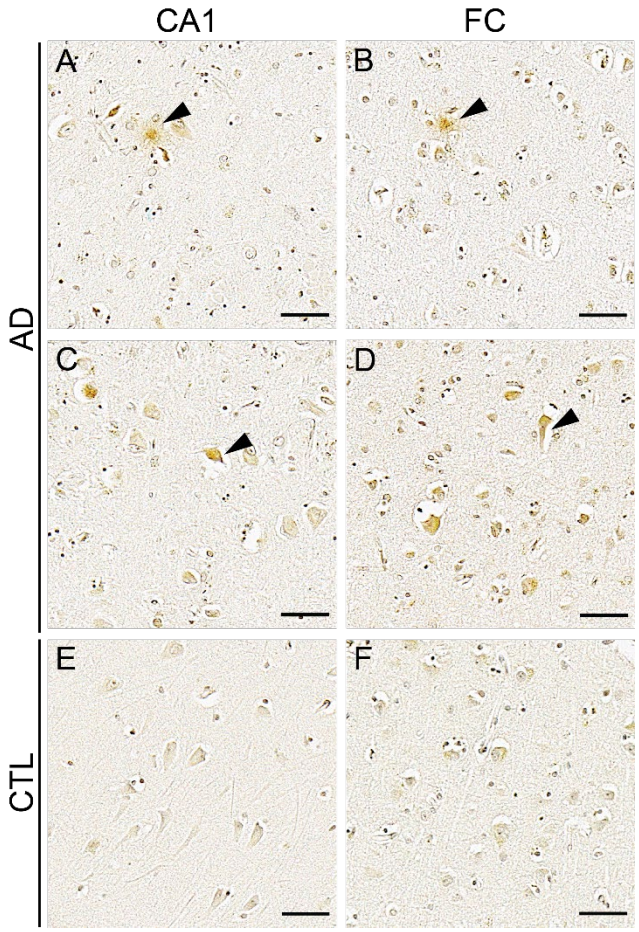

Figure 2.5. ITSN1 is Present in Neurons and Tangle-like Structures in AD Brains.

Representative brightfield images of ITSN1 IHC in AD and CTL hippocampus (CA1 subregion; A, C, E) and frontal cortex (FC; B, D, F). Arrows indicate staining present in AD cases but not in CTL. Scale bars = 50 μm.

Clathrin Light Chain A and B are Not Altered by AD in the Human Brain

Composed of three heavy chains and three light chains, Clathrin is a protein heavily involved in CME and cellular trafficking (*4*). ITSN1 interacts with clathrin heavy chain (CHC) and both paralogs of clathrin light chain (CLC), CLCA and CLCB which result from two separate genes *CLTA* and *CLTB* (*147*). Thus, we evaluated levels of CLCA in AD and CTL FC and HP by immunoblot. In the FC, there was no effect of disease, but a significant sex effect ($p = 0.047$) on CLCA with increased levels in CTL males versus CTL females ($p = 0.024$), but no difference between AD males and females (**Figure 2.6A**). For CLCB there was also a significant sex effect ($p = 0.019$) but no disease or interaction effects. Post-hoc tests did not reveal significant differences between CLCB in CTL male and females but levels did trend down in females ($p = 0.066$) (**Figure 2.6B**). In the HP, there were no significant differences CLCA levels (**Figure 2.6C**) or CLCB (**Figure 2.6D**). All statistics are shown for the FC in **Table 2.5** and HP in **Table 2.6**.

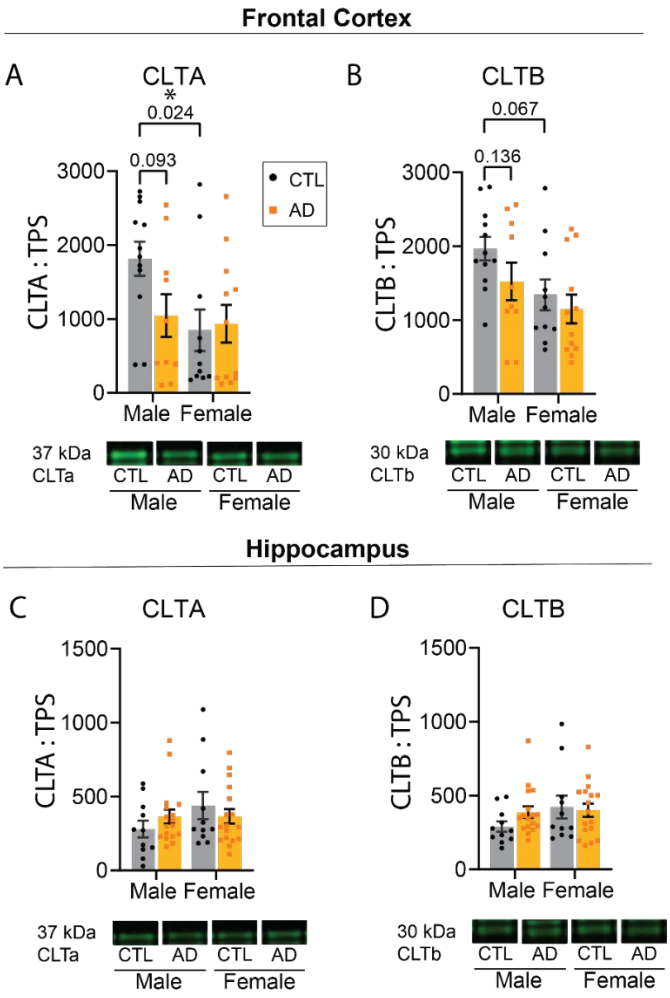

Figure 2.6. Clathrin Light Chain Shows No Change In AD, But a Sex-Difference in CTL Cortex. Comparison of Clathrin Light Chain A (CLTA) and Clathrin Light Chain B (CLTB) between males and females in AD and CTL frontal cortex (FC) and hippocampus (HP). For each analysis, all graphs (A, B, C, D) show protein intensity values normalized to total protein stain (TPS) with representative immunoblot bands underneath. Data are represented as mean ± SEM. Statistical significance was determined by two-way ANOVA, with post-hoc Šídák multiple comparisons tests for analyses with significant group effects. *P<0.05

Other CME Proteins are Not Altered by AD in the Human Brain

We examined other proteins also involved in the CME pathway, which were predicted targets of the AD miRNAs, interactors with ITSN1 (*144*), and/or already known to be related to AD (*41, 126-130, 133*) **(Table 2.2)**. Thus, we examined phosphatidylinositol binding clathrin assembly protein (PICALM), FCH domain only 1 (FCHO1), adaptor-related protein complex 2, alpha 1 subunit (AP2A1), dynamin 2 (DNM2) in the FC and HP by immunoblot. Previously, PICALM was shown to have differences in AD between isoforms (*124, 125, 148*), so we evaluated the effect of AD on both isoforms 1,2 (65-75kDa), and isoform 4 (50 kDa). In our sample cohort, PICALM isoforms 1,2 showed no significant effect of disease, sex, or an interaction in either the FC (**Figure 2.7A**) or HP (**Figure 2.8A**). Likewise, evaluation of PICALM isoform 4 showed no significant effect of disease, sex, or an interaction in the FC (**Figure 2.7B**), but in the HP there was a trending disease by sex interaction ($p = 0.051$, **Figure 2.8B**) with a potential increase in male AD and decrease in female AD compared to same sex CTLs. FCHO1, AP2A1, and DNM2 levels were not significantly affected by disease, sex, or their interaction in the FC (**Figure 2.7C-E**) or HP (**Figure 2.8C-E**). All statistics are shown for the FC in **Table 2.5** and HP in **Table 2.6**.

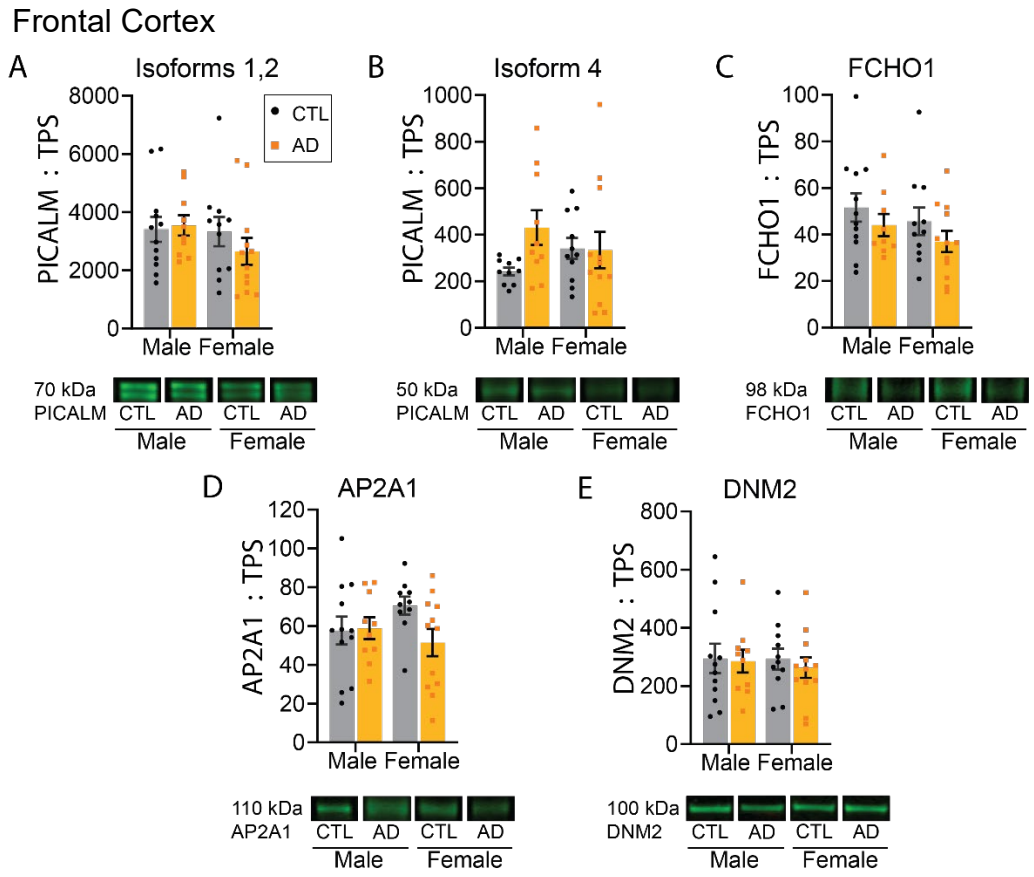

Figure 2.7. Other CME Proteins Are Not Changed in AD Frontal Cortex. Comparison of proteins involved in CME between males and females in AD and CTL frontal cortex (FC). Proteins examined include PICALM isoforms 1,2 (A) and isoform 4 (B), FCHO1 (C), AP2A1 (D), and DNM2 (E). For each analysis, all graphs show protein intensity values normalized to total protein stain (TPS) with representative immunoblot bands underneath. Data are represented as mean ± SEM. Statistical significance was determined by two-way ANOVA, with post-hoc Šídák multiple comparisons tests for analyses with significant group effects. *P<0.05

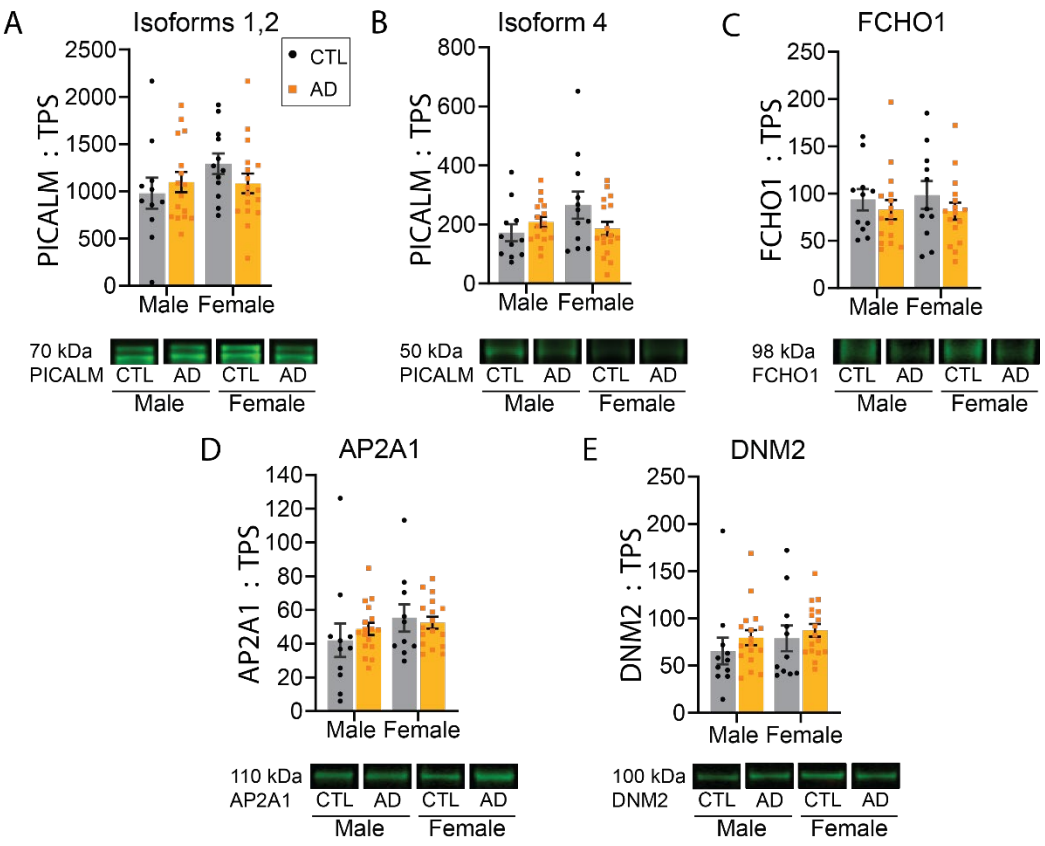

Figure 2.8. Other CME Proteins Are Not Changed in AD Hippocampus. Comparison of proteins involved in CME between males and females in AD and CTL hippocampus. Proteins examined include PICALM isoforms 1,2 (A) and isoform 4 (B), FCHO1 (C), AP2A1 (D), and DNM2 (E). For each analysis, all graphs show protein intensity values normalized to total protein stain (TPS) with representative immunoblot bands underneath. Data are represented as mean ± SEM. Statistical significance was determined by two-way ANOVA, with post-hoc Šídák multiple comparisons tests for analyses with significant group effects. *P<0.05

2.5 Discussion

The goal of this study was to use candidate AD miRNA biomarkers to discover and evaluate potential pathways contributing to AD mechanisms. We found that CME may be regulated by the candidate miRNAs and examined several CME hub proteins based on their existing association with AD, their potential to be regulated by the AD CSF candidate biomarkers, and how essential they are in the pathway. Our study is the first to perform a comprehensive evaluation of major CME hub proteins in the same cohort of samples and multiple brain regions. By immunoblot, protein levels of the scaffolding protein ITSN1 showed isoform and brain region specific differences between AD and CTL brains. However, there were no appreciable differences between AD and CTL in the other CME proteins assessed herein.

CME is a ubiquitous process by which cells internalize material from the cell surface and mediates many cellular functions (*1, 2*). As such, disruption of CME function is associated with many diseases (*4, 8*). In AD, genetic links have been made to *AP-2* and *PICALM* (*7, 9*) and many proteins involved in CME have reported changes at the RNA and protein level (*40-44*) over a wide variety of brain regions. There are many cellular functions known to be disrupted in AD that are downstream of CME or use CME machinery. For example, one of the earliest pathologies specific to sporadic AD is the enlargement of early endosomes in pyramidal cells (*25, 26*). This in turn results in endolysosomal disruption and various neuropathological outcomes such as $A\beta_{1-42}$ over production and clearance deficits as well as dystrophic neurites (*22-24*). Increased size and/or number of endosomes correlates with increased endocytosis (*34*) and suggests that CME changes may contribute to downstream endolysosomal changes in AD. Synapse dysfunction is another well characterized neuronal phenotype in AD (*56*) which correlates with cognitive impairment and leads to severe synaptic loss in early stages of disease (*53, 149*). One facet of synapse dysfunction in AD is the reduction of pre-synaptic vesicle recycling, which normally relies on CME to maintain a readily available pool of vesicles for fast

transmission (*58, 59, 73*). Blocking CME significantly reduces vesicle recycling in pre-synaptic terminals (*1*). Post-synaptic CME may contribute to AMPA receptor trafficking which contributes to cognitive function (*63-66*). This together suggests that alterations of CME could contribute to both pre- and post-synaptic dysfunction in AD.

ITSN1 is a scaffolding protein (*150*) and both the neuronal specific, ITSN1-L, and ubiquitous, ITSN1-S, isoforms are highly involved in CME and can interact with many essential proteins (*151, 152*). ITSN1-L has an additional role in actin-cytoskeletal dynamics due to its additional functional domains (*153, 154*). There is evidence that both overexpression (*155, 156*) and under-expression (*157, 158*) reduce CME, indicating that any alteration in ITSN1 levels is disruptive to CME function. Interestingly, total knock out of ITSN1-L in mice results in learning and memory deficits (*159*) and ITSN1 total knock out results in deficits of neurotransmission (*160, 161*). Thus far, few studies have evaluated ITSN1 in the context of AD. At the RNA level, *ITSN1-S* was the most significantly upregulated gene in AD FC, but *ITSN1-L* showed no expression changes (*126*). Another transcriptomic study found *ITSN1* significantly upregulated in AD temporal cortex with increasing neurofibrillary tangle pathology (*162*) though specific isoform was not specified. The only study to evaluated ITSN1 protein levels in AD brains found no difference in frontal or temporal cortex compared to CTL in either isoform (*127*).

Our study revealed that protein levels of ITSN1-L were decreased in the FC of AD males compared to CTL males but not changed between female CTL and AD brains. Our data may differ from the previous protein study due to differences in male to female ratios of the AD and CTL groups (*127*). The prior study had more female CTL cases than males and more male AD cases than females. In males, the decrease of ITSN1-L we report could be masked because of the comparison of female prominent CTL cases to male prominent AD cases. It is interesting though that *ITSN1-L* RNA was not previously found to be changed in the FC (*126*). This suggests a potential post-translational regulation of *ITSN1-L*, for example, regulation by

miRNAs. As our AD miRNA candidates have ordered changes over disease progression (*116*), and *ITSN* mRNA was found to increase with an increased tangle burden (*162*), it may be interesting to evaluate ITSN1 levels over disease progression. This study was not designed to evaluate whether ITSN1-L expression levels correlate with disease progression so future studies that include MCI groups would be valuable to answer this question.

In the HP, ITSN1-L protein changed differently in females and males. In AD females compared to CTL females, we observed an decrease in ITSN1-L but no changes between male CTL and AD. There was also a significant increase in ITSN1-L in CTL females compared with CTL males, but not between AD males and females. Increased ITSN1-L in CTL females is particularly interesting given that females are more likely to develop AD (*50, 51*) and that in the HP we demonstrate a decrease in ITSN1 in AD females, but no change in males. Additionally, females with MCI and AD show faster hippocampal deterioration and connectivity changes (*163, 164*), and in rodent models females can exhibit less learning and cognition compared to males (*165*). The decrease in ITSN1-L we observe in AD female HP could be connected to their increased vulnerability to neurodegeneration. Future studies should continue to include both sexes to evaluate whether ITSN1-L is specifically related to these sex differences.

In the FC, ITSN1-S was not observable at a high enough level to measure accurately. This suggests a brain region specific function of ITSN1-S and highlights the importance of brain region specific studies. In the HP, we observed a significant increase in ITSN1-S in both male and female AD brains. The directional difference between ITSN1-L and ITSN1-S changes in the HP could be due to the additional functions of ITSN1-L in actin cytoskeletal dynamics (*153, 154*).

To our knowledge, this is the first evaluation of ITSN1 staining pattern in the human brain by IHC. In both AD and CTL HP and FC this revealed complex differences from our immunoblot data. While there was staining present in AD brains that was not in CTL brains, it

ranged from subtle cytoplasmic staining, to intense staining of what appeared as neuronal intracytoplasmic structures. It should be noted that the antibody used detects both isoforms and so we cannot distinguish between ITSN1-L and -S and whether one signature of staining is specific to one isoform. Taking this into consideration, the staining does seem to be neuronal specific which could mean that ITSN1-L and -S are both changing in neurons in different directions and thus we again cannot appreciate whether their individual differences are being masked. Additionally, not all neurons exhibited staining and ITSN1 abundance seemed to be less than Tauopathy. Immunofluorescent co-staining with ITSN1 isoform specific antibodies and Tau would illuminate potential differences. However, due to technical challenges resulting from the use of archival tissue, we were not able to include immunofluorescence in this study.

Of the other CME proteins we evaluated, DNM2 (*131, 132*), AP2A1 (*41*), CLCA (*128*), and PICALM (*124, 125, 148*) have been shown to exhibit various protein, RNA, or localization changes associated with AD. While we observed no changes by immunoblot in any of these proteins, our study differed from many of these in several ways. *DNM2* is a susceptibility gene for AD (*131*) and its mRNA decreases in AD temporal cortex but has otherwise not been studied at the protein level (*132, 166*). Our finding that DNM2 protein levels do not change in AD could be masking a region or cell type specific localization change, though as of yet DNM2 has not been evaluated by IHC in the human brain. AP-2 was previously found to be decreased only in layer II of the superior frontal gyrus by IHC (*41*) while a separate study showed localization with Tau pathology in the temporal cortex and a decreased level by immunoblot in AD amygdala (*130*). CLTA localization is altered in the AD HP depending on which domain the antibody used was targeting (*128*). Our studies of AP2A1 and CLTA did not evaluate staining by IHC and its possible that these proteins have different localization in AD but no difference in gross levels. Additionally, our AP2A1 immunoblots examined the HP not the amygdala, and as we see with ITSN1, and brain region is an important factor to consider. FCHO1 is essential to the initiation of

CME (*4*) but has only tenuously been linked to AD as a potential genetic variant (*129*), thus our study is the first to examine it in the context of AD.

Of particular interest, our analysis of PICALM levels does not recapitulate previous studies, which show PICALM isoform 4 as both increased (*148*) or decreased (*124, 125*) in AD depending on if the soluble or insoluble protein fraction was extracted. As our sample preparation protocol captures both soluble and insoluble protein fractions, we may not capture the difference in PICALM levels seen previously in each fraction. However, the prior studies used primarily male AD brains due to the challenges of sample access. Our inclusion of both males and females allowed us to observe a trending interaction between sex and disease on PICALM isoform 4 levels ($p = 0.051$) in the HP with a potential increase in male AD and decrease in female AD compared to same sex CTLs. This points to a potential difference in how PICALM isoform 4 levels may change differently in AD between males and females.

In summary, we show that ITSN1-L and -S are both changed in AD brains and could be involved in AD pathogenesis. Additionally, ITSN1 staining seems to be associated with Tau pathology in AD brains. The change of only ITSN1 and no other CME proteins could indicate that other functions of ITSN1, such as actin-cytoskeletal dynamics, but not CME are altered in AD. Alternatively, since ITSN1 is an important scaffolding protein in CME and any disruption is detrimental to the proper function of the pathway, it is possible that changes in ITSN1 alone are enough to disrupt CME. Further studies are required to tease apart the nuanced differences in AD brain changes between ITSN1 isoforms, how they may contribute differently to AD pathogenesis, and which of their functions are involved, CME or otherwise.

Chapter 3. ITSN1-L Changes Transiently Over Disease Progression in the 5xFAD Model.

3.1 Abstract

Intersectin 1 (ITSN1) has two isoforms, long (-L) and short (-S) that have similar functions as scaffolding proteins in clathrin mediated endocytosis. ITSN1-L is additionally important for synaptic plasticity and learning and memory, all of which are implicated in Alzheimer's disease (AD). Both ITSN1-L and ITSN1-S change in AD brains at the RNA and protein level in the frontal cortex and hippocampus (HP). It is unknown which specific functions of each ITSN1 isoform are affected by these changes and how they may contribute to AD pathogenesis. We evaluated ITSN1-L levels in cortex (CTX) and HP of the 5xFAD mouse model a different timepoints during disease progression by immunoblot (n = 5-8 per group) and immunohistochemistry (IHC, n = 3 per group) in both males and females. At 3 months, female 5xFAD exhibited an increase of ITSN1-L in CTX and at 6 months male 5xFAD showed a decrease in HP. Immunofluorescent staining at 6 months revealed ITSN1-L loss in the male 5xFAD dentate gyrus (DG) and CA1. Additionally, immunofluorescent staining of 5xFAD primary HP neurons over 28 days in vitro (DIV) showed an increase of ITSN1-L in matured 5xFAD neurons at 21 and 28 DIV. Our data suggest that ITSN1-L changes transiently over disease progression in the 5xFAD model, with levels increasing in CTX during early Aβ accumulation and decreasing in HP during later progression, specifically in areas important for synaptic plasticity.

3.2 Introduction

As Alzheimer's disease (AD) is the most common form of dementia, much research has been put into discovering disease mechanisms and developing disease modifying treatments. The hallmark pathologies of AD, amyloid beta (Aβ) plaques and neurofibrillary Tau protein tangles (*12, 167*), have long been targeted for therapeutic development, but as of yet no treatments have been successful (*168*) . To further our understanding of AD and recapitulate facets of its pathologies and cellular dysfunction, different animal models have been developed which introduce human genes, such as amyloid precursor protein (*APP*) and Presenilin1 (*PSEN1*) that contain mutations found in some AD populations (*23, 31-33*). By utilizing these transgenic animal models, potential disease mechanisms can be studied more extensively *in vivo*. Each mutation introduced causes gene associated AD pathology (*169*) and related disruptions such as APP internalization and pathogenic processing of Aβ, synaptic plasticity dysfunction, neuron loss, and deficits in learning and memory which develop as the mice age (*47, 48, 170, 171*). Importantly, no single mouse model develops pathology and cognitive symptoms that exactly recapitulate AD in humans. When further investigating a change initially observed in humans, it is important to choose a model carefully and first evaluate whether the same change can be found.

We and others (*126, 162*) have previously observed a difference in intersectin-1 (ITSN1) in human AD brains, which showed an isoform and brain region specific change (see **Chapter 2**). ITSN1 has two distinct isoforms resulting from alternative splicing (*172*), ITSN1-long (-L) which is neuronal specific and ITSN1-short (-S) which is ubiquitous (*145*). ITSN1-L and -S both act as essential scaffolding proteins in clathrin mediated endocytosis (CME) which bring together proteins at each step of the pathway (*150*). Both an increase or a decrease in ITSN1 has been shown to reduce CME (*155, 157, 173*) suggesting ITSN1 is tightly regulated. Importantly, APP is internalized via CME and in AD processed into toxic Aβ (*20, 68, 72*).

Inhibition of CME both reduces internalization of APP (*72*) and prevents Aβ induced axon damage (*79*). ITSN1-L has several additional neuronal specific functions (*174, 175*). These include dendritic spine development (*79, 154*), fast neurotransmission (*161, 176*), synaptic plasticity through reelin (*177*) and mitogenic signaling pathways (*159, 178*).

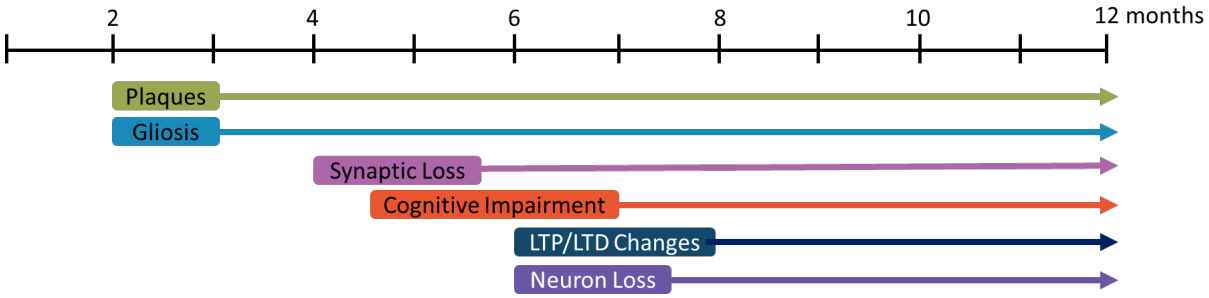

Figure 3.1. 5xFAD Mice Develop Amyloid Pathology and Cognitive Deficits Over Time. Timeline of 5xFAD mouse pathology and behavioral effects over 12 months. Amyloid plaques and gliosis appear at 2 months, synaptic loss and cognitive impairment between 4 and 6 months, then after 6 months changes in synaptic transmission (long-term potentiation (LTP) and long-term depression (LTD)) and neuron loss.

The goal of this study is to evaluate whether ITSN1 is changed the 5xFAD mouse cortex (CTX) and hippocampus (HP) and to determine if this model can be used to further study ITSN1 and CME mechanisms in the context of AD. 5xFAD mice have human *APP* and *PSEN1* transgenes with 5 AD-linked mutations between them (*48*). As they age, they develop Aβ pathology and many cognitive symptoms associated with AD which have been extensively studied (*179-181*). Briefly, as shown in **Figure 1**, Aβ plaques and increased glial activity begins at 2 months, by 6 months there is significant synaptic loss and cognitive impairment and by 8 months neuronal loss impacts processes involved in memory. Here we examined protein levels and cellular distribution of ITSN1-L in 5xFAD and WT littermate controls in the CTX and HP, at

1, 3, and 6 months. We found that ITSN1-L in 5xFAD mice increases early in disease in the CTX and decreases in later disease in the HP. This, and our finding that ITSN1-L increases in 5xFAD primary hippocampal neurons, illustrates the potential for ITSN1-L to be compensatory as Aβ pathology develops in the CTX and in the HP ITSN1-L loss could become detrimental. Further, these differences in ITSN1-L between brain region and disease stage point to the potential of ITSN1-L changes to affect multiple mechanisms in AD.

3.3 Methods

Animals

All animal experiments were approved by the OHSU Institutional Animal Care and Use Committee (TR01_IP00000040) and were conducted in compliance with relevant ethical regulations for animal research. The 5xFAD mice were obtained from JAX (The Jackson Laboratory, #034840-JAX). These mice contain three familial AD mutations in humanized *APP* (K670N/M671L, 1716V, V717I) and two familial AD mutations in humanized *PSEN1 (*M146L, L286V). Male 5xFAD hemizygous were crossed with female B6SJLF1/J (JAX Strain #:100012). Animals were housed in standard conditions of temperature, light, and enrichment, and provided food and water *ad libitum*. After genotyping and weaning at 21 days, mice were social housed with littermates and aged until the correct timepoint reached. Some male mice developed aggression after 4 months of age and were subsequently housed individually.

Genotyping

For genotyping, primers that detect the mutant and wild-type (WT) APP amplicon (Forward: 5'-ACCCCCATGTCAGAGTTCCT-3', mutant reverse: 5'-CGGGCCTCTTCGCTATTAC-3', and WT reverse: 5'-TATACAACCTTGGGGGATGG-3') were used to determine presence of the transgenes. DNA extraction and PCR on tail snips (collected from weanlings or embryos) was performed with the REDExtract-N-Amp Tissue PCR Kit (Sigma Aldrich) and bands resolved on an agarose gel. The PCR thermal cycling protocol used is as follows: initial denaturation (94ºC, 3 minutes, 1 cycle), denaturation (94ºC, 30 seconds), then 10 1 minute cycles starting at 65 ºC and decreasing by 0.5ºC each cycle (65ºC to 61ºC) followed by 28 1 minute cycles at 60ºC.

Tissue Collection

Mice were euthanized at 1, 3, 6, and 8 months via CO_2 inhalation, followed by cervical dislocation. Brains were removed and hemispheres separated along the midline. The left hemisphere was dissected to collect the hippocampus and cortex, which were frozen on dry ice and stored at -80ºC until immunoblot analysis. The right hemisphere was immersed and fixed in 4% paraformaldehyde (PFA) overnight then transferred to 30% sucrose in PBS for two days, all at 4ºC. The right hemisphere was then frozen over dry ice and sectioned coronally at 30 µm using a cryostat (Cryostar NX50, Epredia). Serial sections were collected into 12-well plates containing cryoprotectant (30% sucrose in PBS) and stored at -20ºC for subsequent free-floating tissue staining.

Primary Neuronal Cultures

Primary hippocampal neurons were collected, frozen as in (*182*), and grown in sandwich culture with glia as in (*183*) to enable lower density culture. Briefly, E15 embryos were collected from timed pregnant 5xFAD hemizygous mice and the hippocampus dissected from the brain. To determine the embryo genotypes, PCR with embryo tails was run simultaneously with dissection. After genotypes were confirmed, hippocampi of each genotype were pooled and incubated in 0.25% trypsin at 37ºC for 115 minutes. Cells were then gently homogenized with a flame polished glass pipet into single cell suspension and counted. 500,000 cells were then added to cryovials containing freezing media (80% Fetal bovine serum, 20% DMSO), frozen and stored in liquid nitrogen.

To prepare sandwich culture, 18mm round coverslips were cleaned in 70% nitric acid for 48 hours, sterilized by glass autoclave, and then had wax feet applied. They were then coated with 1mg/mL poly-l-lysine on the same side as the wax feet overnight at room temperature and washed with PBS the next day. One week ahead of neuronal plating, 50,000 mouse neural stem

cells were seeded into Primaria 60 mm cell culture dishes (Corning, 353802) in differentiation media (10% fetal bovine serum, 10% 10X N2 supplement (*183*), 100U/mL penicillin-streptomycin) and new media added every other day, these become glial feeder cells. 24 hours before neuronal plating, glial feeder medium is replaced with neuronal media (B27 Plus Neuronal culture system, Thermo Fisher).

Frozen neurons were thawed gently in a 37ºC water bath for 2 minutes. In a separate 60mm dish from glial feeders, neurons were plated at 150,000 cells/dish on the prepared side of the coverslips in neuronal plating media (0.6% wt/vol D-Glucose, 10 % fetal bovine serum in minimum essential medium). After 3-4 hours, neurons have attached and coverslips were flipped into dishes with glial feeder cells. The neurons grow on the underside of the coverslip held above the glial cells by wax feet, enabling trophic support from the glia. Once established, cultures were fed with neuronal medium once per week and coverslips collected and fixed with 10% neutral buffered formalin for 30 minutes at room temperature at 7, 14, 21, and 28 days *in vitro* (DIV). Coverslips were dehydrated in a gradient of ethanol (50% to 70% to 100%, 1 minute each) and stored in 100% EtOH at -20ºC until stained. For each time-point, n=2-3 separate primary culture preparations were used with three coverslips collected from each culture preparation at each timepoint for a total n=30-50 neurons. Within each time-point all coverslips were stained together for analysis.

ITSN1 Immunoblots

Fresh frozen tissue, collected as described above, was thawed and incubated in RIPA lysis buffer (Thermo Fisher) with Halt protease/phosphatase inhibitor (Thermo Fisher). Tissue was homogenized with a handheld mechanical pestle (Fisher Scientific) for 10 seconds and then digested in the RIPA buffer for 30 minutes, then vortexed once more halfway through the digestion. After protein extraction, samples were centrifuged at 12,000 x g for 20 minutes at

4ºC. Supernatant was collected and aliquoted for BCA analysis (Pierce BCA Protein Assay kit, ThermoFisher Scientific) and immunoblot. Laemmli running buffer was added to samples, which were then boiled, cooled, and stored at -80ºCuntil 10 µg of protein was loaded onto pre-cast Nupage 3-8% Tris-Acetate gels (Invitrogen) and separated by electrophoresis. Protein was then transferred onto polyvinylidene difluoride (PVDF) membranes in transfer buffer containing 10% methanol for better transfer of high molecular weight proteins. Before primary antibody incubation, membranes were dried overnight at 4ºC then activated with methanol and stained with Revert 700 Total Protein Stain Kit Total protein stain (TPS, LI-COR Biosciences), imaged on the Odyssey CLx Imager (LI-COR Biosciences), then destained and blocked with Intercept (TBS) Blocking Buffer (LI-COR Biosciences). After blocking, membranes were incubated with ITSN1 primary antibody (1:2500, Novus Biologicals) for two hours at room temperature in Intercept blocking buffer (LI-COR Biosciences) with 0.2% Tween-20. After washing (4 x 5 min, TBS-T, 0.2% Tween-20). Membranes were then incubated with IRDye 800CW Donkey anti-Rabbit (1:20,000, LI-COR Biosciences) in Intercept blocking buffer with 0.2% Tween-20 and 0.02% SDS for 1 hour at room temperature. Membranes were washed (4 x 5 min, TBS-T) and bands visualized on the Odyssey CLx Imager. The intensity of each signal was determined with Empiria Studio software version 2.2 (LI-COR Biosciences) using the Quantitative western blot function that employs automatic lane detection and background subtraction to reduce variability of between gel analyses. Signals were first normalized within gels to TPS, and as multiple gels were needed to include all samples, bands were normalized to a repeated sample run on every gel to account for between gel variation.

Brain and Primary Neuron Immunofluorescence Staining

Tissue sections were removed from cryoprotectant and washed three times in PBS then blocked with 10% normal goat serum in PBS for two hours at room temperature. Rabbit anti-

ITSN1 (1:500, Novus Biologicals) and rat anti-alpha tubulin (1:500, Thermo Fisher) primary antibodies were applied overnight at 4ºC in 10% normal goat serum. After washing in PBS, Alexa Fluor 488 Goat anti-Rabbit IgG (1:500) and Alexa Fluor 647 Goat anti-Rat IgG (1:1,000, Thermo Fisher) secondary antibodies in 10% normal goal serum were incubated for two hours at room temperature and counterstained with DAPI. Sections were then mounted onto slides and dried before applying coverglass with ProLong Gold antifade mountant (Thermo Fisher).

Fixed primary hippocampal neurons were rehydrated by incubation for 1 minute each in 70% ethanol, 50% ethanol, and then PBS. They were then permeabilized in PBS-T (0.1% Tween-20) for 10 minutes at room temperature then blocked for 30 minutes. Rabbit anti-ITSN1 (1:500, Novus Biological) and chicken anti-MAP2 (1:10,000, Thermo Fisher Scientific) primary antibodies were applied overnight at 4ºC. After washing with PBS, Alexa Fluor 647 Donkey anti-Chicken IgY (1:500, Thermo Fisher) and Alexa Fluor 488 Donkey anti-Rabbit IgG (1:500, Thermo Fisher) secondary antibodies were incubated for 1 hour at room temperature and counterstained with (4′,6-diamidino-2-phenylindole) DAPI. Blocking, primary, and secondary antibody incubation were all in 3% bovine serum albumin. Coverslips were mounted on glass slides with ProLong Gold antifade mountant (Thermo Fisher).

Brain and Primary Neuron Image Acquisition & Analysis

Stained mouse hemispheres, 3 animals from each group (timepoint x sex) and 4 sections per animal, were fluorescently imaged over multiple z planes via Zeiss Axioscan 7 Slidescanner and a Plan-Apochromat 10X/0.45 M27 objective. Images were stitched together and max projections created for comparison of staining across groups. All images within each time-point are displayed with the same settings.

Primary hippocampal neurons were imaged using confocal laser scanning microscopy using an LSM 900 Axio Observer.Z1/7 (Zeiss) inverted microscope equipped with a Plan-

Apochromat 63x/1.40 NA oil immersion objective, 1.00 Airy Units/56 µm pinhole for each channel. 5-10 cells were imaged in three dimensions from each coverslip for total n = 30-50 neurons for each genotype at each timepoint. For analysis, maximum projections of each image were created from 5 z steps around the focus plane with sharpest signal. Signal intensities of maximum projections were collected using the Intellesis automated segmentation package in Zeiss ZEN 3.6. Intellesis segmentation is a machine learning segmentation tool in which a model is trained to segment image objects in complex images such as neurons. We trained the program to segment neurons based on microtubule associated protein 2 (MAP2) signal and collected the signal intensity of the ITSN1 staining within the MAP2 segmentation to analyze.

Statistical Analysis

Data were analyzed with GraphPad Prism software v10.1.0 (GraphPad Software, Inc., San Diego, CA). Immunoblot data are shown as mean ± standard error of the mean (SEM) of ITSN1 protein levels normalized to total protein within each age group for both the cortex and hippocampus of male and female 5xFAD and littermate WT mice. Immunoblots for each timepoint were run together. Biological replicates are displayed as individual symbols on each graph. To assess differences between protein levels in 5xFAD and WT mice while considering sex (male vs. female) we used a two-way ANOVAs (genotype x sex) followed by Šídák multiple comparisons tests when appropriate. Data from primary neurons are shown as mean signal intensity of ITSN1 within the MAP2 segmentation for each genotype at 7, 14, 21, and 28 DIV. Experiments were carried out independently 2-3 times per group and imaged across three coverslips per repetition for a total n=30-45 cells per group. To assess differences in ITSN1 signal intensity between 5xFAD and WT neurons we used unpaired, two-tailed, t-tests at 7, 21 and 28 DIV, and Welch's corrected t-test at 14 DIV. Data were not compared between time-

points for either immunoblot or primary neuron experiments as samples of each time-point were prepared and assayed at different times.

3.4 Results

Decreased ITSN1-L in the Aged 5xFAD Hippocampus

To examine if the changes in ITSN1 we observed in human brains also occurs in an AD mouse model with amyloid pathology, we performed immunoblots on the CTX and HP of 5xFAD and WT littermate controls. As ITSN1 is involved in neurodevelopment (*177*) and AD pathology does not appear until adulthood, we examined ITSN1 levels between 5xFAD and WT at 1-, 3-, 6-, and 8- months in both males and females. (**Figures 3.2 and 3.3**). ITSN1-S was much less abundant than ITSN1-L and did not have high enough signal to noise ratio to measure by immunoblot. In the CTX, there was no effects of genotype on ITSN1-L levels at 1 (**Figure 3.2A**) or 6 months (**Figure 3.2C**). However, at 3 months, we found a significant effect of genotype on ITSN1-L ($p = 0.0095$) (**Figure 3.2B**). Subsequent post-hoc tests revealed a significant increase of ITSN1-L in 5xFAD females compared to CTL females. At 8 months, tentatively, there is a trend towards decreased ITSN1-L in both male and female 5xFAD mice, compared to WT (**Figure 3.2D**). Note that 8 month protein lysates were derived from mice raised in a separate facility (generous donation from Dr. Nora Gray) from the 1-, 3-, and 6- month time-point mice. Thus, these data are preliminary and were not statistically analyzed. Mice raised in the same conditions as earlier time-points are currently aging and will be used for statistical comparison to include in this data set. In the HP, there was no significant effect of genotype at 1 and 3 months (**Figure 3.3A, B)**. However, at 6 months we observed a significant main effect of genotype ($p = 0.0002$) and a significant interaction between genotype and sex ($p = 0.038$) (**Figure 3.3C**). Post-hoc tests revealed a significant decrease of ITSN1 levels in 5xFAD males as compared to WT males ($p = 0.0002$). Interestingly, there was also a trending decrease in female WT mice compared to male WTs ($p = 0.061$) indicating a baseline difference between sexes. At 8 months we observed a trend towards decreased ITSN1-L in both male and female 5xFAD, compared to WT (**Figure 3.3D**). Full statistical results for ITSN1 in the CTX and HP are reported in **Table 1**.

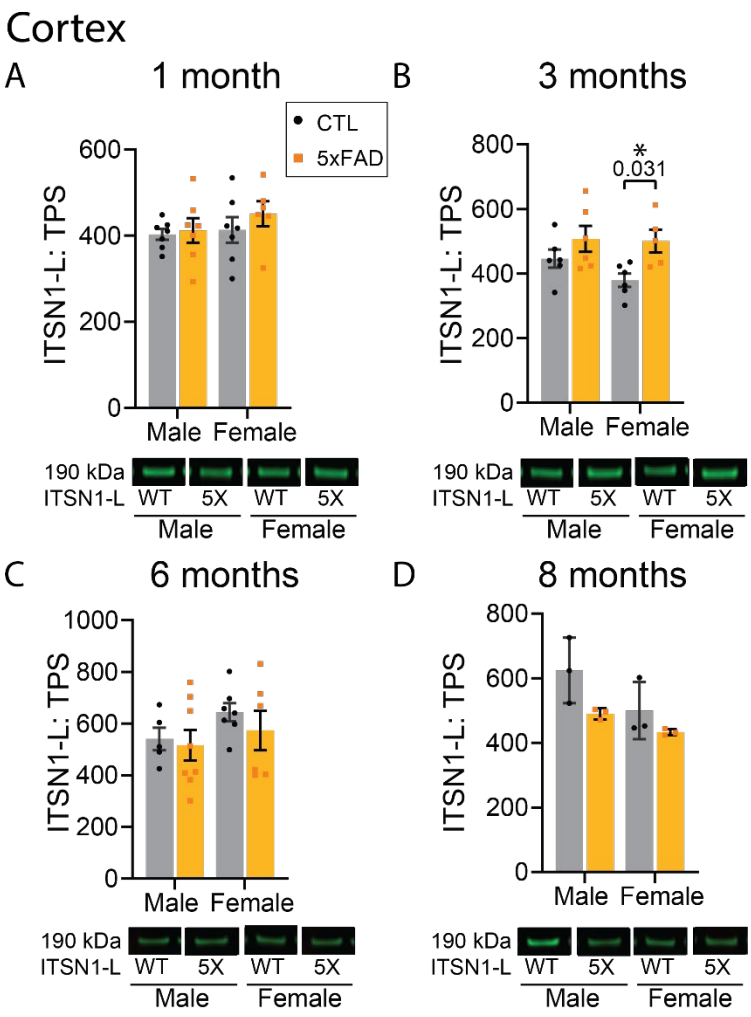

Figure 3.2. ITSN1 Expression Is Increased in Female 5xFAD Cortex At 3 Months of Age. Immunoblot comparison of ITSN1-L between males and females in 5xFAD and WT littermate controls in the cortex at 1, 3, 6, and 8 months of age. For each analysis, all graphs (A, B, C, D) show protein intensity values at 1, 3, 6, and 8 months normalized to total protein stain (TPS) with representative immunoblot bands underneath. Data are represented as mean ± SEM. Statistical significance was determined by two-way ANOVAs followed by Šídák multiple comparisons post-hoc tests for analyses with a significant main effect. *P<0.05

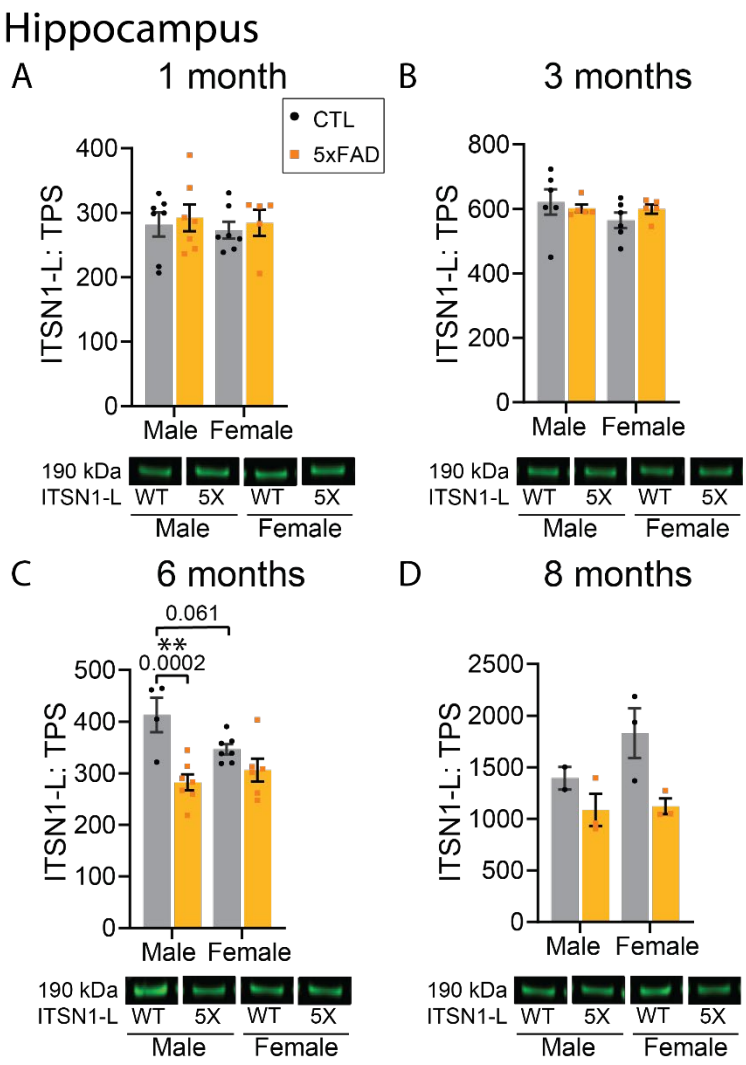

Figure 3.3. ITSN1-L Is Decreased in Male 5xFAD Hippocampus At 6 Months of Age.

Immunoblot comparison of ITSN1-L between males and females in 5xFAD and WT littermate controls in the hippocampus at 1, 3, 6, and 8 months of age. For each analysis, all graphs (A, B, C, D) show protein intensity values at 1, 3, 6, and 8 months normalized to total protein stain (TPS) with representative immunoblot bands underneath. Data are represented as mean ± SEM. Statistical significance was determined by two-way ANOVAs followed by Šídák multiple comparisons post-hoc tests for analyses with a significant main effect. **P<0.01

Table 3.1. Statistics for Cortical and Hippocampal ITSN1 Immunoblot Results. This table shows the 2-way ANOVA results for hippocampal and cortex immunoblots of ITSN1-L in 5xFAD and WT mice over time. Statistically significant results are in bold and trends italicized.

		2-way ANOVA		Post-Hoc tests	
Cortex		F (DFn, DFd)	P value	Šídák multiple comparisons test	
1 month	Interaction	F (1, 23) = 0.299	P=0.590	–	–
	Sex	F (1, 23) = 0.910	P=0.350		
	Genotype	F (1, 23) = 0.846	P=0.367		
3 months	Interaction	F (1, 19) = 0.909	P=0.353	Male WT-5X	P=0.324
	Sex	F (1, 19) = 1.341	P=0.261		
	Genotype	F (1, 19) = 8.320	**P=0.0095**	Female WT-5X	**P=0.031**
6 months	Interaction	F (1, 22) = 0.157	P=0.696	–	–
	Sex	F (1, 22) = 1.916	P=0.180		
	Genotype	F (1, 22) = 0.660	P=0.425		
Hippocampus		F(DFn, DFd)	p-value		
1 month	Interaction	F (1, 22) = 0.0006	P=0.981	–	–
	Sex	F (1, 22) = 0.205	P=0.655		
	Genotype	F (1, 22) = 0.355	P=0.558		
3 months	Interaction	F (1, 18) = 1.053	P=0.318	–	–
	Sex	F (1, 18) = 1.217	P=0.285		
	Genotype	F (1, 18) = 0.080	P=0.781		
6 months	Interaction	F (1, 22) = 4.901	**P=0.038**	Male WT-5X	**P=0.0002**
	Sex	F (1, 22) = 1.368	P=0.255	Female WT-5X	P=0.222
	Genotype	F (1, 22) = 20.13	**P=0.0002**	WT Male-Female	*P=0.061*
				5X Male-Female	P=0.697

Age-Related Changes in ITSN1 Staining Patterns

To evaluate whether ITSN1 localization changes between 5xFAD and WT mice at each timepoint, we performed immunofluorescence to detect ITSN1 and α-Tubulin, a neuronal marker which marks the axon and cell body (*184, 185*). There were no gross differences in ITSN1 observed between males and females of each group so representative images in **Figure 3.4-6** are from only males at each time-point. White boxes in **Figure 3.4-6A** indicate the area of hippocampal (CA1 and DG) and cortical regions shown in **Figures 3.4-6 B, C,** and **D**. Comparisons between intensity values of images at different time-points was not valid as tissues were processed at different times. Thus, overall signal intensity was not compared between time-points. There were no differences in ITSN1 patterning between 5xFAD and WT at 1 month (**Figure 3.4B**). Generally, ITSN1 showed staining across the tissue with some bright puncta in HP CA1 and dentate gyrus (DG) subregions, but this was not always concentrated around the α-Tubulin neurons. Areas which include ITSN1 staining unique to α-Tubulin were the corpus callosum and a band in the medial entorhinal cortex. In the cortex, ITSN1 was sometimes seen to be more concentrated in the soma of neurons where the nucleus is located (**Figure 3.4B**, WT, white arrows,). However, some cells that were α-Tubulin negative also contain concentrated ITSN1 near the nucleus (**Figure 3.4B**, 5xFAD, white arrows,). Similarly, at 3 months no gross differences in ITSN1 can be seen between 5xFAD and WT mice. White arrows indicate bright puncta, also seen at 1 month, in both 5xFAD and WT brains (**Figure 3.5C**). At 6 months, where immunoblot of whole hippocampal tissue showed a decrease of ITSN1 in 5xFAD mice (**Figure 3.3**), a similar trend was seen in the DG and CA3 (**Figure 3.6B, D**). As expected, the 6 month mice showed amyloid plaques throughout the cortex and a few in the HP. They appeared as holes in the tissue devoid of staining, were relatively uniform in shape, and were primarily in the deeper cortical layers (**Figure 3.4B** circles,). Interestingly, ITSN1 infiltrates into the area of plaques which have no α-Tubulin (white circles, **Figure 3.4B**).

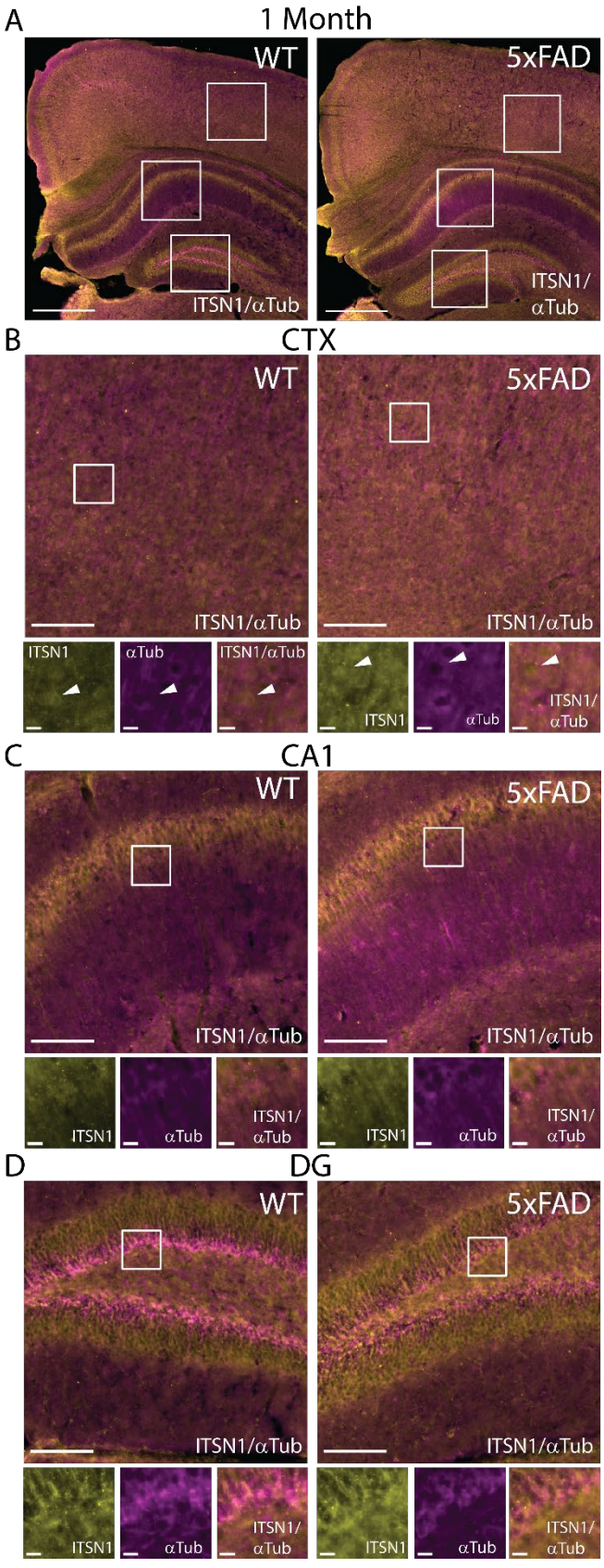

Figure 3.4. ITSN1 Is in Neuronal and Non-Neuronal Cells At 1 Month. (A) Representative wide field images of male 5xFAD and WT brains stained for ITSN1 (yellow) and α-Tubulin (violet) and 1 month of age. White boxes in A indicate areas magnified in B, C, and D in the cortex (CTX, top box), hippocampal CA1 (middle box), and dentate gyrus (DG, bottom box). Each region is shown with inlay at a higher magnification underneath. Arrows indicate cells with both ITSN1 and α-Tubulin (WT) and only ITSN1 (5xFAD) Scale bars are 500 μm in A, 100μm and 10 μm in B, C, and D.

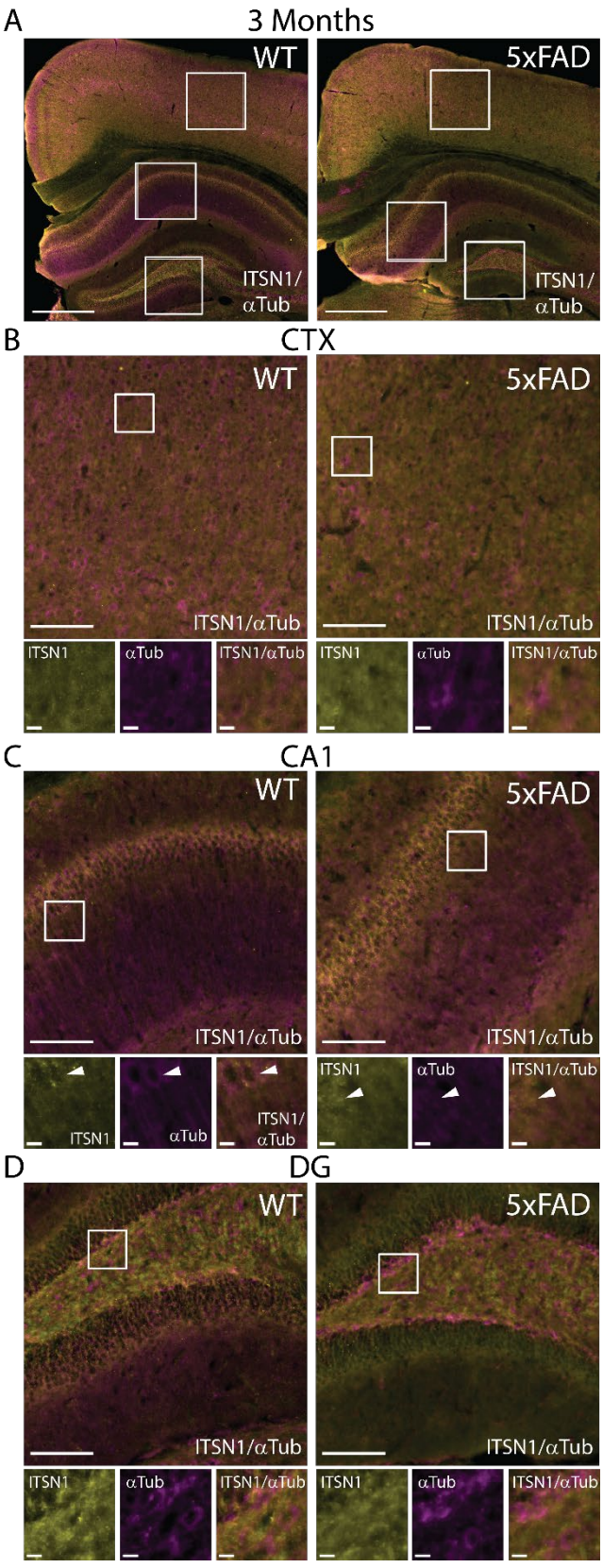

Figure 3.5. 5xFAD ITSN1 Staining Does Not Differ from WT at 3 Months. (A) Representative wide field images of male 5xFAD and WT brains stained for ITSN1 (yellow) and α-Tubulin (violet) and 3 months of age. White boxes in A indicate areas magnified in B, C, and D in the cortex (CTX, top box), hippocampal CA1 (middle box), and dentate gyrus (DG, bottom box). Each region is shown with inlay at a higher magnification underneath. White arrows indicate areas with bright puncta of ITSN1 in both WT and 5xFAD. Scale bars are 500 μm in A, 100μm and 10 μm in B, C, and D.

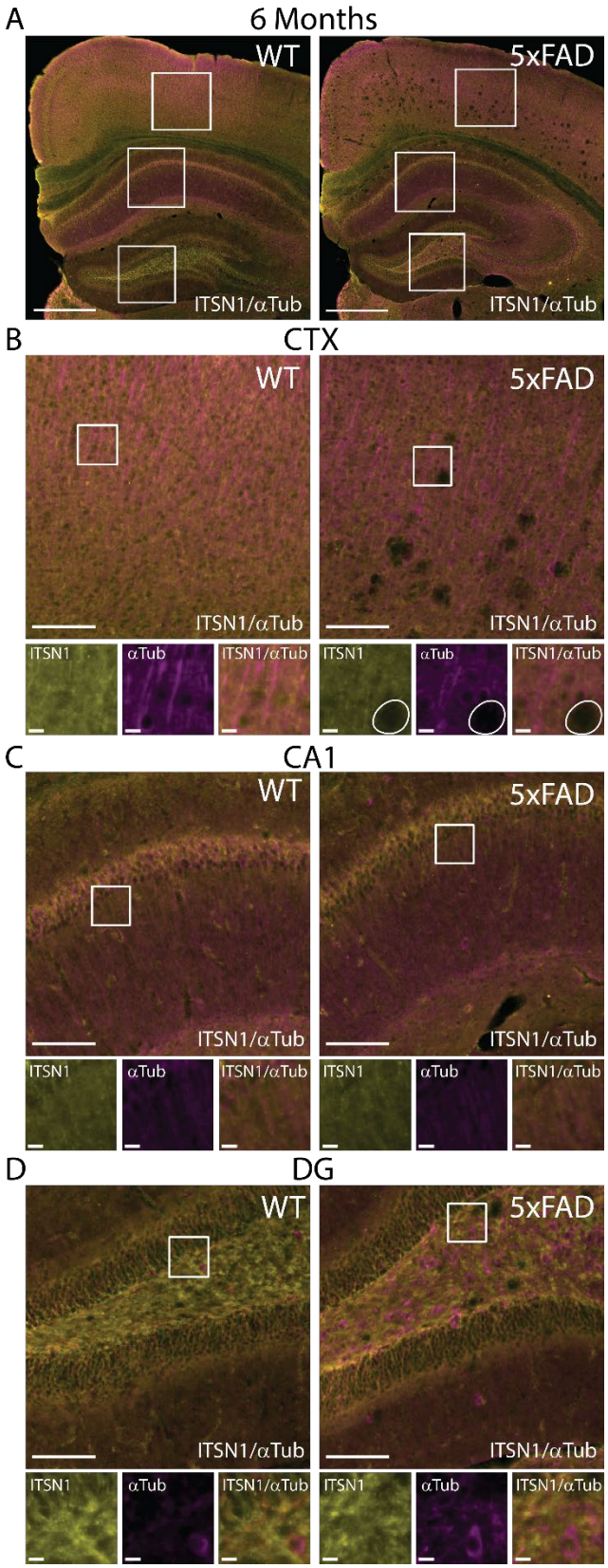

Figure 3.6. ITSN1 is Decreased in 5xFAD DG and CA3 at 6 months. (A) Representative wide field images of male 5xFAD and WT brains stained for ITSN1 (yellow) and α-Tubulin (violet) and 6 months of age. White boxes in A indicate areas magnified in B, C, and D in the cortex (CTX, top box), hippocampal CA1 (middle box), and dentate gyrus (DG, bottom box). Each region is shown with inlay at a higher magnification underneath. White circles indicate borders of an Aβ plaque as defined by lack of α-Tubulin signal (B, right inset). Scale bars are 500 μm in A, 100μm and 10 μm in B, C, and D.

Increased ITSN1 in 5xFAD Aged Hippocampal Neurons

To further evaluate the impact of ageing on ITSN1 in 5xFAD neurons we grew primary hippocampal neurons in sandwich culture with glia. We performed immunofluorescence of 5xFAD and WT neurons at 7, 14, 21, and 28 DIV and imaged individual cells at each time-point. Analysis of staining in neurons has historically been challenging as traditional segmentation methods cannot automatically detect the intricate processes of a neuron. To mitigate this, we used Zeiss Zen Intellesis trainable segmentation. The segmentation algorithm was trained on a subset of images across time-points to identify the neuron and processes by evaluating MAP2, which was then applied it to all images to create an object that encompasses the neuronal cell body as well as dendrites. Mean ITSN1 signal was measured within the MAP2 segmentation and compared between 5xFAD and WT neurons. At 7 and 14 DIV, there were no significant differences in ITSN1 (**Figure 3.7A**, **B**). At 21 DIV, we observed a significant increase of ITSN1 in 5xFAD cells ($p = 0.023$) and again at 28 DIV ($p = 0.025$) (**Figure 3.7C, D**). Interestingly once neurons reached maturity at 21 DIV, ITSN1 localized to the axon initial segment in both 5xFAD and WT neurons (white arrows, **Figure 3.7D**).

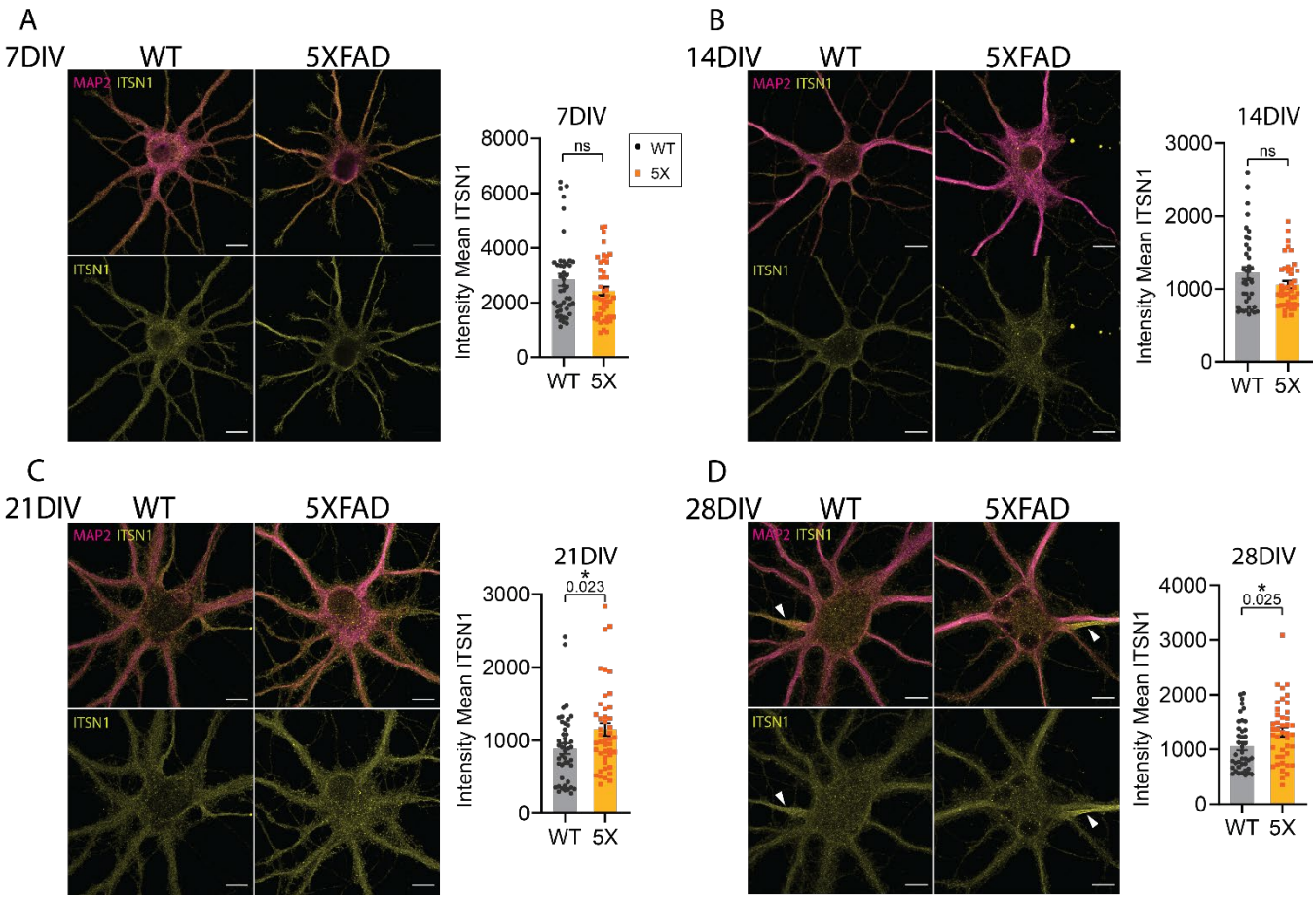

Figure 3.7. ITSN1 is Increased in Aged Cultured 5xFAD Hippocampal Neurons. Confocal microscopy images of 5xFAD and WT primary hippocampal neurons at 7 (A), 14 (B), 21 (C) and 28 (D) days in vitro (DIV). Both WT and 5X neurons were stained with ITSN1-L (yellow) and microtubule associated protein 2 (MAP2, violet). Neurons were individually segmented by MAP2 using Zeiss Zen Intellesis trainable artificial intelligence segmentation. For each set of images, graphs show the intensity mean values of ITSN1 in the MAP2 segmented area with each data point corresponding to one neuron. Experiments were carried out independently 2-3 times per group and imaged across three coverslips per repetition for a total n=30-45 cells per group. *P<0.05, all scale bars 10 μm.

3.5 Discussion

The goal of this study was to evaluate ITSN1, which we and others (*126, 162*) have found altered in human postmortem AD brains, in an AD mouse model. A mouse model that recapitulates human ITSN1 expression levels could be used to mechanistically examine CME and other ITSN1 functions in the context of AD. By immunoblot we found that in the 5xFAD mice, ITSN1-L in the CTX is increased in females at 3 months, but in the HP decreased in males at 6 months. Additionally, we gained further resolution of this loss in males at 6 months with immunofluorescence staining of ITSN1 which showed decreased levels in DG and CA3. 5xFAD primary neurons showed a similar age-related phenotype with ITSN1-L increased compared to WT upon neuron maturation to 21 and 28 DIV.

CME has been implicated in AD through both human and mouse model studies that evaluated RNA and protein levels of essential proteins in the pathway (*40-44*). For example, mice with a mutation in *APP* (*45*) that exhibit an AD-like Aβ pathology, show a decrease in essential CME proteins dynamin I and adaptor protein-180 in the HP (*44*) but in cortex other CME proteins APP, clathrin, and dynamin II (*46*) are increased. This suggests CME could be changed differently between brain regions, a similar trend to our observations in humans (see **Chapter 2**) and here where we observe an increase of ITSN1 in the CTX but a decrease in the HP of 5xFAD mice.

ITSN1 has two distinct isoforms resulting from alternative splicing (*172*), ITSN1-long (-L) which is neuronal specific and ITSN1-short (-S) which is ubiquitous (*145*). ITSN1-L and -S both act as essential scaffolding proteins in CME which bring together proteins at each step of the pathway (*150*). In this role ITSN1 interacts with many essential CME proteins such as adaptor-protein 2, clathrin, dynamin, and AD risk factor *PICALM* (*59, 146, 151, 160*). Both an increase or a decrease in ITSN1 has been shown to reduce CME (*155, 157, 173*) suggesting that ITSN1 is tightly regulated. Importantly, APP is internalized via CME and in AD is processed into toxic Aβ

(*20, 68, 72*). Inhibition of CME both reduces internalization of APP (*72*) and prevents Aβ induced axon damage (*79*). A change in ITSN1 which affects CME function may therefore affect the internalization of APP and production of toxic Aβ.

To begin to elucidate what pathological mechanism(s) (e.g., Aβ vs. Tau) impact ITSN1 changes in AD, we evaluated ITSN1 levels in the 5xFAD mouse model over the lifespan. We found that ITSN1-S was not abundant enough to measure by immunoblot, but did observe changes in ITSN1-L at different time-points. Interestingly, the changes observed in 5xFAD mice in each brain region are in opposite directions and at different time-points. In the CTX, we saw an increase of ITSN1-L in 3 month female 5xFAD mice. This is interesting as female 5xFAD mice exhibit more plaques earlier than males (3) which could suggest that an increase in ITSN1-L is associated with the increase of Aβ burden in early stages of pathology development in female 5xFAD mice. However, at later timepoints (6, 8 months) this increase in ITSN1-L is not sustained and may even transition to a decrease in ITSN1-L by 8 months. This could suggest a transient mechanism by which ITSN1-L is compensatory early in disease to combat the effects of increased Aβ burden by decreasing CME. It's unclear what specific mechanisms may be involved as early plaques begin to accumulate because most studies characterizing 5xFAD models typically begin observations at 4 months, after significant pathology has developed (*179-181, 186*). Those at earlier time-points have exhibited gene expression changes between 5xFAD and WT mice at 2 months (*48*) and as early as postnatal day 1 (*187*). Interestingly CME has changed expression patterns in 5xFAD at this early postnatal time (*187*). How an increase in ITSN1 could be contributing to a difference in CME in a compensatory manner and whether this function changes over disease progression is yet to be revealed.

In pursuit of a model to examine ITSN1 changes mechanistically, we compared ITSN1 levels via immunofluorescence in 5xFAD and WT primary hippocampal neurons. We found that ITSN1 was significantly increased in 5xFAD neurons at 21 and 28 DIV. As previously shown in

WT primary hippocampal neurons, CME and production of APP is increased in 28 DIV 'aged' neurons compared to younger neurons (*72*). The same study also showed that inhibition of CME limits Aβ production which reverts *in vitro* age-related synaptic loss (*72*). Thus, the increase we saw in ITSN1 at 21 and 28 DIV 5xFAD primary hippocampal neurons, which correspond to increased CME and APP production, could also function as a compensatory mechanism to reduce CME and Aβ and prevent subsequent synaptic loss. This further supports the above hypothesis that the early ITSN1-L increase in 5xFAD females is a protective response to Aβ.

In the HP, the decrease of ITSN1-L in 5xFAD males, but not females, corresponds with the expected age when synaptic and neuron loss occur in the 5xFAD model, 4 months and onward (*48, 170*). This suggests that ITSN1-L changes in the HP, which we specifically observe in the DG and CA3, could be related to mechanisms causing neuron loss through synaptic plasticity dysfunction. Recently, ITSN1 has been discovered as an important component of synaptic plasticity. ITSN1-L knockout mice exhibit behavioral deficits in learning and long-term spatial memory (*159*), loss of long-term potentiation (LTP) through the reelin pathway (*188*), and loss of LTP via mitogen-activated protein kinase (MAPK) pathway (*159*). LTP and long-term depression (LTD) are key forms of synaptic plasticity changes which affect cognitive function and memory formation and are known to be affected in AD (*189-192*). The DG and CA3, where we see ITSN1 changes, are both regions important in how synaptic LTP and LTD affect learning and memory (*193, 194*).

Immunofluorescence staining of ITSN1 in brain sections revealed interesting age and genotype related staining patterns. While we cannot compare the signal intensity between time-points, as samples in each time-point were prepared and assayed separately, there are some noticeable expression pattern changes as the mice age. In general, the ITSN1 staining does not appear to be solely neuronal. This could indicate that ITSN1 has different functions, or is more

prominent in different cell types, during different times in the lifespan. Between 5xFAD and WT mice, there were no dramatic differences in localization, but notably in 6-month 5xFAD mice where plaques appeared ITSN1 overlapped the empty space where α-Tubulin staining had been lost. It is likely that this staining is ITSN1-S in microglia or astrocytes which can be found in close proximity to plaques (*195*). Further evaluation of ITSN1 in more specific brain regions with markers of neuronal subtypes and non-neuronal cells would help to get a better idea of cell types involved in the ITSN1 changes we observed.

Limitations of this study include the inability to compare ITSN1 immunoblots, IHC, or primary neuron levels between time-points due to processing samples in time-point batches. As there seems to be an association with disease progression and ITSN1 has developmental importance, how levels compare over the lifetime in each brain region may help point to which specific function of ITSN1 may be altered in 5xFAD mice and when. Additionally, the 5xFAD model does not develop Tauopathy. According to our human data (see **Chapter 2**), ITSN1 is potentially associated with Tau, but evaluating Tau associations in 5xFAD is not possible.

In summary, we show that ITSN1-L is changed in the CTX and HP at different time-points in the 5xFAD mouse model. An increase in ITSN1 earlier in disease progression, as Aβ begins accumulating, which we saw at 3 months in 5xFAD females and in 21 and 28 DIV 5xFAD primary hippocampal neurons, could point to a potential early compensatory mechanism in which CME is reduced to decrease pathogenic Aβ production. Additionally, the loss of ITSN1 in the DG and CA3 of 6 month 5xFAD males, could indicate loss of ITSN1 functions in synaptic plasticity that contribute to later cognitive decline. Interestingly, we see a similar decrease of ITSN1-L in the HP of human female AD brains (See **Chapter 2**) so further characterization of these ITSN1-L changes in the 5xFAD HP may be relevant to human disease mechanism. These data suggest that ITSN1-L function may be associated with pathology progression in the 5xFAD

model and further supports the potential for ITSN1 to have different functions in specific brain regions.

Chapter 4. Additional Experiments and Data

This chapter includes studies and methods I performed over the course of my research which did not result in complete data for technical reasons or did not fit into the scope of my overall work. Methods are categorized by the research question I aimed to answer with each technique.

4.1 Does MiR-193a-5p Regulate ITSN1-S mRNA And Affect Protein Levels?

Our initial target prediction results identified that the candidate AD miRNA biomarker miR-193a-5p could bind Intersectin1-short (ITSN1-S). To test the hypothesis that miR-193a-5p binds to and regulates ITSN1-S mRNA, and decreases ITSN1 protein levels, we performed *in vitro* assays in HT-1080 and HEK293T cells. In HT-1080 cells, we performed luciferase assays which examine whether miR-193a-5p can bind to ITSN1-S mRNA to repress luciferase expression. In HEK293T cells, we used qPCR and immunoblots to evaluate if mRNA or protein levels of ITSN1-S decreased following transfection with miR-193a-5p mimic. The luciferase assay in HT-1080 cells revealed no regulation of ITSN1-S by miR-193a-5p as measured by relative luminescence. If ITSN1-s mRNA is regulated by miR-193a-5p, we expect to see the transfection of a miR-193a-5p mimic to reduce the relative luminescence of the ITSN1 3' UTR as we see with the miR-193a-5p positive control 3' UTR. Instead we say no significant change in luminescence between any of the conditions. This outcome indicated that miR-193a-5p does not bind to the 3'UTR of ITSN, where expected miRNA translational repression occurs, or was not able on its own to reduce ITSN1 expression (**Figure 4.1**). In parallel we transfected HEK293T cells, which express endogenous ITSN1-S mRNA and protein, with miR-193a-5p mimic (**Figure 4.2A**). As higher amounts of miR-193a-5p were added, ITSN1 mRNA levels decreased, but unexpectedly, protein levels increased, which is inverse to the expected outcome of decreased protein. Additionally, a miR-193a-5p inhibitor did not reverse this effect in

either mRNA or protein (**Figure 4.2B**). These data suggest that ITSN1-S levels may be affected by miR-193a-5p but through a more complicated mechanism than direct miRNA-mRNA binding.

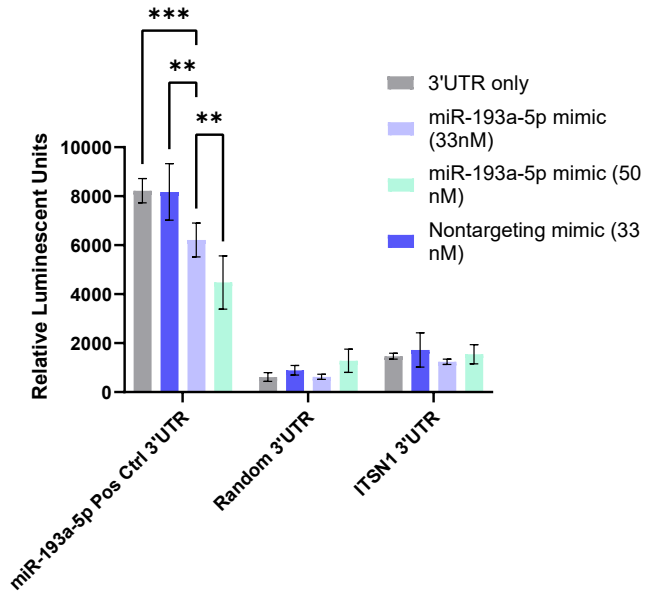

Figure 4.1. Luciferase Assay Shows No Regulation of ITSN1-S by MiR-193a-5p. Relative luminescent units of HT-1080 cells transfected with a miR-193a-5p mimic and plasmids containing a positive control 3' UTR, a random 3' UTR, or the ITSN1-S 3' UTR downstream of a luciferase open reading frame.

A

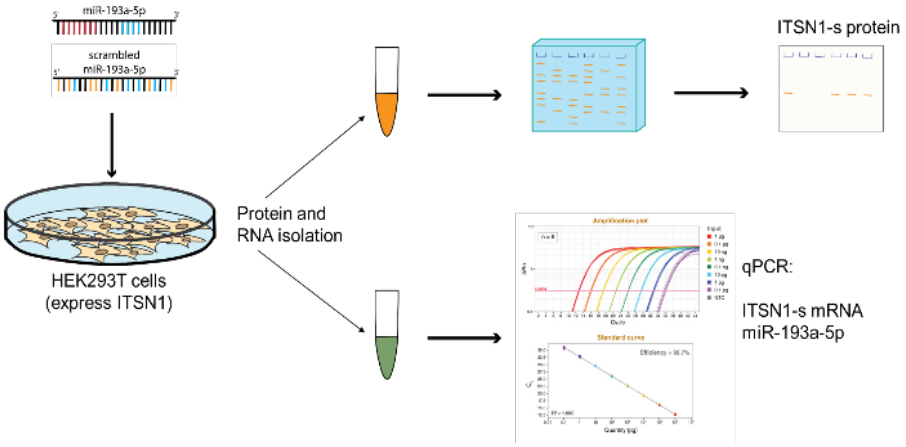

B

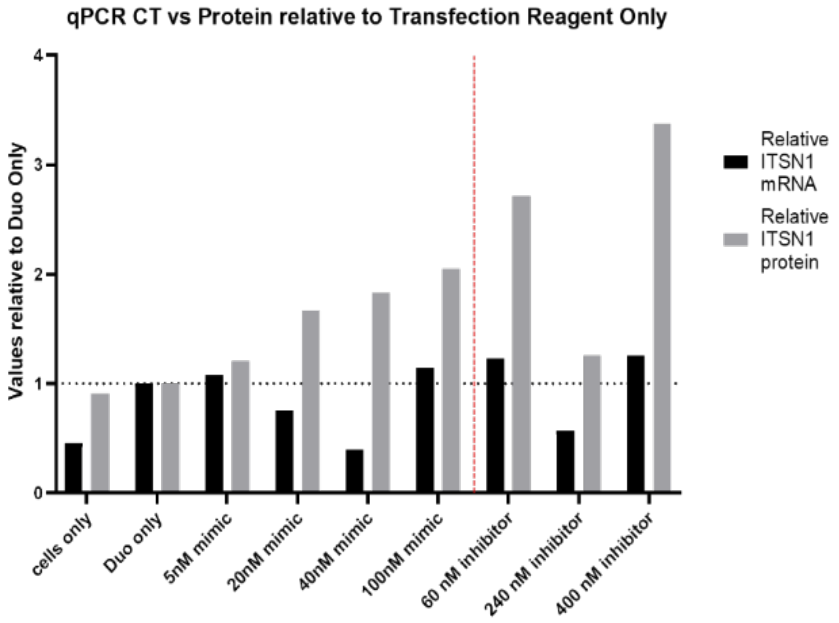

Figure 4.2. MiR-193a-5p Effects on Endogenous ITSN1 mRNA and Protein in HEK293T Cells. (A) Experimental workflow to evaluate RNA and protein from the same sample after transfection with miR-193a-5p mimic or inhibitor. (B) Levels of ITSN1 RNA and protein relative to a transfection reagent only condition (Duo).

4.2 What Cell Type(s) Show ITSN1 Change in AD Brains?

Following my immunoblot results that ITSN1 is changed in an isoform specific manner in AD brains, we wanted to visualize how this change may be happening in different cell types. Unfortunately, ITSN1-S cannot be distinguished from ITSN1-L by antibody due to their identical structure before the additional distinct domains in ITSN1-L. To visualize ITSN1-S only, we used RNAscope to label the distinct ITSN1-S mRNA 3' UTR in archival formalin fixed paraffin embedded (FFPE) brain tissue. To examine potential cell types in which ITSN1 expressed we used fluorescent immunohistochemistry in fresh frozen archival brain tissue. We first validated the RNAscope assay and probes in HE293T cells (**Figure 4.3A**) and wild-type (WT) mouse cortex (**Figure 4.3B**). *ITSN1-S* Signal was clearly visible in both cells and mouse tissue but very sparse compared to positive control Peptidylprolyl Isomerase B (PPIB) in mouse brain. However, in human FFPE hippocampus, RNAscope signal of both *PPIB* and *ITSN1-S* could not be seen above background levels in the bacterial DAPB negative control (**Figure 4.3C**). When adjusting assay parameters did not improve signal, we isolated RNA from FFPE tissue of one AD and one CTL hippocampus and analyzed RNA at the OHSU Gene Profiling Shared Resource. Bioanalyzer results showed the RNA isolated from FFPE tissue was highly degraded as determined by low RNA integrity (RIN) scores of 2.5 and DV200s of less than 30%. This indicates that less than 30% of the RNA in each sample is more than 200 base pairs, illustrated by the displayed bioanalyzer traces (**Figure 4.3D**). As all of the RNAscope probes used are well over 200 base pairs, it is unlikely that they could bind to any of the small degraded RNA in FFPE tissue.

We encountered similar difficulties with fluorescent IHC in FFPE tissue with the ITSN1 antibody we use. Again, ITSN1 fluorescence levels did not rise above negative control background with two different fluorophores, though NeuN did (**Figure 4.4A**). This could mean that the processing of FFPE tissue masks the epitope of ITSN1 that the antibody targets. As a

preliminary test, we obtained fresh frozen tissue from the OHSU Layton Ageing and Alzheimer's Disease Center/Oregon Brain Bank, and performed immunofluorescence of ITSN1 with NeuN or GFAP in one AD and one CTL hippocampus. Interestingly, ITSN1 corresponded to cell bodies associated with GFAP staining (**Figure 4.4C**) and not NeuN staining (**Figure 4.4B**) in the AD sample. This pattern was not apparent in the CTL sample but is hard to draw conclusions as the tissue was severely impacted by damage from ice artifacts. Repeating this study in cryoprotected fresh frozen tissue would be extremely illuminating as to what cell types are involved in ITSN1 changes in AD brains.

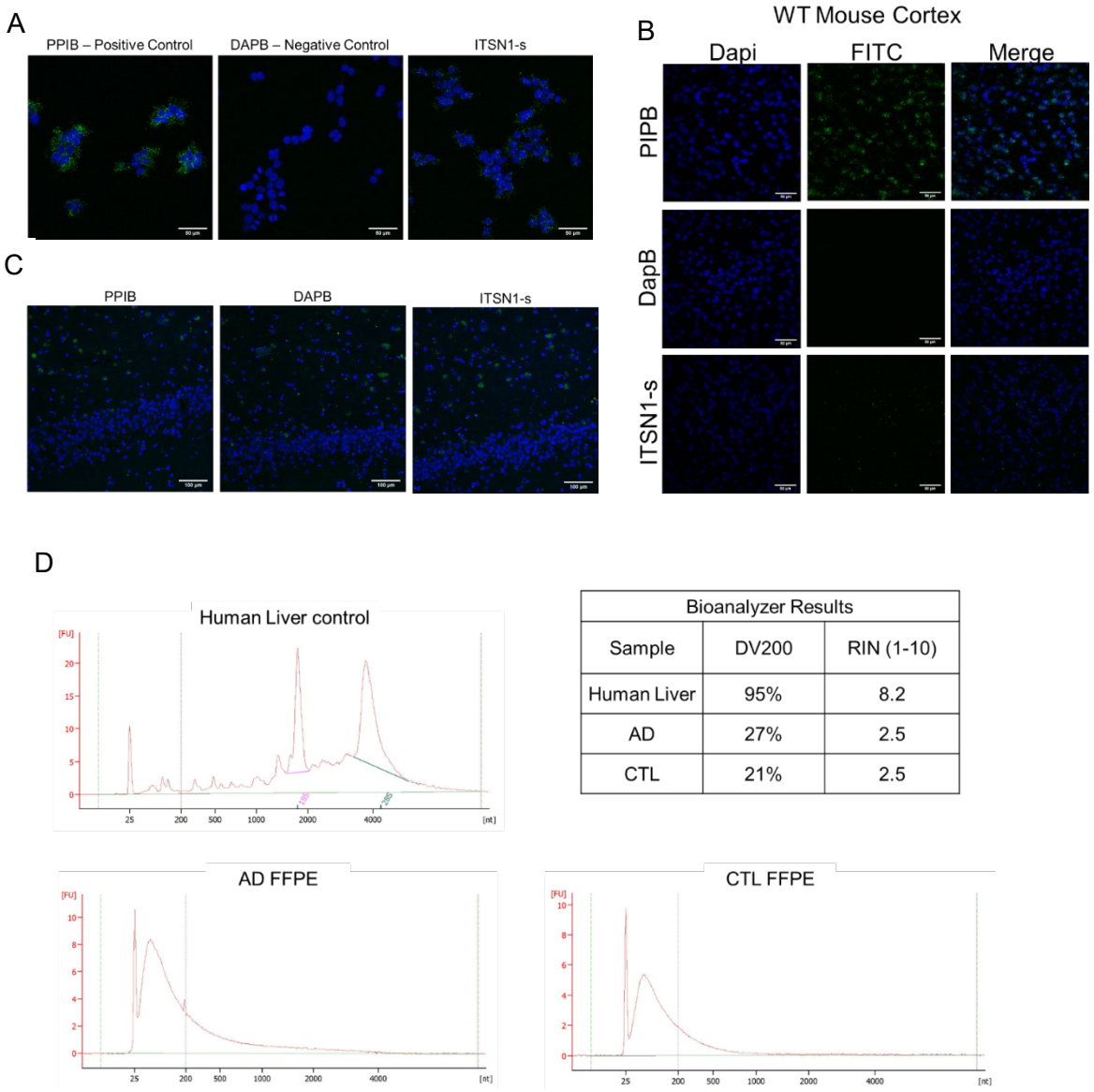

Bioanalyzer Results		
Sample	DV200	RIN (1-10)
Human Liver	95%	8.2
AD	27%	2.5
CTL	21%	2.5

Figure 4.3. RNAscope Signal of ITSN1 Does Not Show Above Background due to RNA Degeneration in Archival Tissue. Fluorescent RNAscope (green) with a positive control probe (PPIB), a negative control probe (DAPB), and ITSN1-S probe in HEK293T cells (A) and mouse cortex (B) and human formalin fixed paraffin embedded hippocampus (C). RNA isolated from human liver, FFPE AD hippocampus and CTL hippocampus were examined using an Agilent Bioanalyzer. RNA Integrity Numbers (RINs) were calculated from the Bioanalyzer traces (D). Scale bars 50 μm.

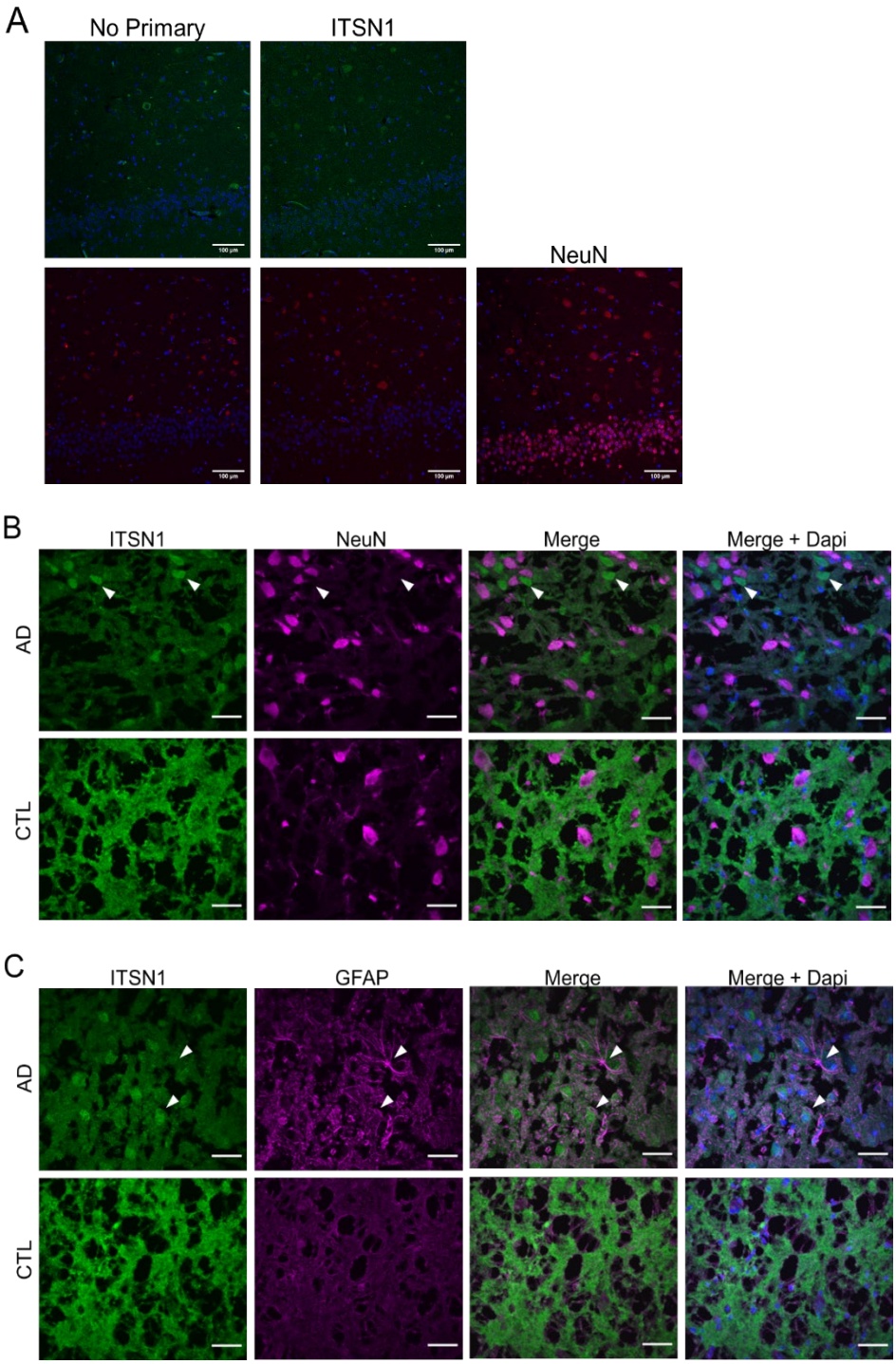

Figure 4.4. Fluorescent IHC in FFPE and Fresh Frozen tissue. (A) Fluorescent IHC of ITSN1 and NeuN using both green and red fluorophores in human hippocampal FFPE tissue. Fluorescent IHC of ITSN1 and NeuN (B) or GFAP (C) in fresh frozen human post mortem hippocampus of one AD and one CTL brain. Scale bars 50 μm.

4.3 Are CSF EV MiRNAs Changed in AD Brains?

In our published paper, Sandau et al., 2022 (*196*), we found four miRNAs increased in AD CSF extracellular vesicles (EVs). **Figure 4.5** and legend are taken directly from the publication. For this study, I performed target prediction and pathway analysis in **Figure 4.5F** and **G**. We found that the synaptogenesis pathway is a target of multiple AD CSF EV miRNAs and that a key component, SNAP-25, is a predicted target of miR-16-5p. To establish if the CSF EV miRNA miR-16-5p is also changed in AD brains we visualized the miR-16-5p using miRNAscope and quantified the amount of miR-16-5p between a preliminary set of AD and CTL FFPE cortex sections (**Figure 4.6A**). Because miRNAs are much smaller than mRNAs, the degradation of FFPE mRNA did not seem to affect the miRNA signal. We measured the percent area of miRNA puncta in each, and compared these values for AD and CTL separately in white matter versus gray matter (**Figure 4.6B**). We did not perform statistics on these data, but there is a trend of increased miR-16-5p in AD white matter but not gray matter, which is the same direction of change of miR-16-5p in CSF EVs. Additionally, we evaluated if a target of miR-16-5p, SNAP-25 which is highly involved in synaptogenesis, also changes in AD brains by immunoblot. Indeed, SNAP-25 is decreased in AD frontal cortex, which is the expected from repression of mRNA translation resulting from an increase in miR-16-5p and subsequent binding to SNAP-25 mRNA (**Figure 4.7A, B**). This preliminary data is a proof of concept that we are able to quantitatively measure miRNAs in FFPE tissue and potentially relate it to targeted protein changes. Future studies will confirm miRNA-mRNA binding of miR-16-5p and *SNAP-25* mRNA and perform dual miRNAscope immunohistochemistry to visualize if miR-16-5p and SNAP-25 are in the same cell type.

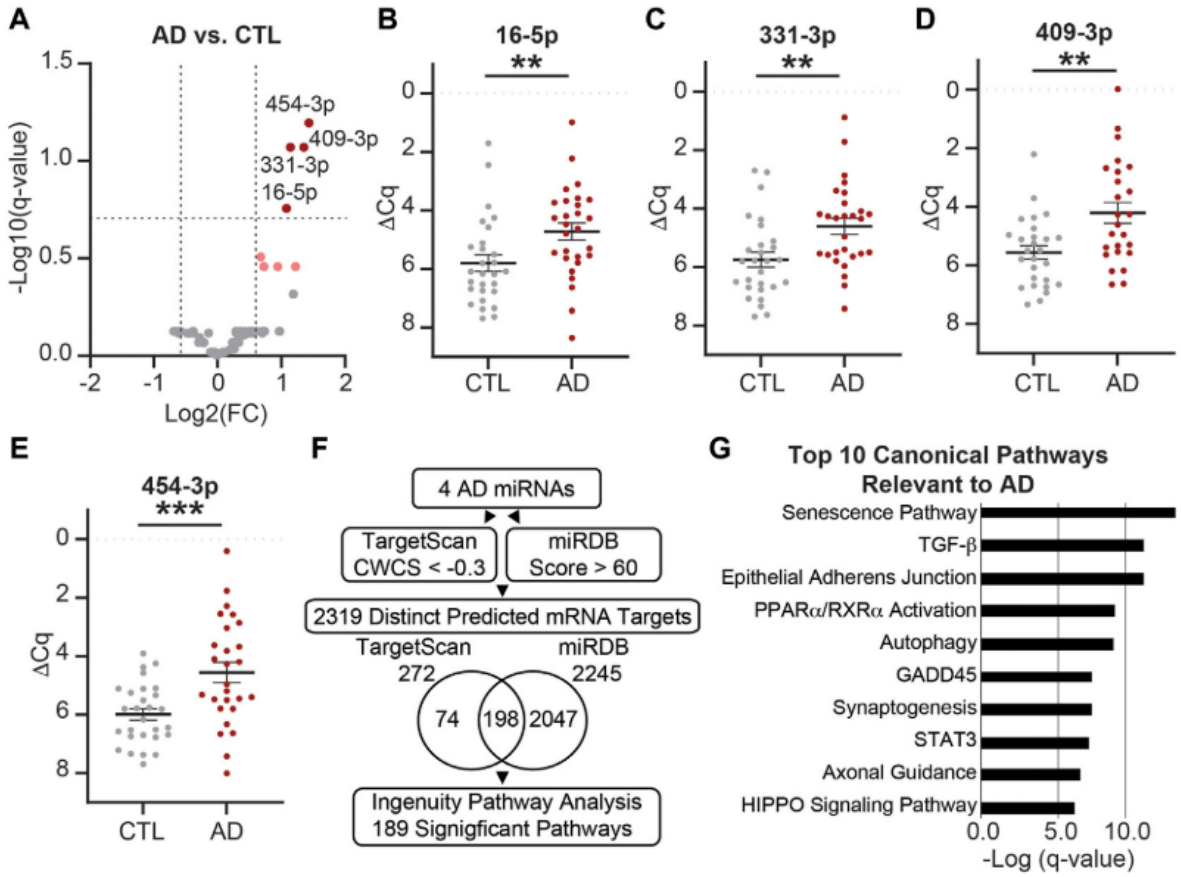

Figure 4.5. Hsa-miR-16-5p is Predicted to Regulate SNAP-25 mRNA (*196*). MiRNAs are differentially expressed in AD vs. CTL CSF EVs. For legend descriptions of A-E see full figure in **Appendix C**. (F) Workflow of the target prediction analysis for the four significant miRNAs: miR-16-5p, -331-3p, -409-3p, and -454-3p. MiRNAs were queried using TargetScan 7.2 with a CWCS of < −0.3 (272 MiRNAs total) and miRDB with a target score >60 (2,245 MiRNAs total). The Venn diagram shows the overlap in miRNA targets predicted by TargetScan 7.2 and miRDB. Of the 2,319 predicted mRNA targets (74 from TargetScan +2047 from miRDB +198 in common to both), we identified 189 significant pathways (B-H FDR 0.01). (G) Top 10 canonical pathways predicted by the mRNA targets, all of which are relevant to AD. Note all 10 pathways were in the top 17 of all 189 significant pathways, and senescence, TGF-β signaling, and epithelial adherens junction signaling pathways were the top three overall.

A

postmortem summary	age	sex	PMI
ad	80	m	9
ad	75	m	7
ad	72	f	18
ad	53	f	10.5
ctl	54	f	17
ctl	69	f	24
ctl	81	m	8

B

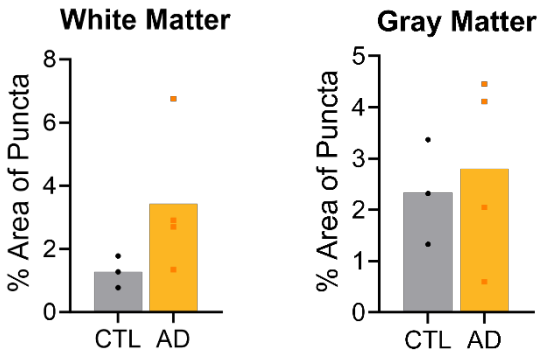

C

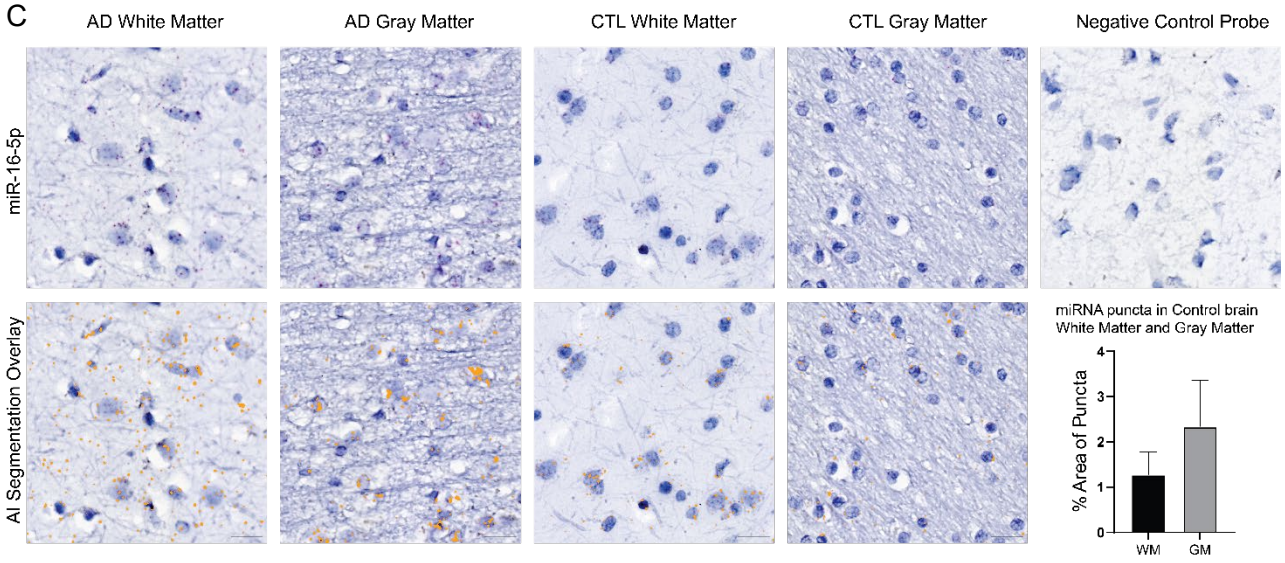

Figure 4.6. MiRNAscope Can Be Used to Visualize and Quantify MiR-16-5p Levels in Human Post-mortem Brains. Four AD and four CTL post mortem frontal cortex (A) were probed for miR-16-5p via miRNAscope. After brightfield slide scanning, Zeiss Zen Intellesis trainable segmentation was used to identify and quantify miRNA signal (C). Segmentation shown as an orange overlay of miRNA puncta (C). Percent area of miRNA segmentation is shown for white matter and gray matter separately (B) as they were segmented with differently trained analysis modules.

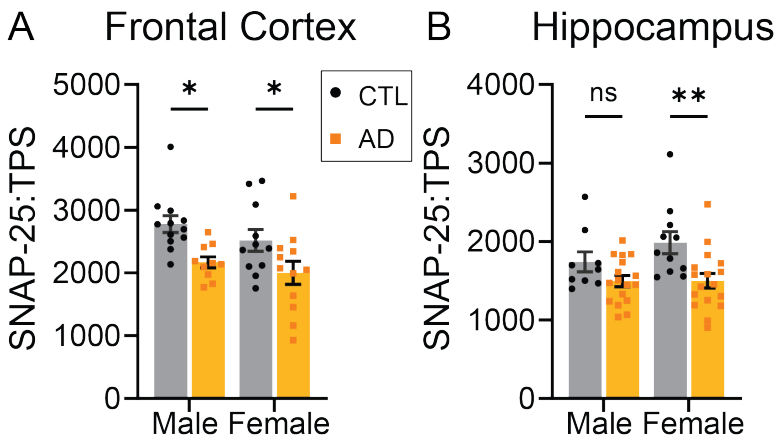

C

		2-way ANOVA		Post-Hoc tests	
FC				Šídák multiple comparisons test	
SNAP-25	Interaction	F (1, 41) = 0.09306	P=0.762	CTL-AD	
	Sex	F (1, 41) = 1.932	P=0.172	Male	**P=0.0016**
	Diagnosis	F (1, 41) = 13.51	**P=0.0007**	Female	**P=0.040**
HP		F(DFn, DFd)	p-value		
SNAP-25	Interaction	F (1, 50) = 1.292	P=0.261	CTL-AD	
	Sex	F (1, 50) = 1.381	P=0.245	Male	P=0.223
	Diagnosis	F (1, 50) = 11.93	**P=0.0011**	Female	**P=0.0031**

Figure 4.7. SNAP-25 Decreases in AD Brains Compared to CTL. Comparison of SNAP-25 between males and females in AD and age-matched normal control (CTL) frontal cortex (A) and hippocampus (B). Data are represented as mean ± SEM. Statistical significance was determined by two-way ANOVA with post-hoc Šídák multiple comparisons test. *P<0.05, **P<0.005

4.4 Methods

Luciferase Assay

HT-1080 cells (ATCC- CCL-121) were seeded into solid white bottom 96-well plates at 5000 cells/well the day before transfection. We used GoClone plasmid constructs (Active Motif) containing a luciferase reporter open reading frame upstream of experimental 3' UTRs. 3' UTR constructs used included the ITSN1-S 3' UTR containing two target sites for miR-193a-5p, a positive control 3' UTR containing the complimentary sequence match to miR-193a-5p, and a negative control 3' UTR with a random sequence. Approximately 24 hours after cells were seeded, each luciferase reporter construct were added to serum and antibiotic free DMEM and combined with either a miR-193a-5p mimic or a nontargeting miRNA mimic (Active Motif). The 3' UTR-miRNA mimic mixes were then incubated with DharmaFECT Duo transfection reagent (Horizon) for 30 minutes at room temperature. Media was then removed from the cells and 100uL of transfection mix added to each well. We used 100ng of luciferase reporter plasmid, up to 100nM of each miRNA mimic and 0.163 µL DharmaFECT Duo per well transfected, with three replicate wells per condition. 24 hours after transfection mix added, we added 100µL of the LightSwitch Luciferase Assay system (Active Motif) directly to each well, incubated for 30 minutes at room temperature, then luminescence of each well recorded for 2 seconds using the SpectraMax iD3 (Molecular Devices) microplate reader.

miRNA mimic transfection in HEK cells

HEK293T cells (ATCC- CRL-1573) were seeded at 300,000 cells/well in 6 well tissue culture plates. 24 hours later, 100 ng of miR-193a-5p mimic or inhibitor (Active Motif) was incubated with 6 µL/well of DharmaFECT Duo (Horizon Discovery) in 2 mLs of serum and antibiotic free DMEM for 20 minutes at room temperature. Media was then removed from the cells and transfection mix added. 24 hours after transfection, cells were trypsinized, spun down

resuspended in 500 µL cold PBS, and then divided. 100 µL of cell suspension was used for RNA isolation and 400 µL for protein analysis.

RNA isolation and qPCR

RNA from cells was isolated post transfection using the MagMAX™ mirVana™ Total RNA Isolation Kit 9 (Thermo Fisher) protocol for adherent cells. RNA was stored at 20ºC until RT-qPCR performed. We used TaqMan assays for *ITSN1-S* and beta actin (*ACTB)* (Thermo Fisher), Samples were prepped using SuperScript VILO cDNA Synthesis Kit (Thermo Fisher) and TaqMan Universal Master Mix II (Thermo Fisher) run in 96 well PCR plates on a QuantStudio12K Flex, and analyzed with Quant Studio Design and Analysis Software version 2.6.0 (Thermo Fisher). Values are represented as *ITSN1* relative to *ACTB*.

Human Brain Samples

This study consisted of post-mortem tissue of 119 donors from the Oregon Health & Science University Layton Aging and Alzheimer Disease Center. All donors were aged individuals from the community and had either no known neurological disease (CTL) or a clinical history established, as previously described (AD)(*140, 141*). After consent was given from the next of kin, brain autopsy was performed on all participants in accordance with Oregon Health & Science University guidelines. Tissue was either stored unfixed at -80ºC, or formalin fixed and paraffin embedded. Patient demographics can be found in **Chapter 2, Table 2.2**. Note that two samples represented there were removed here due to degradation or postmortem interval time of over 24 hours.

Immunoblots

Archived frozen brain tissue was thawed and while thawing white matter and leptomeninges were dissected away. 40-60 mg of post-mortem grey matter from AD and CTL frontal cortex (FC; AD n=22, CTL n=23) and hippocampus (HP; AD n=34, CTL n=22) was collected and total protein extracted by sonication for 25 seconds in lysis buffer (62.5 mM Tris pH 6.8, 2% SDS and 10% glycerol) followed by centrifugation at 14,000 x g for 10 minutes. The supernatant was aliquoted and stored at -80ºC until used for immunoblot analysis. Before use, protein lysates were analyzed for protein content using the Pierce BCA Protein Assay kit (ThermoFisher Scientific), loading buffer (50 mM DTT, 0.01% bromophenol blue) added, boiled and cooled before protein (10 µg) was loaded onto precast NuPAGE 3-8% Tris-Acetate gels (Invitrogen) and separated by electrophoresis.

Cells post transfection, collected as described above, were incubated with RIPA lysis buffer (Thermo Fisher) with Halt protease/phosphatase inhibitor (Thermo Fisher). After protein extraction, samples were centrifuged at 12,000 x g for 20 minutes at 4ºC. Supernatant was collected and aliquoted for BCA analysis (Pierce BCA Protein Assay kit, ThermoFisher Scientific) and immunoblot. Laemmli running buffer was added to samples, which were then boiled, cooled, and stored at -80ºC until protein (10 µg) was loaded onto precast NuPAGE 3-8% Tris-Acetate gels (Invitrogen) and separated by electrophoresis.

Protein was then transferred onto polyvinylidene difluoride (PVDF) membranes in transfer buffer containing 10% methanol for better transfer of high molecular weight proteins. Before primary antibody incubation, membranes were dried overnight at 4ºC then activated with methanol and stained with Revert 700 Total Protein Stain Kit Total protein stain (TPS, LI-COR Biosciences), imaged on the Odyssey CLx Imager (LI-COR Biosciences), then destained and blocked with Intercept (TBS) Blocking Buffer (LI-COR Biosciences). After blocking, membranes were incubated with the specified primary antibodies (SNAP-25 1:1000 Santa Cruz

Biotechnologies, ITSN1 1:2500 Novus Biologicals) for two hours at room temperature in Intercept blocking buffer (LI-COR Biosciences) with 0.2% Tween-20. After washing (4 x 5 min, TBS-T, 0.2% Tween-20). Membranes were then incubated with the appropriate IRDye secondary antibodies (IRDye 800CW Donkey anti-Rabbit, IRDye 680RD Donkey anti-Mouse, LI-COR) in Intercept blocking buffer with 0.2% Tween-20 and 0.02% SDS for 1 hour at room temperature. Membranes were washed (4 x 5 min, TBS-T) and bands visualized on the Odyssey CLx Imager. The intensity of each signal was determined with Empiria Studio software version 2.2 (LI-COR Biosciences) using the Quantitative western blot function that employs automatic lane detection and background subtraction to reduce variability of between gel analyses. Signals were first normalized within gels to TPS, and as multiple gels were needed to include all samples, bands were normalized to a repeated sample run on every gel to account for between gel variation.

RNAscope and miRNAscope

Post mortem FFPE human hippocampus on glass slides were baked at 60˚C for 1 hour, then incubated in xylene for 10 minutes, followed by 100% EtOH for 5 minutes. Tissue was then treated with hydrogen peroxide for 10 minutes at room temperature and underwent target retrieval for 15 minutes in 100ºC buffer (ACD Bio) and RNAscope protease plus (ACD Bio) treatment for 30 minutes at 40C. After pre-treatment we used RNA probes for *PPIB* (RNAscope 3-plex Positive Control Probe_Hs, RNAscope 3-plex Positive Control Probe_Mm, ACD Bio), *DAPB* (RNAscope 3-plex Negative Control Probe, ACD Bio), and *ITSN1-S* (RNAscope 3-plex Positive Control Probe_Hs, RNAscope Probe- Mm-ITSN1-O1, ACD Bio) and the RNAscope Multiplex Fluorescent Detection Reagents v2 (ACD Bio) with fluorophore in the Opal 520 Reagent Pack (Akoya Biosciences). For miRNAscope, the same deparaffinization and pretreatment protocol as RNAscope is used followed by the miRNAscope HD detection kit –

RED (ACD Bio). miRNA probes used were positive control *RNU6* (miRNAscope positive control probe - SR-RNU6-S1, ACD Bio), negative control RNA scramble (miRNAscope negative control probe- SR-Scramble-S1, ACD Bio) and miR-16-5p (miRNAscope singleplex target probe- miR-16-5p, ACD Bio).

Image acquisition

miRNAscope images were taken in brightfield using a Zeiss Axioscan 7 Slidescanner and a Plan-Apochromat 10X/0.45 M27 objective. Tiles were stitched together and then images compressed using the Zeiss JpgXr compression method. Fluorescent images were taken using an Olympus CX3 inverted confocal with a 20X or 40X objective lens.

RNA isolation from FFPE and quality analysis

The Oregon Health & Science University Gene Profiling Shared Resource isolated total RNA from FFPE tissue using the RNeasy FFPE Kit (Qiagen) and assessed RNA quality using the Agilent Bioanalyzer (Agilent).

Fluorescent IHC- FFPE and Fresh Frozen Tissue

Post mortem FFPE human hippocampus on glass slides were baked at 60˚C for 1 hour, then incubated in xylene for 30 minutes, followed by 100% to 95% to 70% EtOH for 10 minutes each. Slides were then fixed in 10% neutral buffered formalin at 4ºC for 20 minutes and rinsed with water. Fresh frozen sections were fixed in chilled 10% neutral buffered formalin at 4ºC for 1 hour followed by 50% to 70% to 100% EtOH for 5 minutes each. From this point on FFPE and fresh frozen samples were treated the same. After preparation, sections underwent heat induced epitope retrieval for 15 minutes in 100ºC AR6 buffer (Akoya Biosciences) then rinsed with TBS + 0.1% Tween (TBST) and blocked with Opal Antibody Diluent/Block (Akoya Biosciences) for 10

minutes at room temperature in a humidity tray. Primary antibody (NeuN 1:1000, Abcam or GFAP 1:1000, Abcam) incubated in Opal Antibody Diluent/Block (Akoya Biosciences) overnight at 4ºC and then washed in TBST. Opal Secondary Antibody - OPAL POLYMER ANTI-RABBIT HRP KIT (Akoya Biosciences) was applied for 10 minutes and washed in TBST. Then Opal 620 Reagent Pack (Akoya Biosciences) working solution was applied for 10 minutes and again washed in TBST. Samples underwent heat induced epitope retrieval again for 15 minutes in 100ºC AR6 buffer (Akoya Biosciences). ITSN1 primary antibody (1:500, Novus Biologicals) was applied overnight at 4ºC in Opal Antibody Diluent/Block (Akoya Biosciences) and then washed in TBST. Opal Secondary Antibody - OPAL POLYMER ANTI-RABBIT HRP KIT (Akoya Biosciences) was applied to 10 minutes and washed in TBST and then Opal 520 Reagent Pack (Akoya Biosciences) working solution was applied for 10 minutes and then washed in TBST. Samples underwent a third heat induced epitope retrieval as before and then were counterstained with DAPI and mounted with Prolong Diamond Antifade Mountant (Thermo Fisher).

Target prediction (Sandau et al., 2022)

We used TargetScan 7.2 (*134*) and miRDB (*135, 136*) to predict target mRNAs of the four CSF EV miRNAs significantly associated with AD (miRs-16-5p, 331-3p, 409-3p, 454-3p). These algorithms use the miRNA sequence and properties of mRNA sequences to predict the likelihood of a miRNA binding to an mRNA (*137*). To limit number of genes input for later pathway analysis, predicted targets were excluded if they had a Cumulative Weighted Context Score above –0.3 in TargetScan or a target score of below 60 in miRDB. To increase sensitivity and potential for predicting novel targets, we used the union of targets predicted by both TargetScan and miRDB (*137, 138*). The sensitivity, specificity, and precision of this method were calculated using validated miRNA-target pairs from miRTarBase, a database of

experimentally validated miRNA-target interactions(*139*). The resulting values ranged from 0-1 with high quality results performing closer to 1 (*137, 138*). The union of TargetScan and miRDB resulted in higher values of sensitivity (0.35), specificity (0.833), and precision (0.98) when compared with an intersection (only targets predicted by both algorithms). Pathway analysis of the union set of 2319 predicted targets with QIAGEN Ingenuity Pathway Analysis (IPA) revealed 189 pathways in which the targets are significantly overrepresented. For this analysis we excluded cancer cell lines and related tissues to avoid the knowledge bias towards cancer in the IPA database.

Chapter 5. Summary and Conclusion

5.1 Biomarkers as Clues for AD Disease Mechanisms

Alzheimer's disease (AD) is diagnosed through several modalities that attempt to classify clinical symptoms and pathological decline as disease progresses. Brain pathologies such as amyloid beta (Aβ) plaques and Tau tangles, along with their associated cellular changes, begin to appear in patients long before they exhibit enough symptoms to diagnose (*13*). Additionally, there are few treatments which can slow or counteract the progression of pathology, and they have only emerged in recent years. Currently, all treatments are Aβ-targeting monoclonal antibodies and have varying success in reducing Aβ burden and slowing cognitive decline (*168*). However, they are also most effective in early stages of disease, as characterized by Aβ and Tau levels. Aβ burden can be decreased in some patients, but progression is not completely halted (*197-200*) suggesting that targeting Aβ is not sufficient to significantly alter other molecular pathways involved in later stage AD pathophysiology.

Historically, AD was not always distinguishable from other neurodegenerative diseases, but in 1976 it was revealed to be much more common than initially thought (*201*). The 1980's and 90's brought an abundance of research on AD and led to diagnoses based on specific types of cognitive decline which are distinct from other dementias (*202, 203*). Since then, in addition to cognitive assessments, diagnostic criteria for AD have incorporated a variety of biomarkers such as: cerebrospinal fluid (CSF) levels of $A\beta_{1-40}$, $A\beta_{1-42}$, total Tau, phosphorylated Tau, ratio of $A\beta_{1-40}$: $A\beta_{1-42}$,, and neuroimaging of Aβ and Tau by positron emission tomography (*204-207*). Recently, the National Institute on Aging and Alzheimer's Association (NIA-AAA) has developed an updated research framework for defining AD that centers biological measurements of biomarkers (*208*). Progression of AD biomarkers is continuous and begins before symptoms (*209, 210*). For example, CSF Aβ and phosphorylated Tau begin to increase

long before symptoms appear, however, patients do not usually seek medical treatment at this time. By the time cognitive impairments appear in patients and they begin to receive medical care, CSF Aβ and phosphorylated Tau levels are near plateau in contrast to early disease when biomarkers are changing rapidly (*12, 209*). Thus, discovering biomarkers for this period of time between disease onset and when patients seek medical help may be valuable in starting available treatments early enough to be more beneficial.

Recently, research has focused on identifying circulating extracellular RNA biomarkers to fill this gap (*211-215*), specifically microRNAs (miRNAs). MiRNAs are short, non-coding RNAs that regulate protein expression via complementary binding to targeted sequences in the untranslated regions (UTR) of messenger RNAs (mRNAs). This interaction leads to suppression or degradation of the targeted mRNA transcripts (*120-122, 216*) and subsequently reduced translation of the corresponding protein. This regulation of protein translation is highly utilized by cells to control specific functions through suppression or de-repression of mRNA targets, which initiate or inhibit downstream signaling cascades (*217, 218*).

Factors like disease can affect miRNA levels and alter their regulation of target mRNA protein translation (*122*). MiRNAs in extracellular biofluids serve as sensitive biomarkers for altered physiological states, including disease and injury (*117, 219*). We previously discovered (*117*) and validated (*118*) a set of candidate miRNA biomarkers in human cerebrospinal fluid (CSF) that distinguish AD patients from neurologically normal controls (CTL). Five of the miRNAs (miRs-142-3p, 146a-5p, 146b-5p, 193a-5p, 365a-3p) showed a trend towards decreased median expression across ordered diagnoses from CTL to mild cognitive impairment (MCI) to AD (*119*), suggesting that these miRNAs track with disease progression. It is unknown how these miRNAs may relate to or result from disease mechanisms in the brain. However, if biomarkers such as Aβ and Tau can be associated with pathophysiology, it is reasonable to examine other biomarkers, like miRNAs, for clues to novel mechanisms.

We designed a miRNA target prediction pipeline to evaluate if potential targets of the AD CSF miRNAs are involved in AD-relevant disease pathways. This pipeline involves collecting a list of predicted mRNA targets and then running pathway analyses to evaluate which cellular processes are overrepresented in the targets. However, miRNA-mRNA interactions are not solely influenced by sequence matching (*220*), and other factors, such as secondary structure, context of sequence around the miRNA recognition element, including the abundance and evolutionary conservation of miRNA recognition elements (*138, 221-223*) affect the likelihood of an miRNA-mRNA interaction. A wide variety of target prediction algorithms have been developed (*224, 225*), each taking a different approach in using and categorizing influencing factors. Algorithm effectiveness can be tested against experimentally validated miRNA-mRNA interactions, collected in the miRTarBase database (*226*).

The diversity of parameters used in each algorithm can make selecting one to use challenging (*227*). Additionally, miRNA-mRNA regulation can be extremely complex, as one miRNA can modulate hundreds of genes and one gene can be regulated by many different miRNAs at multiple sites (*228, 229*), which can lead to hundreds or thousands of predicted targets. To increase sensitivity of predictions, multiple algorithms can be combined by either taking all targets predicted by each algorithm (union) or for higher specificity only targets predicted by both (intersection) (*137*). I took the union of TargetScan 7.2 (*134*) and miRDB (*135, 136*), which when combined, evaluated over 20 parameters of miRNA-mRNA interactions. Amazingly, the resulting analysis of predicted targets using Ingenuity pathway analysis (IPA) found many pathways already known to be involved in AD, which illustrates how candidate AD miRNA biomarkers can and do reveal AD related pathways. We chose to follow up on clathrin-mediated endocytosis (CME), as the mechanisms of other pathways such as axonal guidance (*230, 231*), synaptic long-term potentiation (*232-234*), and synaptogenesis (*235, 236*) have been extensively studied in the context of AD.

There are several limitations of our target prediction. First, in our study, there is no expression data associated with predicted miRNA targets, so pathway analysis does not consider potentially altered levels of mRNAs or proteins. Second, interactions cannot happen if the miRNA and mRNA are not in the same cell or brain region, so when evaluating any one predicted miRNA-mRNA interaction, confirmation of the cellular location of each is important. Future analyses of miRNA biomarkers that include existing AD transcriptomic and proteomic data (*136, 237*) may enable increased accuracy in narrowing of pathways regulated by the miRNAs.

5.2 Intersectin 1 Isoforms: Potential Impacts on Clathrin Mediated Endocytosis and AD Pathogenesis

CME is an essential process for many cells, as its machinery is involved in multiple processes that regulate cellular homeostasis and survival. Given that CME is an indispensable cellular process, many diseases are associated with mutations or changes in the level CME proteins (*4, 6-8*). In AD, there are several ways in which neuronal cellular processes may be affected by CME. For example, neuronal endolysosomal dysfunction, the first step by CME (*21*), is thought to result from enlarged endosomes that cause decreased endosomal transport (*34, 36*) which results in many neuropathological outcomes (*22-24*). CME is also involved in important functions at synapses, both pre- and post-synaptic, which is relevant to AD, as synaptic dysfunction and loss are highly correlated with cognitive decline (*53*). Pre-synaptic vesicle recycling is facilitated by CME machinery and is reduced in AD (*58, 59, 238*). In the post-synaptic terminal, receptors are internalized and recycled through CME (*239*). In AD, dysfunction of AMPA receptor recycling is connected to deficits in long-term potentiation and depression (*56, 60-62*). CME is also strongly involved in Aβ pathology, as neuronal internalization of both amyloid precursor protein (APP) (*20, 68*) and pathogenic Aβ occurs

through CME (*80, 82, 83*) and results in downstream effects on cellular mechanisms (*44, 78, 79*). CME-mediated internalization of pathogenic Aβ by astrocytes and microglia also causes a variety of functional deficits (*100-103, 108, 109, 111, 112*). While all of these observations point to CME disruption in AD as a candidate pathway contributing to pathophysiology, the CME mechanisms and functions that could be altered in AD have not been directly investigated.

In Chapter 2, we started to pursue this by first evaluating the level of CME proteins in AD brains, which are potential targets of the AD CSF miRNAs or are essential to CME function. Our data showed that Intersectin1 (ITSN1) was significantly changed in AD brains. ITSN1 acts as a scaffolding protein to bring together proteins needed for CME (*150*). It interacts with every major CME protein at each step, from the first membrane invagination to clathrin uncoating of the internalized vesicle (*151, 152*). There are a variety of ITSN1 variants (*240-242*), with the most well characterized being neuronal specific ITSN1-long (ITSN1-L) and ubiquitous ITSN1-short (ITSN1-S). There is evidence that both overexpression (*155, 156*) and under-expression (*157, 158*) of ITSN1 reduce CME, indicating that any alteration of ITSN1 levels is disruptive to CME function. Importantly, total knock out of ITSN1 isoforms, and specific knockout of ITSN1-L, in mice resulted in enlarged early endosomes (*157*) and later learning and memory deficits (*159*). In humans, enlarged early endosomes are some of the earliest brain changes observed in AD (*25, 26*). This discovery suggests that ITSN1 disruption might contribute to brain changes in early AD pathogenesis.

However, there does seem to be more to the story. Our finding that ITSN1-L and ITSN1-S each have unique expression changes in the hippocampus (HP) and frontal cortex (FC) suggest that they may be acting in different functions of CME in each region. We found a decrease of ITSN1-L in FC of AD males, whereas in the HP only AD females had decreased ITSN1-L. For ITSN1-S, cortical levels were too low to measure in the FC, but in the AD HP there was a significant increase in ITSN1-S for both sexes. Interestingly, ITSN1 is encoded on

chromosome HSA21, which is triplicated in down syndrome (DS) (*26*). People with DS have a significantly higher risk of developing AD, nearly all developing neuropathology and symptoms by age 65 (*29, 30*). This pathology is thought to be due to several AD related genes encoded on HSA21, such as *APP* and presenilin1 (*PSEN1)* (*23, 31-33*). ITSN1 RNA and protein are increased in DS brains (*243-245*), and when comparing ITSN1 protein levels between CTL, DS alone, and DS + AD diagnosis, ITSN1-L and ITSN1-S were upregulated in DS alone compared to CTLs, but significantly decreased in DS + AD relative to levels in DS alone (*245*). This observation suggests that while ITSN1 is increased due to the triplication of its gene, the increase does not contribute to the development of AD in DS. In fact, it could be that the loss of ITSN1 is related to AD progression. We saw a similar decrease of ITSN1-L in AD FC in both males and females, but in HP, a significant decrease was only seen in AD females. However, this finding is interesting, as females have higher instances of AD (*50, 51*). Additionally, we observed a sex difference in CTL ITSN1-L HP, with females having a higher baseline level than males. This could again point to the reduction of ITSN1-L being involved with AD progression and potentially contributes to the higher instance of AD in females.

In contrast, our findings of increased ITSN1-S do not support the idea that a general decrease in ITSN1 contributes to AD. The difference in ITSN1-S and -L levels in AD point to their having distinct functions. This would not be the first instance of each isoform performing different functions in the same context, as shown in glioma, where ITSN1-S promotes disease progression and ITSN1-L inhibits it (*246*). ITSN1-S is only involved in CME and has identical functional domains as ITSN1-L that interact with CME proteins. However, ITSN1-L has several additional neuronal-specific functions due to the three additional binding domains at the C-terminus (*174, 175*). These functions include dendritic spine development (*79, 154*), fast neurotransmission (*161, 176*), mitogenic signaling (*178, 247*), and RAS/MAPK regulation (*248*) .

So, while the increase of ITSN1-S most likely affects only cellular functions which use CME machinery, the decrease of ITSN1-L may not involve CME at all.

Unfortunately, the subtle differences between isoform function, specifically which CME processes involve ITSN1-S versus ITSN1-L, have not been studied. Our data suggest that future research should focus on distinguishing how changes in each isoform affects specific cellular functions. As a first step, discovering which cell types are driving ITSN1-S changes may help to narrow down the specific function of ITSN1-S in the affected cell type. For example, it is reasonable to expect that ITSN1-S is increased in astrocytes and microglia versus in neurons, as reduction of CME in relation to Aβ uptake is observed in these cells. Our IHC study is not helpful in this analysis as there are no specific antibodies for ITSN1-S. Due to their identical structure, only the additional domains at the C-terminus in ITSN1-L are individually targetable. Future studies might include RNAscope to probe for ITSN1-S-specific 3' UTR sequences paired with IHC of cell type markers. As discussed in Chapter 4, our efforts to perform RNAscope and fluorescent IHC were unsuccessful, due to the lack of available tissue that was not RNA degraded or did not contain ice artifacts.

We did see a preliminary potential difference in ITSN1 expression when staining fresh frozen AD and CTL brain, in which there were several cell bodies with strong ITSN1 signal that localized with GFAP and not NeuN. While this study was limited by the poor quality of available tissue, future studies conducted with fresh tissue specifically stored for fluorescent IHC and RNAscope staining may reveal the potential of ITSN1-S involvement in astrocyte-specific functions. If it is discovered that both ITSN1-L and -S are changed in neurons, super-resolution microscopy studies of ITSN1 localization within different neuronal compartments may help to distinguish their functions. A dual immunofluorescence comparison of with an ITSN1-L-specific antibody and an ITSN1 antibody that does not distinguish isoforms would allow us to infer the location of ITSN1-S in the absence of ITSN1-L-specific antibody staining.

We did observe a potential association with Tau- and ITSN1-stained neurons, which could point towards ITSN1-L dysfunction affecting cytoskeletal disturbances in neurons (*249, 250*). However, only a small subset of neurons showed this phenotype, suggesting that there may be a more vulnerable population of neurons affected by changes in ITSN1. Importantly, there is evidence of select neuronal populations being more vulnerable to Tau pathology (*251*). Experiments which co-stain for ITSN1 with Tau and actin could shed some light on whether this is the case.

There are also several possible explanations for why the ITSN1 isoforms were the only proteins changed in AD brains, compared to the other CME proteins we examined (see Chapter 2). ITSN1-L could be essential to CME functioning, and a decrease could disrupt any major CME functions in the neuron. This interpretation is most likely only partially true, as total knockdown studies of ITSN1 have reported a marked decrease in CME, but not total reduction (*157, 158*) indicating that there are other mechanisms by which CME can continue without ITSN1-L. Alternatively, a change in only ITSN1-L could point to the non-CME related functions of ITSN1-L being disrupted, with CME not changing at all. Outside of CME functions, changes to ITSN1-L in neurons could affect other neuronal specific functions such as fast neurotransmission and dendritic spine development, both cellular functions related to AD. Again, these findings demonstrate the importance of considering that ITSN1-L and ITSN1-S may be impacting cellular processes differently in AD.

5.3 Evaluating ITSN1 and CME in AD Animal Models

Currently, many studies that have evaluated CME proteins in the context of AD use transgenic mouse models containing humanized mutations to mimic aspects of AD pathophysiology. As of yet, these studies have not evaluated how CME is mechanistically changed and are limited to RNA and protein expression studies of CME-related proteins (*45, 46,*

252) and not how changes may affect CME function. However, in order for mechanistic studies to have the potential of translating to human disease, careful evaluation of the model is needed (*253*). To further characterize how changes of ITSN1-L and ITSN1-S may affect CME in AD, we began by measuring ITSN1 by immunoblot in the 5xFAD AD mouse model. If ITSN1-L and ITSN1-S change in a similar manner in 5xFAD mice as they do in humans, this model may be useful in studying their mechanisms and/or involvement in AD.

5xFAD mice contain three AD familial mutations in humanized *APP* and two in *PSEN1*: Swedish (K670N/M671L) (*254*), Florida (I716V) (*255*), and London (V717I) (*256*) in *APP*, and *PSEN1* mutations of M146L and L286V (*257, 258*). They exhibit Aβ plaques, neurodegeneration, and cognitive decline as they age (*48, 170, 180, 181*). Differences in protein expression between 5xFAD and WT mice can be seen as early as postnatal day 1, and pathway analysis of these genes revealed changes in CME (*259*). In Chapter 3, we showed that as animals age, ITSN1-L levels are changed in 5xFAD mice differently in the HP and cortex (CTX). ITSN1-L in the HP is decreased in 5xFAD males at 6 months. While in the CTX, ITSN1-L is increased in 5xFAD females at 3 months, with no changes emerging at later time-points. Additionally, our preliminary evaluation of ITSN1-L in 5xFAD mice at 8 months suggested that in both the cortex and HP, ITSN1-L is decreased in 5xFAD males and females.

5xFAD mice begin extracellular deposition of plaques between 2-4 months, and plaques first appear in the subiculum and cortical layer V (*48*). It's possible that early in disease, changes in 5xFAD, like the cortical increase we saw at 3 months, have a different effect on pathology progression than changes at 6 months, when we see HP ITSN1 increase. An increase at 3 months could correspond with the increase in Aβ plaques in the CTX (*48*) and shows the potential for ITSN1 to be involved in CME dysfunction resulting from Aβ build up. A change of ITSN1 is likely to reduce CME, and could be a compensatory mechanism as Aβ accumulates. We also see evidence of this response in aged 5xFAD primary neurons, where

ITSN1 increases at timepoints corresponding to Aβ accumulation (*72*).Both of these results point towards increased ITSN1 as a response to Aβ production and/or build up early in disease.

ITSN1-L knock out mice exhibit decreased dendritic spine density and learning and memory deficits (*159, 260*). As such, the decrease of ITSN1 we see in male 5xFAD at 6 months could correlate with the onset of cognitive effects in the 5xFAD mice that occur later in disease (*170, 181*) and may be more related to functions of ITSN1-L involved in spine development or synaptic plasticity. However, behavioral assays have not revealed significant learning and memory performance differences between male and female 5xFAD (*180*), so it is unclear if our observed sex specific ITSN1-L changes might contribute to behavior differently. Additionally, that ITSN1-L potentially decreases in both the cortex and HP at 8 months supports the idea that there are distinct ITSN1 functions during ageing.

Another potential consequence of ITSN1-L loss in the HP is the impairment of neurogenesis. The reduction of adult neurogenesis is clearly linked to AD and is especially vulnerable at early disease stages (*261-263*). 5xFAD mice show a reduction in neurogenic markers by 2 months (*262*). ITSN1 has not been directly involved in neurogenesis, but several studies have shown that it plays roles in proliferation of neural stem cells (*264*)and survival of differentiating cells (*265*). Interestingly, there appeared to be a reduction of ITSN1 staining in the CA3 of 6-month 5xFAD mice that we examined. CA3 may regulate neurogenesis (*266, 267*) and as such, a change of ITSN1-L in this region could support the hypothesis of ITSN1-L involvement in this process. If not directly affecting neurogenesis, ITSN1 could be supporting survival of newborn neurons. A loss of ITSN1-L could reduce neuron survival due to loss of its functions supporting neuronal migration (*177*), axonal guidance (*153, 268*), and dendritic spine development (*154, 158*).

A limitation of our study is the inability to compare ITSN1 between age groups in each brain region. Age is the highest risk factor for AD (*269*), and CME proteins increase with age

(*49*). Therefore, as ITSN1 itself is increased with age in a DS mouse model (*270*), there is a high likelihood that age related changes may play an important role in ITSN1 function and dysfunction in AD. Increased ITSN1-L with ageing could even be protective, and loss of that protection from decreased ITSN1-L in aged 5xFAD mice may contribute to further disease progression. In humans, this is similarly illustrated by the decrease of ITSN1-L in people with AD and DS compared to the "normally" elevated ITSN1-L levels in DS alone (*245*). Future studies should examine the relationship between age, genotype, and sex effects on ITSN1-L in 5xFAD mice.

Another significant limitation to our studies in the 5xFAD model is the inability to gain insights to ITSN1 functions potentially involved in AD Tau pathology. Our studies have examined ITSN1 and CME within the framework that Aβ pathology may more impacted by changes of CME than Tau pathology. However, there are several ways in which Tau pathology could be impacted by CME as well. The aggregation of Tau proteins can be spread from cell to cell by secretion to the extracellular space and subsequent internalization by a nearby neuron. This internalization can happen in several ways, one of which is CME (*90, 271*). Future studies could measure levels of ITSN1 in the 3xTg mouse model, which is the only model to develop both amyloid and Tau pathology with aging (*47, 272*).

5.4 Differences in ITSN1 Between Humans and the 5xFAD Mouse Model

Findings from mouse models of AD rarely translate to humans in a manner that can be used for development of therapeutics (*253, 273, 274*). However, transgenic mouse models are often the only option for many researchers, as human tissue can be difficult to obtain and long-term storage of samples varies widely between tissue banks. Additionally, as human brains are collected post-mortem, it is difficult to examine brain changes in early AD progression, and it is impossible to perform mechanistic studies. This is where the utility of transgenic mouse models

comes in. But as stated above, due to the many inter-species differences, careful consideration must be taken when comparing changes in the human AD brain to changes in an AD model.

We found several differences between our human and mouse studies that warrant further investigation. First, and most strikingly, we could not measure ITSN1-S in the 5xFAD HP or CTX, whereas in human AD HP, we observed a significant increase in its levels. This discrepancy could suggest a fundamental species difference in ITSN1-S expression or function. Alternatively, it is possible that ITSN1-S expression does change in 5xFAD mice, but its baseline levels are significantly lower than ITSN1-L, and any specific effect of ITSN-S may be masked by high ITSN1-L expression on the immunoblots. We also found evidence of differences in the abundance of ITSN1 between human and mouse brains in the imaging studies we performed and the amount of protein lysate required for immunoblot. In humans, we observed very sparse ITSN1 in the cortex and HP by IHC, and to evaluate levels by immunoblot, we needed to use 50 µg of protein per lane to gain an optimal signal to noise ratio. In the 5xFAD mice, ITSN1 staining was widely present throughout the brain, and we only needed to load 10 µg of protein per lane to obtain a sufficient signal to noise ratio of ITSN1-L. This result suggests that ITSN1-L may play a much larger role in the adult mouse brain than the adult human brain. Re-evaluation of mouse tissue in a more sensitive manner, such as increasing protein used for immunoblot, qPCR, or the iBind immunoblot technique (used for the human samples), would be helpful to determine if ITSN1-S is also increased in 5xFAD HP. However, if these methods do not work and mice naturally have very little ITSN1-S, a transgenic mouse in which ITSN1-S is overexpressed may help to elucidate how increases in protein levels affect CME functions.

These species differences could be the reason for somewhat conflicting results we found between human AD FC and 5xFAD CTX ITSN1-L levels. We observed CTX levels of ITSN1-L in the 5xFAD were increased in female mice, which contrasts the decrease in ITSN-L that we saw

only in males in human AD FC. Conversely, in human AD HP, ITSN1-L levels were decreased in females but not males, whereas in 5xFAD mice at 6 months ITSN1-L is decreased in males but not females. It is as of yet unknown if sex differences seen in human AD are mechanistically similar to those seen in 5xFAD mice. Indeed, in humans we found that baseline ITSN1-L was lower in CTL males than CTL females whereas in WT mice at 6 months there is potentially increased ITSN1-L in males versus females. These discrepancies may illustrate the limitation that human samples do not represent early stages of the disease, whereas disease progression in 5xFAD mice can be monitored over time. Together, these considerations highlight another reason why species differences must be carefully considered.

However, in human HP, both AD HP and CTX ITSN1-L levels were decreased compared to CTL levels. Similarly, the 5xFAD mice also showed a decrease in HP levels of ITSN1-L. This result suggests that the 5xFAD HP may be a model that can be further used to investigate ITSN1-L mechanisms in the context of AD. **Figure 5.1** summarizes our findings of how ITSN1 levels change in human AD, 5xFAD mice, and 5xFAD primary neurons relative to disease stage.

With all of this in mind, future experiments to elucidate specific ITSN1 isoform functions in relation to AD might utilize either the 5xFAD or 3xTg mouse crossed with a total ITSN1 knock out or ITSN1-L specific knock out mouse. We could then evaluate if ITSN1-L loss induces enlarged early endosomes, synapse dysfunction, and neuronal survivability via immunofluorescence and immunoblot. To evaluate ITSN1-S functions in a human-specific model which captures earlier stages of disease, levels in patient-derived iPSC neurons could be evaluated and ITSN1-S overexpressed if necessary. Then, CME function could be tested with transferrin internalization assays. Alternatively, effects of cell type specific expression of ITSN1-

L and -S on Aβ and Tau pathology could be examined using *in vitro* transfection assays in neurons vs astrocytes s microglia and measuring Aβ and Tau levels.

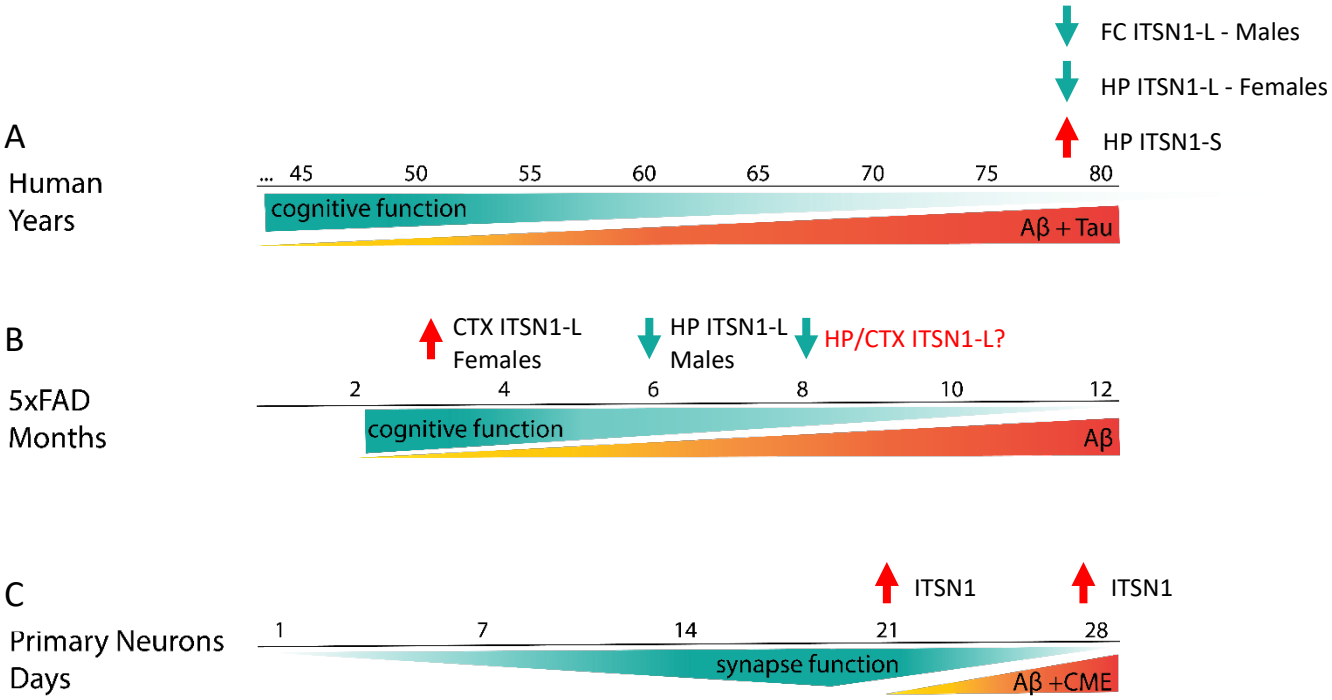

Figure 5.1. Summary Figure. ITSN1-L and -S change in an isoform and brain region specific manner in post-mortem AD human brains (A). In the human HP, ITSN1-S is increased in both AD males and females whereas ITSN1-L is decreased only in AD males. In the FC, ITSN1-L is only decreased in AD males. These changes in ITSN1-L are somewhat recapitulated in the 5xFAD model (B). Interestingly, our 'early stage' models of AD, 5xFAD at 3 months and 5xFAD primary neurons (C), capture disease states earlier than possible with human post-mortem tissue and show an interesting increase in ITSN1-L illustrating a potential transient mechanism in which ITSN1-L is increased during early-stage disease and decreased during late-stage disease.

5.5 Conclusion

The pathophysiology of AD is extremely complex, affecting many cell types, brain regions, and higher order brain functions. The results of this dissertation work illustrate how target prediction of candidate miRNA AD biomarkers leads to AD related cellular pathways. Here, we began to evaluate one of these pathways, CME, for specific changes in AD. Of the CME proteins we assayed, ITSN1 was revealed as the only protein significantly changed in AD postmortem brains. ITSN1 isoform and brain region specific changes of ITSN1, in both human AD brain and 5xFAD mice, suggest distinct functions of ITSN1-L and -S, and the possibility of different ITSN1-L functions in early vs late disease stages. Our results develop a compelling reason to further investigate specific ITSN1-L and -S functions in AD, while also illustrating that those future studies must be carefully designed with specific models that can capture different points in disease progression.

References

1. G. J. Doherty, H. T. McMahon, Mechanisms of Endocytosis. *Annual Review of Biochemistry* **78**, 857-902 (2009).
2. M. Kaksonen, A. Roux, Mechanisms of clathrin-mediated endocytosis. *Nature Reviews Molecular Cell Biology* **19**, 313-326 (2018).
3. S. Boulant, C. Kural, J.-C. Zeeh, F. Ubelmann, T. Kirchhausen, Actin dynamics counteract membrane tension during clathrin-mediated endocytosis. *Nature Cell Biology* **13**, 1124-1131 (2011).
4. H. T. McMahon, E. Boucrot, Molecular mechanism and physiological functions of clathrin-mediated endocytosis. *Nature Reviews Molecular Cell Biology* **12**, 517-533 (2011).
5. M. Mettlen, G. Danuser, Imaging and Modeling the Dynamics of Clathrin-Mediated Endocytosis. *Cold Spring Harbor Perspectives in Biology* **6**, a017038-a017038 (2014).
6. T. Mitsunari *et al.*, Clathrin adaptor AP-2 is essential for early embryonal development. *Mol Cell Biol* **25**, 9318-9323 (2005).
7. T. Azarnia, H. López, Maritzen, Endocytic Adaptor Proteins in Health and Disease: Lessons from Model Organisms and Human Mutations. *Cells* **8**, 1345 (2019).
8. A. M. A. Schreij, E. A. Fon, P. S. McPherson, Endocytic membrane trafficking and neurodegenerative disease. *Cellular and Molecular Life Sciences* **73**, 1529-1545 (2016).
9. T. Raj *et al.*, Integrative transcriptome analyses of the aging brain implicate altered splicing in Alzheimer's disease susceptibility. *Nature Genetics* **50**, 1584-1592 (2018).
10. 2020 Alzheimer's disease facts and figures. *Alzheimer's & Dementia* **16**, 391-460 (2020).
11. H. Braak, E. Braak, Neuropathological stageing of Alzheimer-related changes. *Acta Neuropathologica* **82**, 239-259 (1991).
12. D. J. Selkoe, J. Hardy, The amyloid hypothesis of Alzheimer's disease at 25 years. *EMBO Molecular Medicine* **8**, 595-608 (2016).
13. M. A. Deture, D. W. Dickson, The neuropathological diagnosis of Alzheimer's disease. *Molecular Neurodegeneration* **14**, (2019).
14. A. Theerasri, S. Janpaijit, T. Tencomnao, A. Prasansuklab, Beyond the classical amyloid hypothesis in Alzheimer's disease: Molecular insights into current concepts of pathogenesis, therapeutic targets, and study models. *WIREs Mechanisms of Disease*, (2022).
15. R. A. Nixon, A. M. Cataldo, P. M. Mathews, The endosomal-lysosomal system of neurons in Alzheimer's disease pathogenesis: a review. *Neurochem Res* **25**, 1161-1172 (2000).
16. J. Hardy, D. Allsop, Amyloid deposition as the central event in the aetiology of Alzheimer's disease. *Trends Pharmacol Sci* **12**, 383-388 (1991).
17. J. A. Hardy, G. A. Higgins, Alzheimer's disease: the amyloid cascade hypothesis. *Science* **256**, 184-185 (1992).
18. V. Volloch, S. Rits-Volloch, The Amyloid Cascade Hypothesis 2.0: Generalization of the Concept. *J Alzheimers Dis Rep* **7**, 21-35 (2023).
19. V. Volloch, S. Rits-Volloch, The Amyloid Cascade Hypothesis 2.0: On the Possibility of Once-in-a-Lifetime-Only Treatment for Prevention of Alzheimer's Disease and for Its Potential Cure at Symptomatic Stages. *J Alzheimers Dis Rep* **6**, 369-399 (2022).
20. E. Koo, S. Squazzo, Evidence That Production and Release of Amyloid @Protein Involves the Endocytic Pathwa. *Journal of Biological Chemistry* **269**, (1994).

21. P. J. Cullen, F. Steinberg, To degrade or not to degrade: mechanisms and significance of endocytic recycling. *Nature Reviews Molecular Cell Biology* **19**, 679-696 (2018).
22. R. A. Nixon, Amyloid precursor protein and endosomal-lysosomal dysfunction in Alzheimer's disease: inseparable partners in a multifactorial disease. *The FASEB Journal* **31**, 2729-2743 (2017).
23. D. J. Colacurcio, A. Pensalfini, Y. Jiang, R. A. Nixon, Dysfunction of autophagy and endosomal-lysosomal pathways: Roles in pathogenesis of Down syndrome and Alzheimer's Disease. *Free Radical Biology and Medicine* **114**, 40-51 (2018).
24. M. P. Szabo, S. Mishra, A. Knupp, J. E. Young, The role of Alzheimer's disease risk genes in endolysosomal pathways. *Neurobiology of Disease* **162**, 105576 (2022).
25. A. M. Cataldo, J. L. Barnett, C. Pieroni, R. A. Nixon, Increased Neuronal Endocytosis and Protease Delivery to Early Endosomes in Sporadic Alzheimer's Disease: Neuropathologic Evidence for a Mechanism of Increased β-Amyloidogenesis. *The Journal of Neuroscience* **17**, 6142-6151 (1997).
26. A. M. Cataldo *et al.*, Endocytic Pathway Abnormalities Precede Amyloid β Deposition in Sporadic Alzheimer's Disease and Down Syndrome. *The American Journal of Pathology* **157**, 277-286 (2000).
27. M. A. Israel *et al.*, Probing sporadic and familial Alzheimer's disease using induced pluripotent stem cells. *Nature* **482**, 216-220 (2012).
28. D. Kwart *et al.*, A Large Panel of Isogenic APP and PSEN1 Mutant Human iPSC Neurons Reveals Shared Endosomal Abnormalities Mediated by APP β-CTFs, Not Aβ. *Neuron* **104**, 256-270.e255 (2019).
29. M. McCarron *et al.*, A prospective 20-year longitudinal follow-up of dementia in persons with Down syndrome. *Journal of Intellectual Disability Research* **61**, 843-852 (2017).
30. J. Fortea *et al.*, Alzheimer's disease associated with Down syndrome: a genetic form of dementia. *Lancet Neurol* **20**, 930-942 (2021).
31. A. Filippone, D. Praticò, Endosome Dysregulation in Down Syndrome: A Potential Contributor to Alzheimer Disease Pathology. *Annals of Neurology* **90**, 4-14 (2021).
32. A. Botté, M.-C. Potier. (Elsevier, 2020), pp. 209-243.
33. Y. Jiang *et al.*, Lysosomal Dysfunction in Down Syndrome Is APP-Dependent and Mediated by APP-βCTF (C99). *The Journal of Neuroscience* **39**, 5255-5268 (2019).
34. H. Stenmark *et al.*, Inhibition of rab5 GTPase activity stimulates membrane fusion in endocytosis. *The EMBO Journal* **13**, 1287-1296 (1994).
35. M. S. Song, G. B. Baker, K. G. Todd, S. Kar, Inhibition of beta-amyloid1-42 internalization attenuates neuronal death by stabilizing the endosomal-lysosomal system in rat cortical cultured neurons. *Neuroscience* **178**, 181-188 (2011).
36. N. Kimura, K. Yanagisawa, Traffic jam hypothesis: Relationship between endocytic dysfunction and Alzheimer's disease. *Neurochem Int* **119**, 35-41 (2018).
37. A. Limone, I. Veneruso, V. D'Argenio, D. Sarnataro, Endosomal trafficking and related genetic underpinnings as a hub in Alzheimer's disease. *Journal of Cellular Physiology* **237**, 3803-3815 (2022).
38. A. Hofman *et al.*, The Rotterdam Study: 2016 objectives and design update. *European Journal of Epidemiology* **30**, 661-708 (2015).
39. S. Ahmad *et al.*, Disentangling the biological pathways involved in early features of Alzheimer's disease in the Rotterdam Study. *Alzheimer's & Dementia* **14**, 848-857 (2018).
40. P. J. Yao, R. Morsch, L. M. Callahan, P. D. Coleman, Changes in synaptic expression of clathrin assembly protein AP180 in Alzheimer's disease analysed by immunohistochemistry. *Neuroscience* **94**, 389-394 (1999).

41. P. J. Yao, J. M. Weimer, T. M. O'Herron, P. D. Coleman, Clathrin assembly protein AP-2 is detected in both neurons and glia, and its reduction is prominent in layer II of frontal cortex in Alzheimer's disease. *Neurobiol Aging* **21**, 921-929 (2000).
42. P. J. Yao *et al.*, Defects in expression of genes related to synaptic vesicle trafficking in frontal cortex of Alzheimer's disease. *Neurobiol Dis* **12**, 97-109 (2003).
43. I. S. Piras *et al.*, Association of AEBP1 and NRN1 RNA expression with Alzheimer's disease and neurofibrillary tangle density in middle temporal gyrus. *Brain Res* **1719**, 217-224 (2019).
44. Y. Cao, Y. Xiao, R. Ravid, Z. Z. Guan, Changed clathrin regulatory proteins in the brains of Alzheimer's disease patients and animal models. *J Alzheimers Dis* **22**, 329-342 (2010).
45. K. Hsiao *et al.*, Correlative memory deficits, Abeta elevation, and amyloid plaques in transgenic mice. *Science* **274**, 99-102 (1996).
46. R. S. Thomas, M. J. Lelos, M. A. Good, E. J. Kidd, Clathrin-mediated endocytic proteins are upregulated in the cortex of the Tg2576 mouse model of Alzheimer's disease-like amyloid pathology. *Biochemical and Biophysical Research Communications* **415**, 656-661 (2011).
47. S. Oddo *et al.*, Triple-Transgenic Model of Alzheimer's Disease with Plaques and Tangles. *Neuron* **39**, 409-421 (2003).
48. H. Oakley *et al.*, Intraneuronal β-Amyloid Aggregates, Neurodegeneration, and Neuron Loss in Transgenic Mice with Five Familial Alzheimer's Disease Mutations: Potential Factors in Amyloid Plaque Formation. *The Journal of Neuroscience* **26**, 10129-10140 (2006).
49. M. Alsaqati, R. S. Thomas, E. J. Kidd, Proteins Involved in Endocytosis Are Upregulated by Ageing in the Normal Human Brain: Implications for the Development of Alzheimer's Disease. *The Journals of Gerontology: Series A* **73**, 289-298 (2018).
50. 2023 Alzheimer's disease facts and figures. *Alzheimers Dement* **19**, 1598-1695 (2023).
51. K. B. Rajan *et al.*, Population estimate of people with clinical Alzheimer's disease and mild cognitive impairment in the United States (2020–2060). *Alzheimer's & Dementia* **17**, 1966-1975 (2021).
52. J. Barnes *et al.*, Alzheimer's disease first symptoms are age dependent: Evidence from the NACC dataset. *Alzheimer's & Dementia* **11**, 1349-1357 (2015).
53. R. D. Terry *et al.*, Physical basis of cognitive alterations in alzheimer's disease: Synapse loss is the major correlate of cognitive impairment. *Annals of Neurology* **30**, 572-580 (1991).
54. T. Soykan, T. Maritzen, V. Haucke, Modes and mechanisms of synaptic vesicle recycling. *Curr Opin Neurobiol* **39**, 17-23 (2016).
55. P. J. Yao, Synaptic frailty and clathrin-mediated synaptic vesicle trafficking in Alzheimer's disease. *Trends in Neurosciences* **27**, 24-29 (2004).
56. Y. A. Pei, J. Davies, M. Zhang, H. T. Zhang, The Role of Synaptic Dysfunction in Alzheimer's Disease. *J Alzheimers Dis* **76**, 49-62 (2020).
57. Y. Ratan *et al.*, An Insight into Cellular and Molecular Mechanisms Underlying the Pathogenesis of Neurodegeneration in Alzheimer's Disease. *Biomedicines* **11**, 1398 (2023).
58. I. Milosevic, Revisiting the Role of Clathrin-Mediated Endoytosis in Synaptic Vesicle Recycling. *Frontiers in Cellular Neuroscience* **12**, (2018).
59. A. Pechstein *et al.*, Regulation of synaptic vesicle recycling by complex formation between intersectin 1 and the clathrin adaptor complex AP2. *Proceedings of the National Academy of Sciences* **107**, 4206-4211 (2010).

60. T. E. Chater, Y. Goda, The Shaping of AMPA Receptor Surface Distribution by Neuronal Activity. *Front Synaptic Neurosci* **14**, 833782 (2022).
61. P. Babaei, NMDA and AMPA receptors dysregulation in Alzheimer's disease. *Eur J Pharmacol* **908**, 174310 (2021).
62. R. A. Al-Hallaq, T. P. Conrads, T. D. Veenstra, R. J. Wenthold, NMDA Di-Heteromeric Receptor Populations and Associated Proteins in Rat Hippocampus. *Journal of Neuroscience* **27**, 8334-8343 (2007).
63. E. M. Snyder *et al.*, Regulation of NMDA receptor trafficking by amyloid-β. *Nature Neuroscience* **8**, 1051-1058 (2005).
64. P. N. Lacor *et al.*, Synaptic targeting by Alzheimer's-related amyloid beta oligomers. *J Neurosci* **24**, 10191-10200 (2004).
65. H.-Y. Man *et al.*, Regulation of AMPA Receptor–Mediated Synaptic Transmission by Clathrin-Dependent Receptor Internalization. *Neuron* **25**, 649-662 (2000).
66. S. Guntupalli *et al.*, GluA1 subunit ubiquitination mediates amyloid-β-induced loss of surface α-amino-3-hydroxy-5-methyl-4-isoxazolepropionic acid (AMPA) receptors. *Journal of Biological Chemistry* **292**, 8186-8194 (2017).
67. D. Azarnia Tehran *et al.*, Selective endocytosis of Ca(2+)-permeable AMPARs by the Alzheimer's disease risk factor CALM bidirectionally controls synaptic plasticity. *Sci Adv* **8**, eabl5032 (2022).
68. F. Wu, P. J. Yao, Clathrin-mediated endocytosis and Alzheimer's disease: an update. *Ageing Res Rev* **8**, 147-149 (2009).
69. C. Guimas Almeida, F. Sadat Mirfakhar, C. Perdigão, T. Burrinha, Impact of late-onset Alzheimer's genetic risk factors on beta-amyloid endocytic production. *Cellular and Molecular Life Sciences* **75**, 2577-2589 (2018).
70. R. S. Thomas *et al.*, Decreasing the expression of PICALM reduces endocytosis and the activity of β-secretase: implications for Alzheimer's disease. *BMC Neuroscience* **17**, (2016).
71. Y.-W. Zhang, R. Thompson, H. Zhang, H. Xu, APP processing in Alzheimer's disease. *Molecular Brain* **4**, 3 (2011).
72. T. Burrinha *et al.*, Upregulation of APP endocytosis by neuronal aging drives amyloid-dependent synapse loss. *Journal of Cell Science* **134**, (2021).
73. J. R. Cirrito *et al.*, Endocytosis Is Required for Synaptic Activity-Dependent Release of Amyloid-β In Vivo. *Neuron* **58**, 42-51 (2008).
74. J. R. Cirrito *et al.*, Synaptic Activity Regulates Interstitial Fluid Amyloid-β Levels In Vivo. *Neuron* **48**, 913-922 (2005).
75. G. K. Gouras *et al.*, Intraneuronal Aβ42 Accumulation in Human Brain. *The American Journal of Pathology* **156**, 15-20 (2000).
76. S. S. M. Lai, K. Y. Ng, R. Y. Koh, K. C. Chok, S. M. Chye, Endosomal-lysosomal dysfunctions in Alzheimer's disease: Pathogenesis and therapeutic interventions. *Metabolic Brain Disease* **36**, 1087-1100 (2021).
77. T. Kuboyama, C. Tohda, K. Komatsu, Neuritic regeneration and synaptic reconstruction induced by withanolide A. *British Journal of Pharmacology* **144**, 961-971 (2005).
78. F. M. Laferla, K. N. Green, S. Oddo, Intracellular amyloid-β in Alzheimer's disease. *Nature Reviews Neuroscience* **8**, 499-509 (2007).
79. T. Kuboyama, Y.-A. Lee, H. Nishiko, C. Tohda, Inhibition of clathrin-mediated endocytosis prevents amyloid β-induced axonal damage. *Neurobiology of Aging* **36**, 1808-1819 (2015).
80. E. Wesén, G. D. M. Jeffries, M. Matson Dzebo, E. K. Esbjörner, Endocytic uptake of monomeric amyloid-β peptides is clathrin- and dynamin-independent and results in selective accumulation of Aβ(1–42) compared to Aβ(1–40). *Scientific Reports* **7**, (2017).

81. E. Wesén, R. Lundmark, E. K. Esbjörner, Role of Membrane Tension Sensitive Endocytosis and Rho GTPases in the Uptake of the Alzheimer's Disease Peptide Aβ(1-42). *ACS Chemical Neuroscience* **11**, 1925-1936 (2020).
82. K. E. Marshall, D. M. Vadukul, K. Staras, L. C. Serpell, Misfolded amyloid-β-42 impairs the endosomal–lysosomal pathway. *Cellular and Molecular Life Sciences* **77**, 5031-5043 (2020).
83. J.-M. Shi *et al.*, Endocytosis Is a Key Mode of Interaction between Extracellular β-Amyloid and the Cell Membrane. *Biophysical Journal* **119**, 1078-1090 (2020).
84. S. M. Chafekar, F. Baas, W. Scheper, Oligomer-specific Abeta toxicity in cell models is mediated by selective uptake. *Biochim Biophys Acta* **1782**, 523-531 (2008).
85. S. Jin *et al.*, Amyloid-β(1–42) Aggregation Initiates Its Cellular Uptake and Cytotoxicity. *Journal of Biological Chemistry* **291**, 19590-19606 (2016).
86. R. S. Omtri, M. W. Davidson, B. Arumugam, J. F. Poduslo, K. K. Kandimalla, Differences in the Cellular Uptake and Intracellular Itineraries of Amyloid Beta Proteins 40 and 42: Ramifications for the Alzheimer's Drug Discovery. *Molecular Pharmaceutics* **9**, 1887-1897 (2012).
87. N. V. Mohamed, T. Herrou, V. Plouffe, N. Piperno, N. Leclerc, Spreading of tau pathology in <scp>A</scp>lzheimer's disease by cell-to-cell transmission. *European Journal of Neuroscience* **37**, 1939-1948 (2013).
88. M. Usenovic *et al.*, Internalized Tau Oligomers Cause Neurodegeneration by Inducing Accumulation of Pathogenic Tau in Human Neurons Derived from Induced Pluripotent Stem Cells. *The Journal of Neuroscience* **35**, 14234-14250 (2015).
89. M. Kolarova, U. Sengupta, A. Bartos, J. Ricny, R. Kayed, Tau Oligomers in Sera of Patients with Alzheimer's Disease and Aged Controls. *J Alzheimers Dis* **58**, 471-478 (2017).
90. J. Zhao, H. Wu, X. Q. Tang, Tau internalization: A complex step in tau propagation. *Ageing Res Rev* **67**, 101272 (2021).
91. K. Ando *et al.*, Alzheimer's Disease: Tau Pathology and Dysfunction of Endocytosis. *Front Mol Neurosci* **13**, 583755 (2020).
92. I. D. Vainchtein, A. V. Molofsky, Astrocytes and Microglia: In Sickness and in Health. *Trends Neurosci* **43**, 144-154 (2020).
93. N. F. Al-Ghraiybah *et al.*, Glial Cell-Mediated Neuroinflammation in Alzheimer's Disease. *International Journal of Molecular Sciences* **23**, 10572 (2022).
94. C. Eroglu, B. A. Barres, Regulation of synaptic connectivity by glia. *Nature* **468**, 223-231 (2010).
95. M. V. Sofroniew, H. V. Vinters, Astrocytes: biology and pathology. *Acta Neuropathologica* **119**, 7-35 (2010).
96. B. Torres-Ceja, M. L. Olsen, A closer look at astrocyte morphology: Development, heterogeneity, and plasticity at astrocyte leaflets. *Curr Opin Neurobiol* **74**, 102550 (2022).
97. M. V. Sofroniew, Astrocyte Reactivity: Subtypes, States, and Functions in CNS Innate Immunity. *Trends in Immunology* **41**, 758-770 (2020).
98. S. A. Liddelow *et al.*, Neurotoxic reactive astrocytes are induced by activated microglia. *Nature* **541**, 481-487 (2017).
99. R. G. Nagele *et al.*, Contribution of glial cells to the development of amyloid plaques in Alzheimer's disease. *Neurobiology of Aging* **25**, 663-674 (2004).
100. M. V. Sanchez-Mico *et al.*, Amyloid-β impairs the phagocytosis of dystrophic synapses by astrocytes in Alzheimer's disease. *Glia* **69**, 997-1011 (2021).

101. S. Söllvander *et al.*, Accumulation of amyloid-β by astrocytes result in enlarged endosomes and microvesicle-induced apoptosis of neurons. *Molecular Neurodegeneration* **11**, (2016).
102. N. Kimura, S. Okabayashi, F. Ono, Dynein dysfunction disrupts beta-amyloid clearance in astrocytes through endocytic disturbances. *Neuroreport* **25**, 514-520 (2014).
103. M. Domínguez-Prieto, A. Velasco, A. Tabernero, J. M. Medina, Endocytosis and Transcytosis of Amyloid-β Peptides by Astrocytes: A Possible Mechanism for Amyloid-β Clearance in Alzheimer's Disease. *Journal of Alzheimer's Disease* **65**, 1109-1124 (2018).
104. Y. A. Martens *et al.*, ApoE Cascade Hypothesis in the pathogenesis of Alzheimer's disease and related dementias. *Neuron* **110**, 1304-1317 (2022).
105. J. Kim, J. M. Basak, D. M. Holtzman, The Role of Apolipoprotein E in Alzheimer's Disease. *Neuron* **63**, 287-303 (2009).
106. M. Koistinaho *et al.*, Apolipoprotein E promotes astrocyte colocalization and degradation of deposited amyloid-β peptides. *Nature Medicine* **10**, 719-726 (2004).
107. Y.-T. Lin *et al.*, APOE4 Causes Widespread Molecular and Cellular Alterations Associated with Alzheimer's Disease Phenotypes in Human iPSC-Derived Brain Cell Types. *Neuron* **98**, 1141-1154.e1147 (2018).
108. P. Narayan *et al.*, PICALM Rescues Endocytic Defects Caused by the Alzheimer's Disease Risk Factor APOE4. *Cell Reports* **33**, 108224 (2020).
109. Z. Cai, M. D. Hussain, L.-J. Yan, Microglia, neuroinflammation, and beta-amyloid protein in Alzheimer's disease. *International Journal of Neuroscience* **124**, 307-321 (2014).
110. M. Y. Wendimu, S. B. Hooks, Microglia Phenotypes in Aging and Neurodegenerative Diseases. *Cells* **11**, 2091 (2022).
111. Y. Zhao *et al.*, Aβ and Tau Regulate Microglia Metabolism via Exosomes in Alzheimer's Disease. *Biomedicines* **10**, 1800 (2022).
112. W. J. Streit, H. Khoshbouei, I. Bechmann, The Role of Microglia in Sporadic Alzheimer's Disease. *Journal of Alzheimer's Disease* **79**, 961-968 (2021).
113. S. K. Jang *et al.*, An Aβ42 uptake and degradation via Rg3 requires an activation of caveolin, clathrin and Aβ-degrading enzymes in microglia. *European Journal of Pharmacology* **758**, 1-10 (2015).
114. M. Fujikura *et al.*, CD14 and Toll-Like Receptor 4 Promote Fibrillar Aβ42 Uptake by Microglia Through A Clathrin-Mediated Pathway. *Journal of Alzheimer's Disease* **68**, 323-337 (2019).
115. B. L. Heckmann *et al.*, LC3-Associated Endocytosis Facilitates β-Amyloid Clearance and Mitigates Neurodegeneration in Murine Alzheimer's Disease. *Cell* **178**, 536-551.e514 (2019).
116. U. S. Sandau *et al.*, Performance of Validated MicroRNA Biomarkers for Alzheimer's Disease in Mild Cognitive Impairment. *Journal of Alzheimer's Disease* **78**, 245-263 (2020).
117. T. A. Lusardi *et al.*, MicroRNAs in Human Cerebrospinal Fluid as Biomarkers for Alzheimer's Disease. *Journal of Alzheimer's Disease* **55**, 1223-1233 (2016).
118. J. T. Wiedrick *et al.*, Validation of MicroRNA Biomarkers for Alzheimer's Disease in Human Cerebrospinal Fluid. *J Alzheimers Dis* **67**, 875-891 (2019).
119. U. S. Sandau *et al.*, Performance of validated microRNA biomarkers for Alzheimer's disease in mild cognitive impairment. . *Journal of Alzheimer's Disease. Online ahead of print.*, (2020).
120. A.-B. Shyu, M. F. Wilkinson, A. Van Hoof, Messenger RNA regulation: to translate or to degrade. *The EMBO Journal* **27**, 471-481 (2008).

121. W. Filipowicz, S. N. Bhattacharyya, N. Sonenberg, Mechanisms of post-transcriptional regulation by microRNAs: are the answers in sight? *Nature Reviews Genetics* **9**, 102-114 (2008).
122. L. F. R. Gebert, I. J. Macrae, Regulation of microRNA function in animals. *Nature Reviews Molecular Cell Biology* **20**, 21-37 (2019).
123. R. A. Nixon, Endosome function and dysfunction in Alzheimer's disease and other neurodegenerative diseases. *Neurobiology of Aging* **26**, 373-382 (2005).
124. K. Ando *et al.*, Clathrin adaptor CALM/PICALM is associated with neurofibrillary tangles and is cleaved in Alzheimer's brains. *Acta Neuropathol* **125**, 861-878 (2013).
125. M. Alsaqati, R. S. Thomas, E. J. Kidd, Upregulation of endocytic protein expression in the Alzheimer's disease male human brain. *Aging Brain* **4**, 100084 (2023).
126. B. Wilmot *et al.*, Translational gene mapping of cognitive decline. **29**, 524-541 (2008).
127. N. Malakooti, The Down Syndrome-Associated Protein, Regulator of Calcineurin-1, is Altered in Alzheimer's Disease and Dementia with Lewy Bodies. (2019).
128. Y. Nakamura *et al.*, Involvement of clathrin light chains in the pathology of Alzheimer's disease. *Acta Neuropathologica* **87**, 23-31 (1994).
129. C. C. Teerlink *et al.*, Analysis of high-risk pedigrees identifies 11 candidate variants for Alzheimer's disease. *Alzheimer's & Dementia*, (2021).
130. S. Srinivasan, J. Gal, A. Bachstetter, P. T. Nelson, Alpha adaptins show isoform-specific association with neurofibrillary tangles in Alzheimer's disease. *Neuropathology and Applied Neurobiology* **48**, (2022).
131. N. J. Aidaralieva *et al.*, Dynamin 2 gene is a novel susceptibility gene for late-onset Alzheimer disease in non-APOE-ε4 carriers. *Journal of Human Genetics* **53**, 296-302 (2008).
132. E. Kamagata *et al.*, Decrease of dynamin 2 levels in late-onset Alzheimer's disease alters Abeta metabolism. *Biochem Biophys Res Commun* **379**, 691-695 (2009).
133. S. S. Du *et al.*, Dynamin-2 mediates clathrin-dependent endocytosis for amyloid-beta internalization in brain microvascular endothelial cells. *Microvasc Res* **138**, 104219 (2021).
134. V. Agarwal, G. W. Bell, J.-W. Nam, D. P. Bartel, Predicting effective microRNA target sites in mammalian mRNAs. *eLife* **4**, (2015).
135. Y. Chen, X. Wang, miRDB: an online database for prediction of functional microRNA targets. *Nucleic Acids Research* **48**, D127-D131 (2020).
136. W. Liu, X. Wang, Prediction of functional microRNA targets by integrative modeling of microRNA binding and target expression data. *Genome Biology* **20**, (2019).
137. A. C. Oliveira *et al.*, Combining Results from Distinct MicroRNA Target Prediction Tools Enhances the Performance of Analyses. *Frontiers in Genetics* **8**, (2017).
138. X. Fan, L. Kurgan, Comprehensive overview and assessment of computational prediction of microRNA targets in animals. **16**, 780-794 (2015).
139. C.-H. Chou *et al.*, miRTarBase update 2018: a resource for experimentally validated microRNA-target interactions. *Nucleic Acids Research* **46**, D296-D302 (2018).
140. J. W. Nelson *et al.*, Role of soluble epoxide hydrolase in age-related vascular cognitive decline. *Prostaglandins & Other Lipid Mediators* **113-115**, 30-37 (2014).
141. M. C. Tierney *et al.*, The NINCDS-ADRDA Work Group criteria for the clinical diagnosis of probable Alzheimer's disease. *A clinicopathologic study of 57 cases* **38**, 359-359 (1988).
142. A. Sormunen *et al.*, Comparison of Automated and Traditional Western Blotting Methods. *Methods and Protocols* **6**, 43 (2023).

143. S. G. Greenberg, P. Davies, J. D. Schein, L. I. Binder, Hydrofluoric acid-treated tau PHF proteins display the same biochemical properties as normal tau. *Journal of Biological Chemistry* **267**, 564-569 (1992).
144. R. Oughtred *et al.*, The <scp>BioGRID</scp> database: A comprehensive biomedical resource of curated protein, genetic, and chemical interactions. *Protein Science* **30**, 187-200 (2021).
145. N. K. Hussain *et al.*, Splice Variants of Intersectin Are Components of the Endocytic Machinery in Neurons and Nonneuronal Cells. *Journal of Biological Chemistry* **274**, 15671-15677 (1999).
146. Okamoto, EHSH1/Intersectin, a protein that cintains EH and SH3 domais and binds ti dynamin and SNAP-25. (1999).
147. J. Das, M. Tiwari, D. Subramanyam, Clathrin Light Chains: Not to Be Taken so Lightly. *Front Cell Dev Biol* **9**, 774587 (2021).
148. K. Ando *et al.*, Level of PICALM, a key component of clathrin-mediated endocytosis, is correlated with levels of phosphotau and autophagy-related proteins and is associated with tau inclusions in AD, PSP and Pick disease. *Neurobiology of Disease* **94**, 32-43 (2016).
149. J. Jacobs, M. J. Kahana, Direct brain recordings fuel advances in cognitive electrophysiology. *Trends in Cognitive Sciences* **14**, 162-171 (2010).
150. E. Herrero-Garcia, J. P. O'Bryan, Intersectin scaffold proteins and their role in cell signaling and endocytosis. **1864**, 23-30 (2017).
151. K. A. Wong *et al.*, Intersectin (ITSN) Family of Scaffolds Function as Molecular Hubs in Protein Interaction Networks. **7**, e36023 (2012).
152. O. Gubar *et al.*, Intersectin: The Crossroad between Vesicle Exocytosis and Endocytosis. *Frontiers in Endocrinology* **4**, (2013).
153. N. K. Hussain *et al.*, Endocytic protein intersectin-l regulates actin assembly via Cdc42 and N-WASP. *Nat Cell Biol* **3**, 927-932 (2001).
154. F. Irie, Y. Yamaguchi, EphB receptors regulate dendritic spine development via intersectin, Cdc42 and N-WASP. *Nature Neuroscience* **5**, 1117-1118 (2002).
155. F. Simpson *et al.*, SH3-domain-containing proteins function at distinct steps in clathrin-coated vesicle formation. *Nature Cell Biology* **1**, 119-124 (1999).
156. A. S. Sengar, The EH and SH3 domain Ese proteins regulate endocytosis by linking dynamin and Eps15. (1999).
157. Y. Yu *et al.*, Mice deficient for the chromosome 21 ortholog Itsn1 exhibit vesicle-trafficking abnormalities. *Human Molecular Genetics* **17**, 3281-3290 (2008).
158. S. Thomas *et al.*, Intersectin Regulates Dendritic Spine Development and Somatodendritic Endocytosis but Not Synaptic Vesicle Recycling in Hippocampal Neurons. *Journal of Biological Chemistry* **284**, 12410-12419 (2009).
159. N. Malakooti *et al.*, The Long Isoform of Intersectin-1 Has a Role in Learning and Memory. *Frontiers in Behavioral Neuroscience* **14**, (2020).
160. F. Gerth *et al.*, Intersectin associates with synapsin and regulates its nanoscale localization and function. *Proceedings of the National Academy of Sciences* **114**, 12057-12062 (2017).
161. M. Jäpel *et al.*, Intersectin-Mediated Clearance of SNARE Complexes Is Required for Fast Neurotransmission. *Cell Reports* **30**, 409-420.e406 (2020).
162. T. Dunckley *et al.*, Gene expression correlates of neurofibrillary tangles in Alzheimer's disease. **27**, 1359-1371 (2006).
163. L. G. Apostolova *et al.*, 3D comparison of hippocampal atrophy in amnestic mild cognitive impairment and Alzheimer's disease. *Brain* **129**, 2867-2873 (2006).

164. J. Williamson *et al.*, Sex differences in brain functional connectivity of hippocampus in mild cognitive impairment. *Front Aging Neurosci* **14**, 959394 (2022).
165. S. Yagi, L. A. M. Galea, Sex differences in hippocampal cognition and neurogenesis. *Neuropsychopharmacology* **44**, 200-213 (2019).
166. A. M. González-Jamett *et al.*, Dynamin-2 in nervous system disorders. *Journal of Neurochemistry* **128**, 210-223 (2014).
167. O. Sheppard, M. Coleman. (Exon Publications, 2020), pp. 1-22.
168. G. D. Rabinovici, R. La Joie, Amyloid-Targeting Monoclonal Antibodies for Alzheimer Disease. *JAMA* **330**, 507-509 (2023).
169. G. Esquerda-Canals, L. Montoliu-Gaya, J. Güell-Bosch, S. Villegas, Mouse Models of Alzheimer's Disease. *Journal of Alzheimer's Disease* **57**, 1171-1183 (2017).
170. S. Jawhar, A. Trawicka, C. Jenneckens, T. A. Bayer, O. Wirths, Motor deficits, neuron loss, and reduced anxiety coinciding with axonal degeneration and intraneuronal Abeta aggregation in the 5XFAD mouse model of Alzheimer's disease. *Neurobiol Aging* **33**, 196 e129-140 (2012).
171. W. A. Eimer, R. Vassar, Neuron loss in the 5XFAD mouse model of Alzheimer's disease correlates with intraneuronal Aβ42 accumulation and Caspase-3 activation. *Molecular Neurodegeneration* **8**, 2 (2013).
172. M. Guipponi *et al.*, Two Isoforms of a Human Intersectin (ITSN) Protein Are Produced by Brain-Specific Alternative Splicing in a Stop Codon. **53**, 369-376 (1998).
173. E. Evergren *et al.*, Intersectin Is a Negative Regulator of Dynamin Recruitment to the Synaptic Endocytic Zone in the Central Synapse. *The Journal of Neuroscience* **27**, 379-390 (2007).
174. L. Tsyba *et al.*, Alternative splicing affecting the SH3A domain controls the binding properties of intersectin 1 in neurons. *Biochemical and Biophysical Research Communications* **372**, 929-934 (2008).
175. L. Tsyba *et al.*, Intersectin multidomain adaptor proteins: Regulation of functional diversity. *Gene* **473**, 67-75 (2011).
176. T. Sakaba *et al.*, Fast neurotransmitter release regulated by the endocytic scaffold intersectin. *Proceedings of the National Academy of Sciences* **110**, 8266-8271 (2013).
177. B. Jakob *et al.*, Intersectin 1 is a component of the Reelin pathway to regulate neuronal migration and synaptic plasticity in the hippocampus. *Proceedings of the National Academy of Sciences* **114**, 5533-5538 (2017).
178. J. P. O'Bryan, R. P. Mohney, C. E. Oldham, Mitogenesis and endocytosis: What's at the INTERSECTIoN? *Oncogene* **20**, 6300-6308 (2001).
179. D. K. Kim *et al.*, Deep proteome profiling of the hippocampus in the 5XFAD mouse model reveals biological process alterations and a novel biomarker of Alzheimer's disease. *Experimental & Molecular Medicine* **51**, (2019).
180. S. Forner *et al.*, Systematic phenotyping and characterization of the 5xFAD mouse model of Alzheimer's disease. *Scientific Data* **8**, (2021).
181. A. L. Oblak *et al.*, Comprehensive Evaluation of the 5XFAD Mouse Model for Preclinical Testing Applications: A MODEL-AD Study. *Front Aging Neurosci* **13**, 713726 (2021).
182. Y. Ishizuka, C. R. Bramham, A simple DMSO-based method for cryopreservation of primary hippocampal and cortical neurons. *J Neurosci Methods* **333**, 108578 (2020).
183. S. Kaech, G. Banker, Culturing hippocampal neurons. *Nature Protocols* **1**, 2406-2415 (2006).
184. P. Guedes-Dias, E. L. F. Holzbaur, Axonal transport: Driving synaptic function. *Science* **366**, (2019).

185. Jeffrey, Maria, Jacob, C. Janke, Erika, α-Tubulin Tyrosination and CLIP-170 Phosphorylation Regulate the Initiation of Dynein-Driven Transport in Neurons. *Cell Reports* **14**, 2637-2652 (2016).
186. I. Hong *et al.*, Quantitative proteomic analysis of the hippocampus in the 5XFAD mouse model at early stages of Alzheimer's disease pathology. *J Alzheimers Dis* **36**, 321-334 (2013).
187. A. Boeddrich *et al.*, A proteomics analysis of 5xFAD mouse brain regions reveals the lysosome-associated protein Arl8b as a candidate biomarker for Alzheimer's disease. *Genome Medicine* **15**, (2023).
188. Y. Chen *et al.*, Reelin modulates NMDA receptor activity in cortical neurons. *J Neurosci* **25**, 8209-8216 (2005).
189. M. Tzioras, R. I. McGeachan, C. S. Durrant, T. L. Spires-Jones, Synaptic degeneration in Alzheimer disease. *Nature Reviews Neurology* **19**, 19-38 (2023).
190. D. Balschun, M. J. Rowan, Hippocampal synaptic plasticity in neurodegenerative diseases: Aß, tau and beyond. *Neuroforum* **24**, A133-A141 (2018).
191. G. A. Prieto *et al.*, Pharmacological Rescue of Long-Term Potentiation in Alzheimer Diseased Synapses. *The Journal of Neuroscience* **37**, 1197-1212 (2017).
192. S. X. Jin, L. Liu, S. Li, A. L. Meunier, D. J. Selkoe, Abeta oligomers from human brain impair mossy fiber LTP in CA3 of hippocampus, but activating cAMP-PKA and cGMP-PKG prevents this. *Neurobiol Dis* **172**, 105816 (2022).
193. J. G. Pelletier, J. C. Lacaille, Long-term synaptic plasticity in hippocampal feedback inhibitory networks. *Prog Brain Res* **169**, 241-250 (2008).
194. J. Basu, S. A. Siegelbaum, The Corticohippocampal Circuit, Synaptic Plasticity, and Memory. *Cold Spring Harbor Perspectives in Biology* **7**, a021733 (2015).
195. G. Di Benedetto *et al.*, Role of Microglia and Astrocytes in Alzheimer's Disease: From Neuroinflammation to Ca2+ Homeostasis Dysregulation. *Cells* **11**, 2728 (2022).
196. U. S. Sandau *et al.*, Differential Effects of APOE Genotype on MicroRNA Cargo of Cerebrospinal Fluid Extracellular Vesicles in Females With Alzheimer's Disease Compared to Males. *Frontiers in Cell and Developmental Biology* **10**, (2022).
197. J. Sevigny *et al.*, The antibody aducanumab reduces Abeta plaques in Alzheimer's disease. *Nature* **537**, 50-56 (2016).
198. S. Budd Haeberlein *et al.*, Two Randomized Phase 3 Studies of Aducanumab in Early Alzheimer's Disease. *J Prev Alzheimers Dis* **9**, 197-210 (2022).
199. C. J. Swanson *et al.*, A randomized, double-blind, phase 2b proof-of-concept clinical trial in early Alzheimer's disease with lecanemab, an anti-Abeta protofibril antibody. *Alzheimers Res Ther* **13**, 80 (2021).
200. M. A. Mintun *et al.*, Donanemab in Early Alzheimer's Disease. *N Engl J Med* **384**, 1691-1704 (2021).
201. R. Katzman, Editorial: The prevalence and malignancy of Alzheimer disease. A major killer. *Arch Neurol* **33**, 217-218 (1976).
202. M. W. Bondi, E. C. Edmonds, D. P. Salmon, Alzheimer's Disease: Past, Present, and Future. *J Int Neuropsychol Soc* **23**, 818-831 (2017).
203. D. P. Salmon *et al.*, Alzheimer's disease can be accurately diagnosed in very mildly impaired individuals. *Neurology* **59**, 1022-1028 (2002).
204. B. Olsson *et al.*, CSF and blood biomarkers for the diagnosis of Alzheimer's disease: a systematic review and meta-analysis. *The Lancet Neurology* **15**, 673-684 (2016).
205. K. Blennow, N. Mattsson, M. Scholl, O. Hansson, H. Zetterberg, Amyloid biomarkers in Alzheimer's disease. *Trends Pharmacol Sci* **36**, 297-309 (2015).
206. R. Ossenkoppele, R. van der Kant, O. Hansson, Tau biomarkers in Alzheimer's disease: towards implementation in clinical practice and trials. *Lancet Neurol* **21**, 726-734 (2022).

207. K. Blennow, H. Zetterberg, Biomarkers for Alzheimer's disease: current status and prospects for the future. *J Intern Med* **284**, 643-663 (2018).
208. C. R. Jack, Jr. *et al.*, NIA-AA Research Framework: Toward a biological definition of Alzheimer's disease. *Alzheimers Dement* **14**, 535-562 (2018).
209. A. M. Fagan *et al.*, Longitudinal change in CSF biomarkers in autosomal-dominant Alzheimer's disease. *Sci Transl Med* **6**, 226ra230 (2014).
210. V. L. Villemagne *et al.*, Amyloid beta deposition, neurodegeneration, and cognitive decline in sporadic Alzheimer's disease: a prospective cohort study. *Lancet Neurol* **12**, 357-367 (2013).
211. J. F. Quinn *et al.*, Extracellular RNAs: development as biomarkers of human disease. **4**, (2015).
212. S. Kumar, P. H. Reddy, Are circulating microRNAs peripheral biomarkers for Alzheimer's disease? *Biochimica et Biophysica Acta (BBA) - Molecular Basis of Disease* **1862**, 1617-1627 (2016).
213. V. Van Giau, S. S. An, Emergence of exosomal miRNAs as a diagnostic biomarker for Alzheimer's disease. *J Neurol Sci* **360**, 141-152 (2016).
214. N. Kosikova, M. Cente, V. Cigankova, P. Koson, P. Filipcik, miRNAs as biofluid markers for diagnostics of Alzheimer's disease: recent status and perspectives. *Gen Physiol Biophys* **37**, 495-514 (2018).
215. S. Swarbrick, N. Wragg, S. Ghosh, A. Stolzing, Systematic Review of miRNA as Biomarkers in Alzheimer's Disease. *Mol Neurobiol* **56**, 6156-6167 (2019).
216. H. Guo, N. T. Ingolia, J. S. Weissman, D. P. Bartel, Mammalian microRNAs predominantly act to decrease target mRNA levels. *Nature* **466**, 835-840 (2010).
217. M. R. Fabian, N. Sonenberg, W. Filipowicz, Regulation of mRNA Translation and Stability by microRNAs. *Annual Review of Biochemistry* **79**, 351-379 (2010).
218. J. Hausser, M. Zavolan, Identification and consequences of miRNA–target interactions — beyond repression of gene expression. *Nature Reviews Genetics* **15**, 599-612 (2014).
219. M. S. Batistela, N. D. Josviak, C. D. Sulzbach, R. L. R. De Souza, An overview of circulating cell-free microRNAs as putative biomarkers in Alzheimer's and Parkinson's Diseases. 1-12 (2016).
220. D. Didiano, O. Hobert, Perfect seed pairing is not a generally reliable predictor for miRNA-target interactions. *Nat Struct Mol Biol* **13**, 849-851 (2006).
221. T. Fujuwara, T. Yada, miRNA-target prediction based on transcriptional regulation. *BMC Genomics*, (2013).
222. H. Hamzeiy, J. Allmer, M. Yousef, Computational methods for microRNA target prediction. *Methods Mol Biol* **1107**, 207-221 (2014).
223. A. Grimson *et al.*, MicroRNA targeting specificity in mammals: determinants beyond seed pairing. *Mol Cell* **27**, 91-105 (2007).
224. T. M. Witkos, E. Koscianska, W. J. Krzyzosiak, Practical Aspects of microRNA Target Prediction. **11**, 93-109 (2011).
225. C. E. Vejnar, E. M. Zdobnov, miRmap: Comprehensive prediction of microRNA target repression strength. *Nucleic Acids Research* **40**, 11673-11683 (2012).
226. H. Y. Huang *et al.*, miRTarBase update 2022: an informative resource for experimentally validated miRNA-target interactions. *Nucleic Acids Res* **50**, D222-D230 (2022).
227. A. L. Riffo-Campos, I. Riquelme, P. Brebi-Mieville, Tools for Sequence-Based miRNA Target Prediction: What to Choose? *Int J Mol Sci* **17**, (2016).
228. E. C. Lai, Predicting and validating microRNA targets. *Genome Biol* **5**, 115 (2004).
229. J. Brennecke, A. Stark, R. B. Russell, S. M. Cohen, Principles of microRNA-target recognition. *PLoS Biol* **3**, e85 (2005).

230. M. Mofatteh, Neurodegeneration and axonal mRNA transportation. *Am J Neurodegener Dis* **10**, 1-12 (2021).
231. L. Zhang *et al.*, Roles and Mechanisms of Axon-Guidance Molecules in Alzheimer's Disease. *Mol Neurobiol* **58**, 3290-3307 (2021).
232. M. F. Colavitta, F. J. Barrantes, Therapeutic Strategies Aimed at Improving Neuroplasticity in Alzheimer Disease. *Pharmaceutics* **15**, (2023).
233. Z. Hu *et al.*, Do tau-synaptic long-term depression interactions in the hippocampus play a pivotal role in the progression of Alzheimer's disease? *Neural Regen Res* **18**, 1213-1219 (2023).
234. G. Koch, D. Spampinato, Alzheimer disease and neuroplasticity. *Handb Clin Neurol* **184**, 473-479 (2022).
235. H. Zhang *et al.*, Role of Abeta in Alzheimer's-related synaptic dysfunction. *Front Cell Dev Biol* **10**, 964075 (2022).
236. P. L. Cardozo *et al.*, Synaptic Elimination in Neurological Disorders. *Curr Neuropharmacol* **17**, 1071-1095 (2019).
237. Y. Yu *et al.*, Integrative Analysis of MicroRNAome, Transcriptome, and Proteome during the Limb Regeneration of Cynops orientalis. *J Proteome Res* **18**, 1088-1098 (2019).
238. K. L. Prichard, N. S. O'Brien, S. R. Murcia, J. R. Baker, A. McCluskey, Role of Clathrin and Dynamin in Clathrin Mediated Endocytosis/Synaptic Vesicle Recycling and Implications in Neurological Diseases. *Frontiers in Cellular Neuroscience* **15**, (2022).
239. T. A. Blanpied, D. B. Scott, M. D. Ehlers, Dynamics and regulation of clathrin coats at specialized endocytic zones of dendrites and spines. *Neuron* **36**, 435-449 (2002).
240. C. Pucharcos, C. Casas, M. Nadal, X. Estivill, S. De La Luna, The human intersectin genes and their spliced variants are differentially expressed. **1521**, 1-11 (2001).
241. S. Kropyvko *et al.*, Structural diversity and differential expression of novel human intersectin 1 isoforms. **37**, 2789-2796 (2010).
242. M. Dergai *et al.*, Identification and characterization of a novel mammalian isoform of the endocytic adaptor ITSN1. **485**, 120-129 (2011).
243. C. Pucharcós *et al.*, Alu-splice cloning of human Intersectin (ITSN), a putative multivalent binding protein expressed in proliferating and differentiating neurons and overexpressed in Down syndrome. *European Journal of Human Genetics* **7**, 704-712 (1999).
244. D. J. Keating, C. Chen, M. A. Pritchard, Alzheimer's disease and endocytic dysfunction: Clues from the Down syndrome-related proteins, DSCR1 and ITSN1. **5**, 388-401 (2006).
245. M. P. Hunter *et al.*, Intersectin 1 contributes to phenotypes in vivo. *NeuroReport* **22**, 767-772 (2011).
246. Y. Shao *et al.*, Alternative splicing-derived intersectin1-L and intersectin1-S exert opposite function in glioma progression. *Cell Death & Disease* **10**, (2019).
247. A. Adams, J. M. Thorn, M. Yamabhai, B. K. Kay, J. P. O'Bryan, Intersectin, an adaptor protein involved in clathrin-mediated endocytosis, activates mitogenic signaling pathways. *J Biol Chem* **275**, 27414-27420 (2000).
248. X. K. Tong, N. K. Hussain, A. G. Adams, J. P. O'Bryan, P. S. McPherson, Intersectin can regulate the Ras/MAP kinase pathway independent of its role in endocytosis. *J Biol Chem* **275**, 29894-29899 (2000).
249. T. Arendt, J. T. Stieler, M. Holzer, Tau and tauopathies. *Brain Res Bull* **126**, 238-292 (2016).
250. Y. Gao, L. Tan, J. T. Yu, L. Tan, Tau in Alzheimer's Disease: Mechanisms and Therapeutic Strategies. *Curr Alzheimer Res* **15**, 283-300 (2018).
251. T. Kwon *et al.*, Tau pathology vulnerable neuronal subpopulation in Alzheimer’s disease. *Alzheimer's & Dementia* **18**, (2022).

252. Y. Cao, Y. Xiao, R. Ravid, Z.-Z. Guan, Changed Clathrin Regulatory Proteins in the Brains of Alzheimer's Disease Patients and Animal Models. *Journal of Alzheimer's Disease* **22**, 329-342 (2010).
253. E. Drummond, T. Wisniewski, Alzheimer's disease: experimental models and reality. *Acta Neuropathologica* **133**, 155-175 (2017).
254. M. Mullan *et al.*, A pathogenic mutation for probable Alzheimer's disease in the APP gene at the N-terminus of beta-amyloid. *Nat Genet* **1**, 345-347 (1992).
255. C. B. Eckman *et al.*, A new pathogenic mutation in the APP gene (I716V) increases the relative proportion of A beta 42(43). *Hum Mol Genet* **6**, 2087-2089 (1997).
256. A. Goate *et al.*, Segregation of a missense mutation in the amyloid precursor protein gene with familial Alzheimer's disease. *Nature* **349**, 704-706 (1991).
257. O. Berezovska *et al.*, Familial Alzheimer's disease presenilin 1 mutations cause alterations in the conformation of presenilin and interactions with amyloid precursor protein. *J Neurosci* **25**, 3009-3017 (2005).
258. M. Citron *et al.*, Additive Effects of PS1 and APP Mutations on Secretion of the 42-Residue Amyloid β-Protein. *Neurobiology of Disease* **5**, 107-116 (1998).
259. A. R. Mazi *et al.*, Neonatal Neurodegeneration in Alzheimer's Disease Transgenic Mouse Model. *J Alzheimers Dis Rep* **2**, 79-91 (2018).
260. A. S. Sengar *et al.*, Vertebrate intersectin1 is repurposed to facilitate cortical midline connectivity and higher order cognition. *J Neurosci* **33**, 4055-4065 (2013).
261. Y. Mu, F. H. Gage, Adult hippocampal neurogenesis and its role in Alzheimer's disease. *Molecular Neurodegeneration* **6**, 85 (2011).
262. K. R. Babcock, J. S. Page, J. R. Fallon, A. E. Webb, Adult Hippocampal Neurogenesis in Aging and Alzheimer's Disease. *Stem Cell Reports* **16**, 681-693 (2021).
263. T. A. Kim, M. D. Syty, K. Wu, S. Ge, Adult hippocampal neurogenesis and its impairment in Alzheimer's disease. *Zool Res* **43**, 481-496 (2022).
264. C. Chabu, C. Q. Doe, Dap160/intersectin binds and activates aPKC to regulate cell polarity and cell cycle progression. *Development* **135**, 2739-2746 (2008).
265. M. Das *et al.*, Regulation of neuron survival through an intersectin-phosphoinositide 3'-kinase C2beta-AKT pathway. *Mol Cell Biol* **27**, 7906-7917 (2007).
266. J. X. Liu, S. B. Pinnock, J. Herbert, Novel Control by the CA3 Region of the Hippocampus on Neurogenesis in the Dentate Gyrus of the Adult Rat. *PLoS ONE* **6**, e17562 (2011).
267. Y.-T. Lin, C.-C. Chen, C.-C. Huang, K. Nishimori, K.-S. Hsu, Oxytocin stimulates hippocampal neurogenesis via oxytocin receptor expressed in CA3 pyramidal neurons. *Nature Communications* **8**, (2017).
268. A. S. Sengar *et al.*, Vertebrate Intersectin1 Is Repurposed to Facilitate Cortical Midline Connectivity and Higher Order Cognition. *Journal of Neuroscience* **33**, 4055-4065 (2013).
269. R. Guerreiro, J. Bras, The age factor in Alzheimer's disease. *Genome Med* **7**, 106 (2015).
270. M. M. Ahmed, A. Block, S. Tong, M. T. Davisson, K. J. Gardiner, Age exacerbates abnormal protein expression in a mouse model of Down syndrome. *Neurobiol Aging* **57**, 120-132 (2017).
271. K. Ando *et al.*, Alzheimer's Disease: Tau Pathology and Dysfunction of Endocytosis. *Frontiers in Molecular Neuroscience* **13**, (2021).
272. S. Oddo, Amyloid deposition precedes tangle formation in a triple transgenic model of Alzheimer's disease. *Neurobiology of Aging* **24**, 1063-1070 (2003).
273. J. L. Cummings, T. Morstorf, K. Zhong, Alzheimer's disease drug-development pipeline: few candidates, frequent failures. *Alzheimer's Research & Therapy* **6**, 37 (2014).

274. A. Banik *et al.*, Translation of Pre-Clinical Studies into Successful Clinical Trials for Alzheimer's Disease: What are the Roadblocks and How Can They Be Overcome? *J Alzheimers Dis* **47**, 815-843 (2015).

Appendix A. Performance of Validated MicroRNA Biomarkers for Alzheimer's Disease in Mild Cognitive Impairment

Ursula S. Sandau[a,1], Jack T. Wiedrick[b,1], Sierra J. Smith[a], Trevor J. McFarland[a], Theresa A. Lusardi[c], Babett Lind[d], Christina A. Harrington[e], Jodi A. Lapidus[b,f], Douglas R. Galasko[g], Joseph F. Quinn[h,i] and Julie A. Saugstad[a,*]

[a]Department of Anesthesiology & Perioperative Medicine, Oregon Health & Science University, Portland, OR, USA
[b]Biostatistics & Design Program, Oregon Health & Science University, Portland, OR, USA
[c]Knight Cancer Institute Cancer Early Detection Advanced Research Center, Oregon Health & Science University, Portland, OR, USA
[d]Department of Neurology, Layton Aging and Alzheimer's Center, Oregon Health & Science University, Portland, OR, USA
[e]Integrated Genomics Laboratory, Oregon Health & Science University, Portland, OR, USA
[f]Oregon Health & Science University–Portland State University School of Public Health, Portland, OR, USA
[g]Department of Neurosciences, University of California San Diego, La Jolla, CA, USA
[h]Parkinson Center and Movement Disorders Program, School of Medicine, Oregon Health & Science University, Portland, OR, USA
[i]Portland VAMC Parkinson's Disease Research, Education, and Clinical Center, Portland, OR, USA

Appendix B. Methamphetamine use Alters Human Plasma Extracellular Vesicles and Their MicroRNA Cargo: An Exploratory Study

Ursula S. Sandau[1], Erika Duggan[2], Xiao Shi[3,4,5,6], Sierra J. Smith[1], Marilyn Huckans[3,4,5,7], William E. Schutzer[3,4,5,6], Jennifer M. Loftis[3,4,5,7], Aaron Janowsky[3,4,5,6], John P. Nolan[2], Julie A. Saugstad[1]

[1]Department of Anesthesiology & Perioperative Medicine, Oregon Health & Science University, Portland, Oregon, USA
[2]Scintillon Institute, San Diego, California, USA
[3]VA Portland Health Care System, Portland, Oregon, USA
[4]Department of Psychiatry, Oregon Health & Science University, Portland, Oregon, USA
[5]Methamphetamine Research Center, Oregon Health & Science University, Portland, Oregon, USA
[6]Department of Behavioral Neuroscience, Oregon Health & Science University, Portland, Oregon, USA
[7]Clinical Psychology Program, Oregon Health & Science University, Portland, Oregon, USA

Appendix C. Differential Effects of APOE Genotype on MicroRNA Cargo of Cerebrospinal Fluid Extracellular Vesicles in Females With Alzheimer's Disease Compared to Males

Ursula S. Sandau[1], Trevor J. McFarland[1], Sierra J. Smith[1], Douglas R. Galasko[2], Joseph F. Quinn[3,4,5] and Julie A. Saugstad[1]*

[1]Department of Anesthesiology and Perioperative Medicine, Oregon Health & Science University, Portland, OR, United States
[2]Department of Neurosciences, University of California, San Diego, La Jolla, CA, United States
[3]Department of Neurology, Oregon Health & Science University, Portland, OR, United States
[4]Parkinson Center and Movement Disorders Program, Oregon Health & Science University, Portland, OR, United States
[5]Portland VAMC Parkinson's Disease Research, Education, and Clinical Center, Portland, OR, United States